



Titre: Practical Microstructured and Plasmonic Terahertz Waveguides
Title:

Auteur: Andrey Markov
Author:

Date: 2015

Type: Mémoire ou thèse / Dissertation or Thesis

Référence: Markov, A. (2015). Practical Microstructured and Plasmonic Terahertz Waveguides
Citation: [Thèse de doctorat, École Polytechnique de Montréal]. PolyPublie.
<https://publications.polymtl.ca/1756/>

 **Document en libre accès dans PolyPublie**
Open Access document in PolyPublie

URL de PolyPublie: <https://publications.polymtl.ca/1756/>
PolyPublie URL:

**Directeurs de
recherche:** Maksim A. Skorobogatiy
Advisors:

Programme: Génie physique
Program:

UNIVERSITÉ DE MONTRÉAL

PRACTICAL MICROSTRUCTURED AND PLASMONIC
TERAHERTZ WAVEGUIDES

ANDREY MARKOV

DÉPARTEMENT DE GÉNIE PHYSIQUE
ÉCOLE POLYTECHNIQUE DE MONTRÉAL

THÈSE PRÉSENTÉE EN VUE DE L'OBTENTION
DU DIPLÔME DE PHILOSOPHIAE DOCTOR
(GÉNIE PHYSIQUE)

MAI 2015

UNIVERSITÉ DE MONTRÉAL

ÉCOLE POLYTECHNIQUE DE MONTRÉAL

Cette thèse intitulée:

PRACTICAL MICROSTRUCTURED AND PLASMONIC
TERAHERTZ WAVEGUIDES

présentée par : MARKOV Andrey

en vue de l'obtention du diplôme de : Philosophiae Doctor

a été dûment acceptée par le jury d'examen constitué de :

M. FRANCOEUR Sébastien, Ph. D., président

M. SKOROBOGATIY Maksim A., Ph. D, membre et directeur de recherche

M. MEUNIER Michel, Ph. D, membre

M. YAMILOV Alexey G., Ph. D, membre externe

ACKNOWLEDGEMENTS

I would like to express my heartfelt gratitude to my supervisor and research director Prof. Maksim Skorobogatiy for his guidance during my PhD study, his invaluable assistance and support. Maksim's help allowed me to pursue successfully my scientific dream, become more mature, and enrich my curiosity.

I have been surrounded by wonderful colleagues Bora Ung, Stephan Gorgutsa, Anna Mazhorova, Mathieu Rozé, Hang Qu, Hichem Guerboukha and others. I would like to thank them for the helpful discussions, productive mutual work, and simply support during the five years of my studies.

Finally I would like to give a special acknowledgement to my parents and my fiancé, Stephanie. They have always been understanding and patient, and I could always address to them for the encouragement and support when I needed it.

RÉSUMÉ

La bande térahertz, comprenant les fréquences entre 100 GHz et 10 THz, présente un fort potentiel pour diverses applications technologiques et scientifiques, telles que la détection, l'imagerie, le secteur des communications ainsi que la spectroscopie. La plupart des sources térahertz (THz) sont immobiles et, dans les systèmes THz existants, la propagation de l'onde se fait dans l'air libre, afin de minimiser les pertes de transmission. Le design efficace de guides d'onde THz est important pour des applications pratiques des techniques THz. Ces guides d'onde permettraient une meilleure intégration de plusieurs composants en un système THz unique: les sources, les détecteurs, les filtres etc.

L'application la plus évidente des guides d'onde THz est la livraison de l'onde de la source au détecteur. Les composants optiques encombrants pourraient être remplacés et le tout pourrait être incorporé dans un système compact de spectroscopie THz dans le domaine temporel. L'imagerie et la détection sont d'autres avenues prometteuses pour les guides d'onde THz. Il a déjà été démontré que les guides d'ondes THz peuvent opérer en régime sub-longueur d'onde, offrant ainsi un confinement du mode guidé plus petit que la limite de diffraction. Ainsi, la résolution spatiale de ces guides d'onde surpassent celle des systèmes THz conventionnels.

Pour un design efficace des guides d'onde THz, il est important de minimiser les pertes et la dispersion. Une solution potentielle serait d'augmenter la fraction de la puissance modale qui se propage dans l'air. Dans cette thèse, nous abordons l'utilisation de guides d'onde air/diélectrique, planaires et poreux, ainsi que de guides d'onde hybrides fils métalliques/diélectriques.

D'abord, nous présentons un nouveau design de guide d'onde planaire et poreux. Nous décrivons sa fabrication et nous le caractérisons pour une potentielle application comme guide d'onde et comme senseur dans le spectre THz. Le guide d'onde est formé de plusieurs minces films de polyéthylène (25 - 50 μm) séparés par des couches d'air d'épaisseurs comparables. Une grande portion du champ électrique est guidée dans l'air, permettant ainsi de réduire significativement les pertes par transmission. Également, nous constatons qu'un tel guide d'onde peut s'avérer utile pour des applications de détection biologique et chimique, en plaçant directement les échantillons dans la microstructure. Le guide d'onde planaire proposé possède l'avantage principal de permettre l'accès aisé au mode optique, puisque la majorité de la puissance THz introduite est confiné dans les couches d'air. De plus, le petit espacement entre les couches permet l'introduction rapide

d'analytes par effet capillaire (moins d'une seconde est nécessaire pour remplir un guide d'onde de 10 cm de long). La transmission et l'absorption du guide d'onde a été étudié expérimentalement, avec un système de spectroscopie THz dans le domaine temporel, et théoriquement, avec un logiciel de calcul par éléments finis. L'indice de réfraction modal du guide d'onde poreux est inférieur au guide d'onde plein. Il est possible par ailleurs d'ajuster cet indice en modifiant l'espacement entre les couches, ainsi que le nombre de couches dans le cœur. Également, les pertes de transmission dans le guide d'onde poreux sont considérablement inférieures aux pertes dans le guide d'onde plein.

Dans les chapitres subséquents, nous examinons une autre approche prometteuse pour le design de guides d'onde THz à faibles pertes et peu dispersifs. Le guide d'onde hybride métallique/diélectrique permet la propagation d'un mode plasmonique guidé dans le gap entre deux fils métalliques parallèles. Le tout est encapsulé dans une gaine micro-structurée diélectrique qui permet de donner une stabilité mécanique et d'isoler le guide d'onde de l'environnement. Nous décrivons plusieurs techniques prometteuses d'encapsulation du guide d'onde à deux fils, tout en minimisant l'impact négatif sur la propagation dû à l'ajout de la gaine diélectrique. En particulier, nous détaillons l'utilisation de mousses à faible densité et de plastiques micro-structurés.

Les guides d'ondes hybrides s'avèrent plus commodes pour les applications pratiques que les guides d'onde classiques à deux fils, puisqu'ils permettent la manipulation de la fibre sans risquer de perturber le mode guidé. Nous présentons une analyse détaillée des propriétés de propagation modale du guide d'onde hybride métallique/diélectrique et nous les comparons avec celles d'un guide d'onde à deux fils classique. Aussi, nous discutons des stratégies pour améliorer la performance des guides d'onde, notamment l'utilisation de gaines micro-structurées plus poreuses ou de matériaux intrinsèquement poreux. Nous étudions l'efficacité de couplage de l'onde vers le guide d'onde hybride et nous constatons qu'il peut être relativement élevé (>50%) aux fréquences aux alentours de ~ 0.5 THz.

Sans surprise, les performances de ces guides d'onde sont inférieures à celles des guides d'onde classiques à deux fils, en raison de la présence du diélectrique près du gap entre les deux fils. Parallèlement, l'ajout des fils métalliques permet de surpasser les guides d'onde poreux sans fils, en termes de largeur de bande passante et de dispersion. Nous démontrons que les guides d'onde hybrides métalliques/diélectrique poreux peuvent avoir des largeurs de bande passante très

grandes, car les modes sont confinés dans l'air aux hautes et basses fréquences. Aux hautes fréquences, ceci est dû au mécanisme de propagation ARROW, alors qu'aux basses fréquences, le mécanisme est plutôt de propagation plasmonique, dans le gap entre les deux fils.

Finalement, nous décrivons une propriété de résonance intéressante de certains modes plasmoniques hybrides métalliques/diélectriques. Cette résonance se manifeste lors du passage du confinement dans le diélectrique au confinement dans l'air. Nous discutons de la possibilité d'utiliser cette propriété pour construire des réfractomètres THz. L'introduction d'analytes à très faibles pertes permet tout de même des changements significatifs dans les pertes modales. Ces pertes sont utilisées comme mécanisme de transduction. La résolution du réfractomètre a été étudiée numériquement en fonction de la fréquence d'opération et des paramètres géométriques de la fibre. Avec une résolution de l'indice de réfraction de l'ordre de $\sim 10^{-3}$, le senseur permet l'identification de plusieurs aérosols et analytes gazeux, ainsi que de mesurer la concentration de particules de poussières dans l'air.

ABSTRACT

The terahertz frequency range, with frequencies lying between 100 GHz and 10 THz, has strong potential for various technological and scientific applications such as sensing, imaging, communications, and spectroscopy. Most terahertz (THz) sources are immobile and THz systems use free-space propagation in dry air where losses are minimal. Designing efficient THz waveguides for flexible delivery of broadband THz radiation is an important step towards practical applications of terahertz techniques. THz waveguides can be very useful on the system integration level when used for connection of the diverse THz point devices, such as sources, filters, sensor cells, detectors, etc.

The most straightforward application of waveguides is to deliver electromagnetic waves from the source to the point of detection. Cumbersome free-space optics can be replaced by waveguides operating in the THz range, which could lead to the development of compact THz time domain spectroscopy systems. Other promising applications of THz waveguides are in sensing and imaging. THz waveguides have also been shown to operate in subwavelength regimes, offering mode confinement in waveguide structures with a size smaller than the diffraction limit, and thus, surpassing the resolution of free-space THz imaging systems.

In order to design efficient terahertz waveguides, the frequency dependent loss and dispersion of the waveguide must be minimized. A possible solution would be to increase the fraction of mode power propagating through air. In this thesis, the usage of planar porous air/dielectric waveguides and metal wire/dielectric hybrid terahertz fibers will be discussed.

First, I present a novel design of a planar porous low-loss waveguide, describe its fabrication, and characterize it in view of its potential applications as a low-loss waveguide and sensor in the THz spectral range. The waveguide structure features a periodic sequence of layers of thin (25-50 μm) polyethylene film that are separated by low-loss air layers of comparable thickness. A large fraction of the modal fields in these waveguides is guided in the low-loss air region, thus effectively reducing the waveguide transmission losses. I consider that such waveguides can be useful not only for low-loss THz wave delivery, but also for sensing of biological and chemical specimens in the terahertz region, by placing the recognition elements directly into the waveguide microstructure. The main advantage of the proposed planar porous waveguide is the convenient access to its optical mode, since the major portion of THz power

launched into such a waveguide is confined within the air layers. Moreover, small spacing between the layers promotes rapid loading of the analyte into the waveguide due to strong capillary effect (< 1 s filling of a 10 cm long waveguide with an analyte). The transmission and absorption properties of such waveguides have been investigated both experimentally using THz-TDS spectroscopy and theoretically using finite element software. The modal refractive index of porous waveguides is smaller compared to pure polymer and it is easy to adjust by changing the air spacing between the layers, as well as the number of layers in the core. The porous waveguide exhibits considerably smaller transmission losses than bulk material.

In the following chapters I review another promising approach towards designing of low-loss, low-dispersion THz waveguides. The hybrid metal/dielectric waveguides use a plasmonic mode guided in the gap between two parallel wires that are, in turn, encapsulated inside a low-loss, low-refractive index, micro-structured cladding that provides mechanical stability and isolation from the environment. I describe several promising techniques that can be used to encapsulate the two-wire waveguides, while minimizing the negative impact of dielectric cladding on the waveguide optical properties. In particular, I detail the use of low-density foams and microstructured plastic claddings as two enabling materials for the two-wire waveguide encapsulation.

The hybrid fiber design is more convenient for practical applications than a classic two metal wire THz waveguide as it allows direct manipulations of the fiber without the risk of perturbing its core-guided mode. I present a detailed analysis of the modal properties of the hybrid metal/dielectric waveguides, compare them with the properties of a classic two-wire waveguide, and then present strategies for the improvement of hybrid waveguide performance by using higher cladding porosity or utilizing inherently porous cladding material. I study coupling efficiency into hybrid waveguides and conclude that it can be relatively high ($>50\%$) in the broad frequency range ~ 0.5 THz.

Not surprisingly, optical properties of such fibers are inferior to those of a classic two-wire waveguide due to the presence of lossy dielectric near an inter-wire gap. At the same time, composite fibers outperform porous fibers of the same geometry both in bandwidth of operation and in lower dispersion. I demonstrate that hybrid metal/dielectric porous waveguides can have a very large operational bandwidth, while supporting tightly confined, air-bound modes both at high

and low frequencies. This is possible as, at higher frequencies, hybrid fibers can support ARROW-like low-loss air-bound modes, while changing their guidance mechanism to plasmonic confinement in the inter-wire air gap at lower frequencies.

Finally, I describe an intriguing resonant property of some hybrid plasmonic modes of metal / dielectric waveguides that manifests itself in the strong frequency dependent change in the modal confinement from dielectric-bound to air-bound. I discuss how this property can be used to construct THz refractometers. Introduction of even lossless analytes into the fiber core leads to significant changes in the modal losses, which is used as a transduction mechanism. The resolution of the refractometer has been investigated numerically as a function of the operation frequency and the geometric parameters of the fiber. With a refractive index resolution on the order of $\sim 10^{-3}$ RIU, the composite fiber-based sensor is capable of identifying various gaseous analytes and aerosols or measuring the concentration of dust particles in the air.

TABLE OF CONTENTS

ACKNOWLEDGEMENTS	III
RÉSUMÉ.....	IV
ABSTRACT	VII
TABLE OF CONTENTS	X
LIST OF FIGURES.....	XIV
LIST OF SYMBOLS AND ABBREVIATIONS.....	XXII
LIST OF APPENDICES	XXIII
INTRODUCTION.....	1
Structure of the thesis	3
CHAPTER 1 LITERATURE REVIEW	5
1.1 Terahertz waveguides.....	5
1.1.1 Dielectric multilayered waveguides	6
1.1.2 Single wire waveguides	7
1.1.3 Two-wire waveguides.....	9
1.1.4 Composite metal-dielectric air-core fibers	11
1.1.5 Terahertz waveguides examples	14
1.2 Terahertz waveguides simulation.....	16
1.3 Applications of foams in terahertz photonics.....	18
1.4 Terahertz refractometers	19
1.5 Novelty of the proposed waveguides	20
CHAPTER 2 METHODOLOGY.....	23
2.1 Numerical modelling.....	23

2.2	Experimental setup.....	25
2.3	Fiber fabrication	28
CHAPTER 3 ARTICLE 1: PLANAR POROUS THZ WAVEGUIDES FOR LOW-LOSS GUIDANCE AND SENSING APPLICATIONS		29
3.1	Introduction	29
3.2	Waveguide design	30
3.3	Fundamental mode of the waveguide.....	32
3.4	Details of the numerical modelling of the modal fields	33
3.5	Measurement setup.....	34
3.6	Polyethylene refractive index and absorption losses.....	35
3.7	Waveguide transmission and dispersion measurements	37
3.8	Fitting experimental transmission data with a theoretical model.....	40
3.9	Conclusion.....	43
CHAPTER 4 ARTICLE 2: TWO-WIRE TERAHERTZ FIBERS WITH POROUS DIELECTRIC SUPPORT		44
4.1	Introduction	44
4.2	Classic two-wire waveguide.....	48
4.3	Composite fiber featuring two metal wires in a three-hole porous cladding	51
4.4	The influence of porosity on the fiber optical properties	59
4.5	Composite fiber featuring two metal wires in a seven-hole porous cladding	62
4.6	Conclusion.....	65
CHAPTER 5 ARTICLE 3: HYBRID METAL WIRE-DIELECTRIC TERAHERTZ WAVEGUIDES: CHALLENGES AND OPPORTUNITIES [INVITED]		68
5.1	Introduction	69
5.2	Metallic wire-based THz waveguides operating using plasmonic modes	71

5.3 Two-wire THz fibers with dielectric foam cladding	76
Bulk polystyrene foam	79
Two-wire waveguide with a polystyrene foam cladding.....	81
5.4 Two-wire THz fibers with microstructured dielectric cladding.....	84
Two-wire waveguides encapsulated into porous microstructured claddings featuring subwavelength holes	85
Sensing applications with hybrid two-wire waveguides	89
Experimental characterization of hybrid fibers	92
Fibers with embedded Indium wires	95
Scaling of the hybrid fiber dimensions.....	98
5.5 Conclusion.....	100
CHAPTER 6 ARTICLE 4: HYBRID PLASMONIC TERAHERTZ FIBERS FOR SENSING APPLICATIONS	103
6.1 Introduction	103
6.2 Wave guiding in composite fibers with two metal wires in dielectric cladding	104
6.3 Results and discussion.....	106
6.4 Conclusion.....	106
CHAPTER 7 GENERAL DISCUSSION	111
Additional experimental results	111
Waveguides performance limitations.....	114
Fiber cross section	114
Coupling efficiency	115
Characterization of terahertz waveguides	117
3D printing of terahertz waveguides/preforms.....	118
Foam-based two-wire waveguides	120

Future research in the area.....	121
CHAPTER 8 CONCLUSIONS.....	122
REFERENCES.....	124
APPENDIX:	140

LIST OF FIGURES

Figure 1.1 a) Time-domain electric field waveforms detected with the receiver 3mm above and 3mm below the waveguide. b) Spatial profile of the electric field obtained by moving the THz receiver in a plane perpendicular to the waveguide axis. c) The simulated spatial profile of the electric field propagating along the wire. d) THz waveforms measured after 4 cm (black) and 24 cm (red) of propagation distance along the wire. e) Group velocity of the propagating mode as a function of frequency. f) The electric field amplitude attenuation coefficient of the propagating mode as a function of frequency. g) Experimental setup for the excitation of THz surface wave on a metal wire using scattering configuration [52].....	8
Figure 1.2 a) THz pulse transmitted through a 9.5 cm length of commercially available TV twin-lead antenna cable, with THz emitter and receiver at 90° to one another (solid curve); for comparison in dotted curve free-space THz transmission along a direct line-of-sight between the transmitter and receiver separated by the same 9.5 cm spacing, with no waveguide or optics in between. b) Amplitude spectra for the two THz waveforms. Adapted from [30]...	10
Figure 1.3 a) Cross section of a hollow core Zeonex fiber featuring two indium wires. Core diameter is ~2 mm. The indium wires are located at the left- and right-hand side of the hollow core and are seen silver; b) Field distribution (theory) in the HE ₁₁ -like mode at 1.2 THz. Adapted from [61].....	12
Figure 1.4 a) Loss coefficients as measured (grey) and as simulated (red line) for a two-wire fiber. b) Normalized transmission spectrum of 8 cm two-wire fiber with different wire plane orientation with respect to the electric field polarization as indicated. The indium wires are depicted as grey ellipses while the air region is the filled white space. c) Phase refractive indices as measured (grey) and as simulated (red line) for a two-wire fiber. d) The group velocity dispersion parameter determined from the measured data (grey) and as calculated from the simulation (red line) for a two-wire and fiber. Adapted from [61].	13
Figure 2.1. Experimental setup with the fiber mounted in the apertures.	26
Figure 3.1 (a) Photograph of the planar porous multilayer waveguide fabricated from polyethylene and its metal holder, (b) Microscope image of the waveguide cross-section (in the place where	

the PE layers are separated by the spacers), the thickness of the polyethylene layers is 50 μm , while the thickness of spacers is 75 μm	31
Figure 3.2 Transverse electric field distribution of the fundamental mode of the porous waveguide.....	33
Figure 3.3 Experimental THz-TDS setup with the waveguide fixed between two cylindrical Teflon lenses.	35
Figure 3.4 Absorption losses of the bulk polyethylene. Red line – quadratic fitting curve.	36
Figure 3.5 Experimentally measured electric field (a) in time domain and (b) in frequency domain at the output of the waveguide for different number of layers in the waveguide core. Black line corresponds to the absence of the waveguide.	37
Figure 3.6 Dispersion of the fundamental mode of a porous waveguide; comparison between exact simulation and analytical approximation. Black line – analytically calculated dispersion (see Equation 3.8, red line – dispersion computed using finite element method. Layer width 50 μm , spacer width 75 μm , overall waveguide size 0.55 mm, 5 PE layers.	39
Figure 3.7 Transverse electric field distributions of the lower order modes of the waveguide. The modes in the second and third columns are defined as the side modes of the fundamental (top left) and higher order modes (other modes of the first column) in the text of the chapter. ...	41
Figure 3.8 Black line – normalized experimental transmittance, red line – theoretical normalized transmittance (a) 4 layers waveguide, 11 cm length, (b) 8 layers waveguide, 11 cm length	42
Figure 4.1 a) Schematic of a classic two-wire waveguide. b) Longitudinal flux distribution for the TEM mode of a two-wire waveguide. Arrows show vectorial distribution of the corresponding transverse electric field.....	46
Figure 4.2 a) Effective refractive index, b) absorption losses and c) group velocity dispersion of the fundamental mode of a two metal wire waveguide shown in Figure 4.1.....	46
Figure 4.3 Excitation efficiency of the fundamental mode of a classic two-wire waveguide using Gaussian beam with a frequency-dependent beam diameter . as an excitation source. Dependence of the excitation efficiency on various geometrical parameters, such as: a)	

displacement along the x axis from the core center; b) displacement along the y axis from the core center; c) inter-wire gap size; d) wire radius	50
Figure 4.4 a) Schematic of a composite fiber featuring two metal wires in a three-hole cladding. b) Longitudinal flux distribution of a typical guided mode presents a mixture of the plasmonic mode guided by the metal wires and a TIR mode guided by the porous fiber cladding.	51
Figure 4.5 . Black color: the effective refractive indices, absorption losses and excitation efficiencies for the various modes of a composite two-wire fiber shown in Figure 4.4. Red color: various optical properties of the modes of a corresponding porous cladding (no metal wires).	52
Figure 4.6 a) Effective refractive indices, b) excitation efficiencies, c) absorption losses and d) group velocity dispersion for the various modes of a composite two-wire fiber shown in Figure 4.4. Dips in the excitation efficiency versus frequency graph correspond to the frequencies of anticrossing between the plasmonic modes and the fiber cladding modes. ...	53
Figure 4.7 Longitudinal flux distribution of the fundamental plasmonic mode of a composite fiber at various operation frequencies. The flux is normalized at its maximal value at each frequency.	54
Figure 4.8 Longitudinal flux distribution of the lowest order cladding mode of a composite fiber at various frequencies. The flux is normalized at its maximal value at each frequency.	55
Figure 4.9 Longitudinal flux distribution of the fundamental mode of a porous fiber (same cross section as in Figure 4.4, however, without metal wires). The flux is normalized at its maximal value at each frequency.	56
Figure 4.10 Longitudinal flux distribution of the second plasmonic mode of a composite fiber. The flux is normalized at its maximal value at each frequency.	57
Figure 4.11 a) Schematic of a seven-hole fiber with overlapping holes. b) Absorption losses, c) excitation efficiencies, and d) effective refractive index of the various modes of the seven-hole fiber with overlapping holes.	60
Figure 4.12 Longitudinal flux distribution for the modes of a composite seven-hole fiber with overlapping holes and $r = 110 \mu m$. a) Fundamental plasmonic mode, b) lowest order cladding	

mode, c) second plasmonic mode. The flux is normalized at its maximal value at each frequency.....	61
Figure 4.13 a) Schematic of a seven-hole fiber with two metal wires. b) Longitudinal flux distribution for a typical guided mode of a composite fiber presents a mixture of the plasmonic mode guided by the metal wires and a TIR mode guided by the fiber cladding.....	62
Figure 4.14 a) Effective refractive indices, b) excitation efficiencies, c) absorption losses and d) group velocity dispersion for the various modes of a seven-hole composite fiber shown in Figure 4.14. Solid lines define frequency ranges where the modal excitation efficiency is higher than 10%.	63
Figure 4.15. Longitudinal flux distribution for the modes of a seven-hole composite fiber a) fundamental plasmonic mode, b) lowest order cladding mode, c) second plasmonic mode. The flux is normalized at its maximal value at each frequency.	64
Figure 5.1. a) Time-domain electric field waveforms detected with the receiver 3mm above and 3mm below the waveguide. b) Spatial profile of the electric field obtained by moving the THz receiver in a plane perpendicular to the waveguide axis. c) The simulated spatial profile of the electric field propagating along the wire. d) THz waveforms measured after 4 cm (black) and 24 cm (red) of propagation distance along the wire. e) Group velocity of the propagating mode as a function of frequency. f) The electric field amplitude attenuation coefficient of the propagating mode as a function of frequency. Adapted by permission from Macmillan Publishers Ltd © 2004.....	71
Figure 5.2. a) Schematic of a two-wire waveguide. b) Longitudinal flux distribution for the TEM mode of a two-wire waveguide. Arrows show vectorial distribution of the modal transverse electric field.....	72
Figure 5.3. a) Effective refractive index, b) absorption losses, and c) group velocity dispersion of the fundamental mode of a two metal wire waveguide shown in Figure 5.2.....	73
Figure 5.4. Excitation efficiency of the fundamental mode of a two-wire waveguide using diffraction limited Gaussian beam as an excitation source. Dependence of the excitation efficiency on various geometrical parameters, such as: a) displacement along the x axis from	

the core center, b) displacement along the y axis from the core center, c) inter-wire gap size, and d) wire radius.	74
Figure 5.5. a) A two-wire THz waveguide made in our research group. b) THz waveform at the input of the waveguide. c) THz pulse transmitted through a 10 cm-long waveguide.....	75
Figure 5.6. a) THz pulse transmitted through a 9.5 cm length of commercially available TV twin-lead antenna cable, with THz emitter and receiver at 90° to one another (solid curve); for comparison in dotted curve free-space THz transmission along a direct line-of-sight between the transmitter and receiver separated by the same 9.5 cm spacing, with no waveguide or optics in between. b) Amplitude spectra for the two THz waveforms.....	76
Figure 5.7 a) Time-domain electric field. b) Transmission spectra c) Unwrapped phase relative to the reference. Each color represents a particular length of polystyrene foam.	79
Figure 5.8 a) Effective refractive index. The mean is indicated by the dashed line. b) Extinction losses and fit with a forth order polynomial and Lorentzian function	81
Figure 5.9 Photograph of the two-wire ABS 3D-printed holder a) with and b) without polystyrene foam. c) Magnification of the metal coupler used also as an aperture. d) Holder with two wires between two apertures inside the THz-TDS system.	82
Figure 5.10 Time domain electric field of a) the two-wire waveguide embedded in polystyrene foam, b) the two wires only, and c) the ABS holder only. d) Transmission spectra of the corresponding electric field.	83
Figure 5.11. Cross sections of several hybrid fibers fabricated in our group. Microstructured claddings of these fibers feature: a) three-interconnected holes, b) four-interconnected holes, c) web of thin bridges that is used to support metallic wires, and d) three rings of holes positioned on a hexagonal lattice.	84
Figure 5.12. a) Schematic of a composite three-hole fiber. b) Longitudinal flux distribution for the fundamental plasmonic mode at 0.2 THz of a composite three-hole fiber. c) Effective refractive indices, d) excitation efficiencies, e) absorption losses, and f) group velocity dispersion for the various modes of a composite three-hole fiber. We use dotted curves at frequencies for which modal excitation efficiency drops below 5%. As an excitation source we use linearly polarized, diffraction limited Gaussian beam.	86

Figure 5.13. a) Schematics of a composite three-hole fiber. b) Longitudinal flux distribution for a typical guided mode of a composite seven-hole porous fiber. c) Effective refractive indices, d) excitation efficiencies, e) absorption losses, and f) group velocity dispersion for the various modes of a composite seven-hole fiber. We use dotted curves at frequencies for which modal excitation efficiency drops below 5%. As a source we assume linearly polarized, diffraction limited Gaussian beam.88

Figure 5.14. Longitudinal flux distribution for the second plasmonic mode at a) 0.60THz, b) 0.80 THz. Arrows show vectorial distribution of the corresponding transverse electric field. Changes in the optical properties of the plasmonic mode as a function of the analyte refractive index. c) Modal effective refractive index, d) absorption losses.89

Figure 5.15. a) Absorption losses of the plasmonic mode, and corresponding b) sensitivity of the refractometer as a function the refractive index of the analyte at various values of the operation frequency.91

Figure 5.16. Resolution of the hybrid fiber-based refractometer as a function of a) fiber diameter, b) wire diameter, and c) gap between the wires.91

Figure.5.17 a) Cross section of a hybrid 20cm-long three-hole fiber. b) Experimentally measured transmission spectra, blue curve – wires oriented along the polarization of the input THz field, red curve – wires are perpendicular to the polarization of the input THz field, green curve – wires are removed, thus leaving behind a porous dielectric cladding, purple curve – the fiber is removed from the holders.92

Figure 5.18 a) Cross section of a hybrid 10cm-long fiber with thin bridges supporting metallic wires and b) experimentally measured transmission spectra. c) Cross section of a hybrid 10cm-long fiber with thin bridges supporting larger metallic wires and d) experimentally measured transmission spectra. e) Cross section of a hybrid 5cm-long fiber with hexagonal lattice of air holes with two metallic wires and f) experimentally measured transmission spectra. For all the transmission spectra: blue curves – wires oriented along the polarization of the input THz field, red curves – wires are perpendicular to the polarization of the input THz field, green curves – wires are removed, thus leaving behind a porous dielectric cladding.94

Figure.5.19 a) Cross section of a hollow core Zeonex fiber featuring two indium wires. Core diameter is ~2 mm. The indium wires are located at the left- and right-hand side of the hollow

core and are seen silver; b) Field distribution (theory) in the HE_{11} -like mode at 1.2 THz. Adapted from [61].95

Figure 5.20 a) Loss coefficients as measured (grey) and as simulated (red line) for a two-wire fiber. b) Normalized transmission spectrum of 8 cm two-wire fiber with different wire plane orientation with respect to the electric field polarization as indicated. The indium wires are depicted as grey ellipses while the air region is the filled white space. c) Phase refractive indices as measured (grey) and as simulated (red line) for a two-wire fiber. d) The group velocity dispersion parameter determined from the measured data (grey) and as calculated from the simulation (red line) for a two-wire and fiber. Adapted from [61].97

Figure 5.21 a) Core-bound HE_{11} -like modes similar to those reported in [61]. b) Plasmonic-like modes similar to those described in chapter 4.3 and paper [123]. The number below each graph indicates the size of the air gap between the two wires. Adapted from [126].99

Figure 6.1 a) Schematic of the composite three-hole fiber. b) Longitudinal flux distribution for the plasmonic mode in a composite fiber at 0.71 THz. Arrows show vectorial distribution of the corresponding transverse electric field.104

Figure 6.2 Longitudinal flux distribution for the plasmonic mode of a composite fiber at various frequencies.105

Figure 6.3 Changes in the optical properties of a plasmonic mode as a function of the analyte refractive index. a) Modal effective refractive index, b) absorption losses.107

Figure 6.4 a) Absorption losses of the plasmonic mode, and corresponding b) Sensitivity of the refractometer as a function the refractive index of the analyte at various values of the operation frequency.108

Figure 6.5 Resolution of the refractometer as a function of a) fiber diameter, b) wire diameter, c) gap between the wires.110

Figure 7.1 a) Cross section of a hybrid 20cm-long three-hole fiber. b) Experimentally measured transmission spectra; c) Cross section of a hybrid 10cm-long fiber with thin bridges supporting metallic wires and d) experimentally measured transmission spectra. e) Cross section of a hybrid 10cm-long fiber with thin bridges supporting larger metallic wires and f) experimentally measured transmission spectra. g) Cross section of a hybrid 5cm-long fiber

with hexagonal lattice of air holes with two metallic wires and h) experimentally measured transmission spectra. For all the transmission spectra: blue curves – wires oriented along the polarization of the input THz field, red curves – wires are perpendicular to the polarization of the input THz field, green curves – wires are removed, thus leaving behind a porous dielectric cladding. 112

Figure 7.2. a) Cross section of a hybrid porous fiber with metal wires and b) experimentally measured transmission spectra; c) Cross section of a hybrid 10cm-long fiber with thin bridges supporting metallic wires and d) experimentally measured transmission spectra. e) Cross section of 3 hole fiber with two metallic wires and f) experimentally measured transmission spectra..... 113

Figure 7.3 Two cross sections of the same highly porous hybrid fiber. 115

Figure 7.4. Terahertz field amplitude as a function of frequency for different sizes of the aperture..... 117

Figure 7.5. Cross section of a 3D printed hollow core fiber and a porous 3D printed preform... 120

LIST OF SYMBOLS AND ABBREVIATIONS

FEM – finite element method

GaAs – Gallium arsenide

GVD – group velocity dispersion

HCFC 142b – 1-Chloro-1,1-difluoroethane

LDPE – low density polyethylene

PE – polyethylene

RIU – refractive index unit

TEM – transverse electromagnetic mode

THz – terahertz

THz-TDS – terahertz time-domain spectroscopy

LIST OF APPENDICES

SCIENTIFIC OUTCOMES OF MY DOCTORAL RESEARCH	139
---	-----

INTRODUCTION

The terahertz range, with frequencies between 0.1 and 10 THz, is located between infrared and microwave frequencies. Historically, the THz region has been one of the least explored due to the lack of efficient THz sources and detectors. In the early 1980's, generation and detection of terahertz pulses was demonstrated [1-3] with the use of photoconductive switches (Auston switches). The THz pulses were propagating on coplanar and microstrip transmission lines. These pioneer THz waveguides suffered from a severe pulse degradation even at distances on the order of millimeters. Strong dispersion and losses in the aforementioned waveguides were caused by material dispersion in the dielectric substrate and frequency dependent radiation of leaky waves into the substrate. The first works on terahertz time-domain spectroscopy (THz-TDS) began to emerge in the late 1980's [4-6], with water vapor being the first sample that was thoroughly investigated in the THz range. In order to overcome pulse degradation in media these THz-TDS systems utilized free space propagation where THz beams were navigated, steered and focused using optical hardware, such as mirrors and lenses.

The development of the terahertz range is highly promising for application in high-bit rate communication, chemical and biological sensing, imaging, spectroscopy, security, and others. Terahertz radiation penetrates through a large number of non-conductive materials. At the same time, many molecules have excitation lines at terahertz frequency promoting the usage of terahertz spectroscopy.

THz waves penetrate through the skin surface, nevertheless not damaging the body cells, thus having the potential for non-invasive medical imaging. Being extremely sensitive to the water content of media, terahertz waves offer a modality to measure the water content and density of epithelial tissue, thereby assisting in the detection of skin cancer [7, 8]. Terahertz radiation could potentially offer a safe, non-ionizing alternative to X-rays in dentistry to measure enamel demineralization [9]. In addition, security has the potential to become a major application for THz-TDS. THz waves can penetrate through fabrics and show promise in remote screening for concealed weapons [10]. Explosives and drugs have characteristic terahertz absorptions lines, thus offering the possibility to use imaging and spectral identification simultaneously. THz-TDS has multiple practical applications in gas-phase detection. A THz spectrometer can provide real-time information on the chemical composition of a gas mixture [11] for industrial process control or

trace-gas sensing. Another potential application of THz-TDS is in determining the electron effective mass and scattering times in films [12], and observing transient photoconductivity and the recombination dynamics of quasifree electrons in liquids [13]. Atmospheric pollutant gases, such as sulfur dioxide and hydrogen sulfide, can be efficiently probed with THz spectroscopy [14]. Moreover, investigation of the combustion process can also be carried out using THz-TDS. The simultaneous and direct measurement of heavily contaminated combustion gas, without the need for prefiltration, has been reported in [15]. In [16], terahertz imaging has been proposed as a novel tool to measure the thickness and quality of multiple layers of paint on both metals and non-metal surfaces. The same techniques can be applied in the cultural heritage conservation sector to detect hidden paint layers under coats of plaster or paint in murals [17-19]. With paper, cardboard, and plastics being transparent to terahertz radiation, it has been applied for non-invasive mail inspection [20] and inspection of packaged goods [21]. Furthermore, terahertz systems have set one record after another in wireless data transmission rates, currently achieving 100 gigabits-per-second [22].

The usage of terahertz waveguides may be beneficial for many of the above mentioned applications. Terahertz waveguides would allow us to replace large and cumbersome optical hardware, navigate THz pulses in areas that are otherwise difficult to access, and offer tight or even subwavelength confinement of THz radiation, providing stronger interaction with analyzed samples. Multiple papers have been published in a search for THz waveguides that minimize pulse degradation due to loss and dispersion.

Occupying a position between microwaves and visible light in the electromagnetic spectrum, the terahertz field often borrows the ideas and methods already implemented for the more developed ranges of the spectrum. In this thesis, I will describe two types of terahertz waveguides. To begin, I present a novel design of a planar multilayer terahertz waveguide. The idea of using a multilayer dielectric waveguide came from the visible range, where the radiation modes of such waveguides have been thoroughly investigated [23-26]. The waveguide structure I will discuss features a periodic sequence of layers of thin polyethylene film that are separated by low-loss air layers of comparable thickness. A large fraction of the modal fields in these waveguides is guided in the low-loss air region, thus effectively reducing the waveguide transmission losses.

The idea of using metal wires as terahertz waveguides came from microwaves, where the solution for radiation propagating along a metal wire has been known for decades [27-29]. The classical two metal wire waveguides have been proposed and studied for terahertz propagation confirming their outstanding optical properties [30]. The inconvenience of two wire waveguides in practical applications due to the necessity of cumbersome holders to keep the wires straight and parallel to each other led us in search of cladding for metal wires enabling retention of the optical properties of metal wire waveguides, providing the convenience of operation typical for optical fibers. Our group has performed a study of two different techniques for the encapsulation of metal wires. The first technique involves various porous microstructured cladding, while the alternative approach deals with the usage of low-density foam. The idea of using porous fibers in its turn has come to the THz field from the visible or near-infrared range, where such fibers have been systematically researched.

Structure of the thesis

This thesis is organized as follows:

Chapter 1 provides a literature review of terahertz waveguides and sensors, description of their fabrication techniques, and characterization of their optical properties. Chapter 1.2 provides a literature review of planar terahertz waveguide. In Chapter 1.3, I review recent studies of the terahertz waveguides base on metal wires. In Chapter 1.4, I describe state of the art terahertz sensors for chemical or biological detection.

Chapter 2 provides the methodology of my studies. All the steps of the research work are introduced. The details of the waveguide fabrication and characterization are revealed, as well as the information on the theoretical simulations techniques.

Chapter 3 is based on my paper “Planar porous THz waveguides for low-loss guidance and sensing applications,” published in IEEE Transactions on THz Science and Technology in 2013. This paper is devoted to the experimental and theoretical work concerning THz planar waveguides and includes detailed description of the fabrication and characterization techniques.

Chapter 4 is based on my paper “Two-wire Terahertz fibers with porous dielectric support,” published in Optics Express in 2013. In this chapter I present the results of the theoretical

development of the terahertz waveguide consisted of two metal wires supporting a plasmonic mode and porous dielectric cladding used as a mechanical support.

Chapter 5 is based on my paper “Review: Hybrid metal-dielectric terahertz waveguides: challenges and opportunities,” published in Journal of the Optical Society of America B in 2014. The content of this paper partly coincides with the material of Chapters 4 and 6, however the novel findings are included in this chapter, mainly concerning the experimental investigation of the proposed two-wire waveguides and hybrid metal/dielectric fibers.

Chapter 6 is devoted to further investigation of the two-wire waveguides for their possible application as highly sensible terahertz refractometers and is based on my paper “Hybrid plasmonic terahertz fibers for sensing applications,” published in Applied Physics Letters in 2013.

Finally, general discussion of the achieved results and future research perspectives are presented.

CHAPTER 1 LITERATURE REVIEW

1.1 Terahertz waveguides

Terahertz radiation penetrates through a large number of non-conductive materials. At the same time, many molecules have excitation lines at terahertz frequency promoting. The terahertz frequency range has strong potential for various technological and scientific applications, such as chemical and biological sensing, spectroscopy. Novel implementations of the terahertz range are found in security sector, medicine, environmental sciences, and even in archaeology. Terahertz waveguides are highly promising for the applications in high bit-rate communications, subwavelength imaging and high resolution sensing. .However, most terahertz (THz) sources are immobile and THz systems predominantly utilize free-space propagation, where losses can be minimized. Designing efficient THz waveguides for flexible delivery of the broadband THz radiation is an important step towards practical applications of terahertz techniques. Moreover, THz waveguides can be very useful on the system integration level when used for connection of the diverse THz point devices, such as sources, filters, sensor cells, detectors, etc. Availability of the THz fibers is also crucial for various niche applications such as endoscopy and crevice inspection. In order to design efficient terahertz waveguides, the goal is to minimize the frequency dependent loss and dispersion of the waveguide.

The main complexity with designing terahertz waveguides is the fact that for propagation distances of ~1m almost all materials are highly absorbent in the terahertz spectral range [31]. A traditional way of guiding light would be to use solid-core fibers, such as step index core/clad fibers, or solid-core microstructured fibers. In these fibers, however, the fraction of light guided in the solid core is significant, and, therefore, fiber transmission loss is typically close to the absorption loss of the core material. For completeness, in the 0.1-1 THz spectral range, amorphous materials suitable for fiber drawing (such as glasses and polymers) have losses that are typically higher than $0.1\text{-}0.3\text{ cm}^{-1}$. Moreover, group velocity dispersion of many standard waveguides is high enough to result in significant THz pulse broadening over even modest propagation distances of ~10 cm. On the other hand, metals that function well in microwave range have high Ohmic losses at the THz frequencies.

In fact, the lowest loss materials in THz spectral range are dry gases. Therefore, one of the ways to reduce waveguide absorption loss is to maximize the fraction of light guided in the gas phase. Different types of THz waveguides and fibers have been proposed based on this concept. The simplest of such waveguide is a subwavelength fiber [32-34] that features dielectric core that is much smaller than the wavelength of guided light. As a result, a high fraction of modal power is guided outside of the lossy material and in the low-loss gaseous cladding. Another type of the low-loss fibers includes fibers featuring porous core region with the size of the individual pores much smaller than the wavelength of light [32, 33]. Consequently, guided light has a strong presence in the low-loss gas-filled pores inside the core. Higher modal confinement in the core makes such fibers less prone to bending losses and less sensitive to the environment compared to the simple rod-in-the-air subwavelength fibers [32, 35]. Using this strategy, very low transmission losses in the range of 0.01 cm^{-1} were demonstrated using the abovementioned fibers. Subwavelength and porous fibers, however, can have significant group velocity dispersions as these fibers usually operate in the frequency range where modal confinement changes rapidly from weak at lower frequencies (high modal presence in the cladding) to strong at higher frequencies (high modal presence in the core).

Another important type of the low-loss THz waveguides includes fibers featuring gas-filled hollow core surrounded with a structured cladding serving as a reflector. The main challenge in the design of such fibers is to ensure high reflection at the core-cladding interface. Different hollow-core structures have been investigated including metalized bores [35-37], periodic dielectric multilayers [38], as well as thin-walled dielectric pipes [39-42]. These fibers, however, have a tendency of having a large core size that can easily be 10 times larger than the wavelength of guided light. This is necessary in order to reduce modal absorption losses in the reflector structure. Therefore, such fibers operate mostly in the multimode or in the few-mode regime. Moreover, hollow core waveguides that use photonic crystal cladding usually tend to have large outer diameters (over 1 cm) as they need to contain enough layers for efficient modal confinement.

1.1.1 Dielectric multilayered waveguides

Air-filled parallel plate waveguides [43] and slit waveguides [44] are known for their low losses and strong confinement. An obvious disadvantage of such waveguides is a somewhat

inconvenient form factor. So far in terahertz dielectric multilayered waveguides have been mainly used as substrates for photomixers [45] and surfaces for thin dielectric ridge waveguides [46].

In the edge-coupled photomixer source [45], the two interfering laser beams are guided along the multilayer waveguide, the top layer of which is made of an ultrafast photoabsorbing material and covered by dc-biased electrodes. The laser power is being absorbed in the top layer and converted into the THz signal.

Multilayered periodic structures (two-dimensional photonic bandgap structures) enable surface waves guiding in terahertz range [46]. Periodicity of the underlying structure leads to the appearance of the forbidden band. And with a proper choice of material constituting the multilayered waveguide and the terminating top layer it is possible to achieve deeply subwavelength surface terahertz guiding.

The idea of using a multilayer dielectric structures for wave guiding came from the visible range, where the radiation modes of such waveguides have been thoroughly investigated [23-26]. Planar multilayered materials have been recently studied in a context of birefringent anisotropic materials for THz devices [47, 48].

1.1.2 Single wire waveguides

THz guidance with metal wires was first demonstrated by Mittleman et al. in [49]. In principle, a single metal wire can be used to transport terahertz pulses with virtually no dispersion and low attenuation (see Figure 1.1). In practice, however, it is difficult to realize efficient excitation of the guided mode of a single wire waveguide. This is because the fundamental mode of a single wire is radially polarized (angular momentum $m=0$), while commonly used photoconductive antennas tend to produce linearly polarized THz light ($m=1$). Because of this symmetry mismatch, direct excitation of the guided mode on a single wire is problematic. Furthermore, high bending losses of a single wire waveguide limit its practical applications. Even a slight bending of the wire can lead to considerable increase in the modal transmission loss, e.g. from 0.03 cm^{-1} for a straight wire to 0.05 cm^{-1} for a slightly bent one (bending radius of 90 cm, [50]).

To overcome difficulties with modal excitation, Deibel et al. [51] used a radially symmetric photoconductive antenna instead of a linear dipole antenna, and demonstrated coupling efficiencies

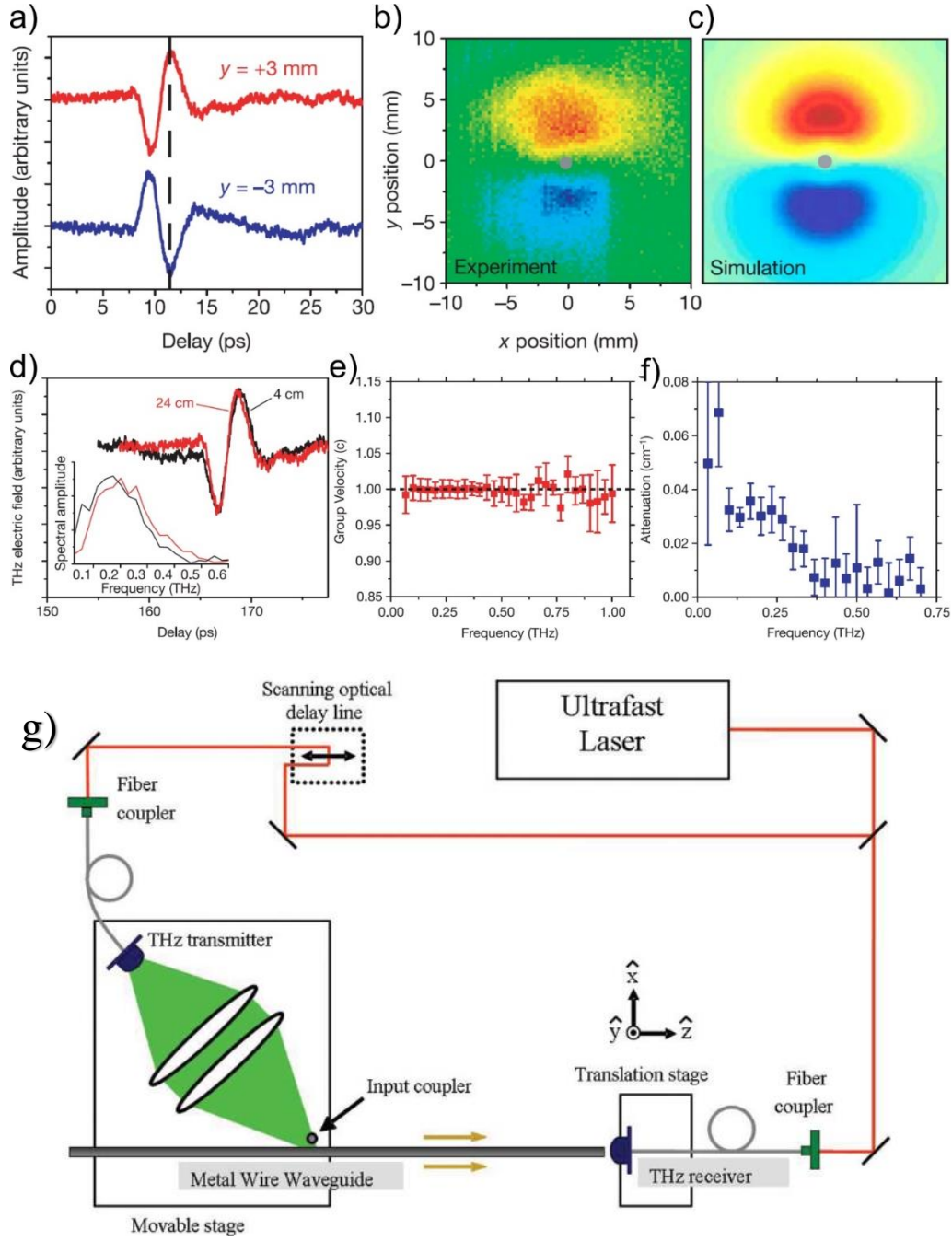


Figure 1.1 a) Time-domain electric field waveforms detected with the receiver 3mm above and 3mm below the waveguide. b) Spatial profile of the electric field obtained by moving the THz receiver in a plane perpendicular to the waveguide axis. c) The simulated spatial profile of the electric field propagating along the wire. d) THz waveforms measured after 4 cm (black) and 24 cm (red) of propagation distance along the wire. e) Group velocity of the propagating mode as a function of frequency. f) The electric field amplitude attenuation coefficient of the propagating mode as a function of frequency. g) Experimental setup for the excitation of THz surface wave on a metal wire using scattering configuration [52].

in excess of 50%. Van der Valk et al. [53] then studied the effect of thin dielectric coatings (deposited on metal wires) on propagation properties of the guided plasmonic mode. Their measurements demonstrated strong distortion of THz pulses even when nondispersive dielectric materials were used in the layer. At the same time, in [26] it was demonstrated that coating the wire with a thin layer of dielectric improves confinement of the THz pulse in the vicinity of the wire due to significant presence of the modal field in the dielectric layer. It was argued that this effect can be potentially exploited for sensitive detection of changes in physical properties of thin dielectric layers. At the same time, from these experiments one can also conclude that outstanding THz guiding properties of a single standing metal wire (low-loss, low-dispersion) can be compromised if the wire surface is not pristine. Later, Cao et al. [54] introduced a novel approach for coupling THz pulses onto the guided mode of a single metal wire using grooves inscribed directly on the wire surface. Adjustment of the groove number, groove geometrical parameters, and inter-groove separation allows controlling bandwidth and center frequency of the excited THz pulse. Finally, conical (tapered) metal wires have been proposed [55] for superfocusing of a THz wave.

1.1.3 Two-wire waveguides

Recently, an efficient solution to the coupling problem has been proposed in [30], where Mittleman et al. suggested using two-wire waveguides that support linearly polarized low-loss and low-dispersion plasmonic modes. Compared to complicated coupling schemes or utilization of specialized THz antennas, two metal wire waveguides can be directly excited with linearly polarized field patterns emitted by the majority of THz sources.

Indeed, field distribution in the fundamental TEM mode of a two-wire waveguide has the same symmetry as that of a wave emitted by a simple THz dipole photoconductive antenna when the wave is polarized along the line joining the two wires. Thus, one expects high excitation efficiencies of the fundamental mode of a two-wire waveguide when using standard dipole terahertz sources. Moreover, efficient confinement of the modal energy between the two wires, as opposed to a highly delocalized Sommerfeld wave on a single wire, makes two-wire waveguides less prone to bending losses. For example, in [30] it was demonstrated that for the same bending radius, bending loss of a two-wire waveguide was 5 times smaller than bending loss of a single wire waveguide. Additionally, absorption losses and group velocity dispersion of the fundamental

mode of a two-wire waveguide are extremely low. Finally, the confinement of the modal power in a small area between the metal wires opens possibilities for various guidance, sensing and even non-linear THz photonics applications. Coupling efficiency into a two-wire waveguide is a sensitive function of the excitation wavelength. It has been established that, the coupling efficiency achieves its maximal value at the wavelength that is comparable to the inter-wire separation, while the coupling efficiency stays relatively low for the wavelengths that are significantly smaller or larger than the optimal one. For a detailed discussion, see for example [56-58], where the authors use a mode-matching technique and a full-wave FEM numerical simulation to study this issue. Ultimately, it is the frequency dependent coupling efficiency that limits practically usable bandwidth in such waveguides.

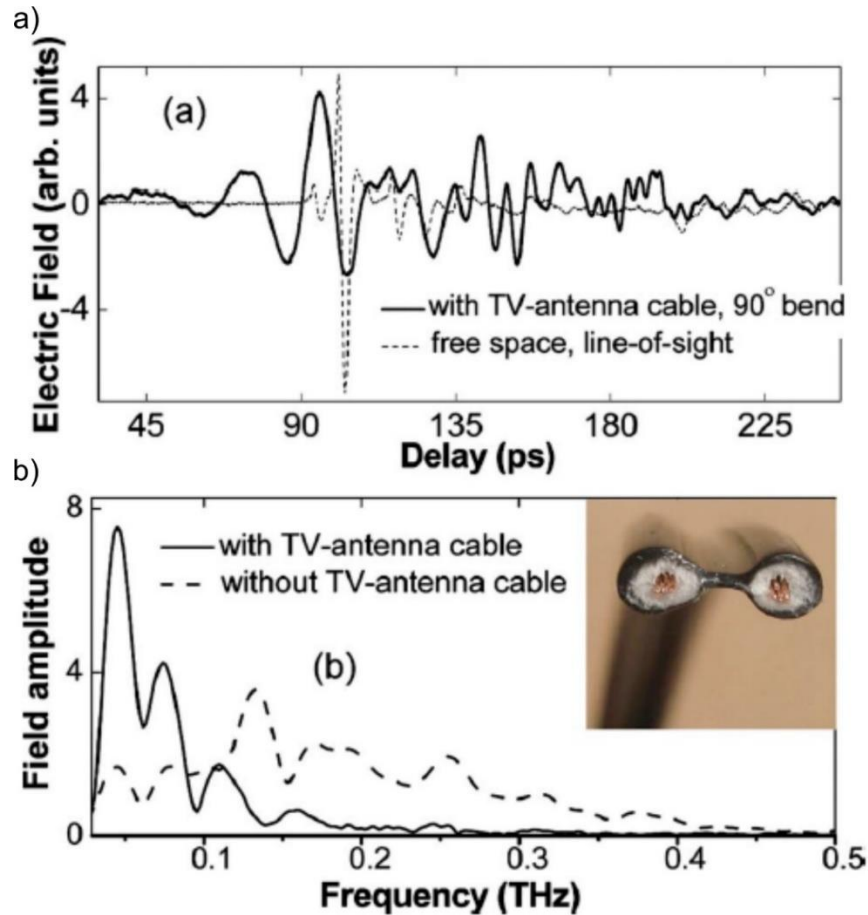


Figure 1.2 a) THz pulse transmitted through a 9.5 cm length of commercially available TV twin-lead antenna cable, with THz emitter and receiver at 90° to one another (solid curve); for comparison in dotted curve free-space THz transmission along a direct line-of-sight between the transmitter and receiver separated by the same 9.5 cm spacing, with no waveguide or optics in between. b) Amplitude spectra for the two THz waveforms. Adapted from [30].

Further improvement of the excitation efficiency of a TEM mode in a two-wire waveguide using realistic THz beams (non diffraction limited) as a source is possible by employing Y-shaped waveguide couplers, as shown in [58]. In this work, the authors used four wires adiabatically merging into a two-wire waveguide. The simulation results show an increased coupling efficiency for the two-wire waveguides without a significant effect on the overall group velocity dispersion or losses.

In [59] the authors have studied potential of the two-wire waveguides for application in chip-to-chip interconnects at operation frequencies up to 100 THz. The authors have shown that a two-wire waveguide with a wire radius of 10-20 μm and the inter-wire separation distance of 50-100 μm can be used to interconnect chips placed several mm apart. Such interconnects were then achieved using standard wire bonding techniques with a loss of less than 1.7 dB/mm.

The first attempt to demonstrate practical two wire waveguides was reported in [30]. There the authors used a ~ 10 cm-long piece of a standard TV antenna cable that is comprised of two metal wires encapsulated into a plastic jacket and separated with a plastic divider (see Figure 1.2). The authors have managed to transmit a THz signal, however, the received pulse was considerably distorted and attenuated. In the same paper, the authors have also demonstrated that traditional bulky metal holders can be partially substituted by foam holders that are highly transparent to THz radiation.

Active two-wire terahertz waveguides have been demonstrated in [60]. THz electric field is generated directly inside the waveguide structure. Efficient excitation of two-wire waveguides coupled with the elimination of power delivery to the waveguide losses allowed achieving 60 times higher power transmittance compared to the passive waveguide of the same structure for the same laser illumination power.

1.1.4 Composite metal-dielectric air-core fibers

Several experimental studies have been reported so far that studied propagation of THz pulses in composite metal-dielectric air-core fibers. Most recently in [61], Argyros et al. have reported a metal-dielectric composite waveguide featuring two or four large indium wires placed into a large hollow plastic tube. The Indium wires were embedded in the preform and then co-drawn together with the supporting material. Indium was chosen because of its low melting

temperature (156.6 °C), appropriate for co-drawing with the chosen dielectric, Zeonex. The main advantage of the co-drawing method is in precise positioning of the thin metal wires inside of the fiber structure compared to manual insertion. Additionally, with the co-drawing method, several-meter-long fibers with wires can be fabricated while with the manual wire insertion method fiber length is typically limited to ~30 cm.

The investigated fiber (see Figure 1.3 (a)) has an inter-wire distance of approximately 2 mm. The wires have an elliptic shape with average diameters of 1.0 mm and 1.8 mm along the minor and the major axis, correspondingly. The fibers were made from Zeonex polymer which is known for its low loss in the THz region [62].

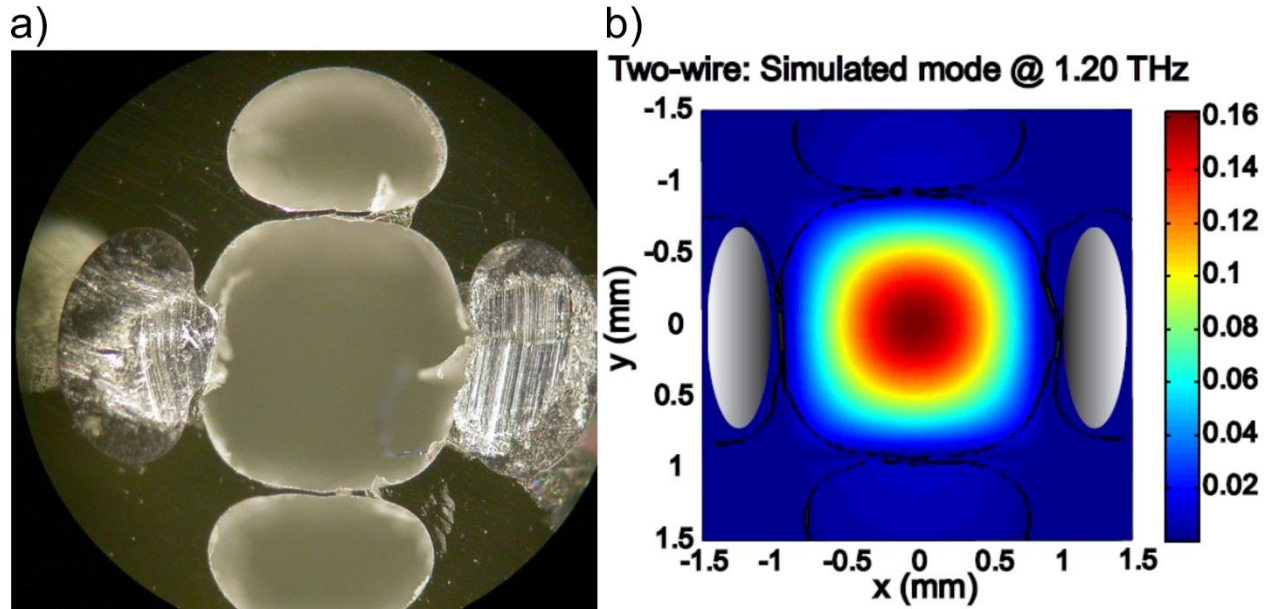


Figure 1.3 a) Cross section of a hollow core Zeonex fiber featuring two indium wires. Core diameter is ~2 mm. The indium wires are located at the left- and right-hand side of the hollow core and are seen silver; b) Field distribution (theory) in the HE_{11} -like mode at 1.2 THz. Adapted from [61].

In the THz frequency range, the lowest-loss mode compatible with the linearly polarized Gaussian beam of a standard THz source is a HE_{11} -like mode shown in Figure 1.3 (b). The numerical simulations indicate strong modal discrimination (with respect to their propagation losses) between the HE_{11} -like mode and the higher order modes. In the two-wire configuration, the HE_{11} -like mode is elliptical, which is most pronounced at low frequencies. At such frequencies, modal fields show significant presence in all three holes of the fiber and the modal sizes can differ

by as much as 20% along the two axes. The authors have also investigated configurations with four metal wires surrounding the hollow core. Unsurprisingly, HE_{11} -like modes of the two-wire and four-wire fibers do not differ much in shape at high frequencies, with most of the modal field concentrated in the central hole. At lower frequencies however, HE_{11} -like mode of a two-wire fiber becomes more elongated compared to the mode of a four-wire fiber due to penetration of its modal field into the two peripheral holes.

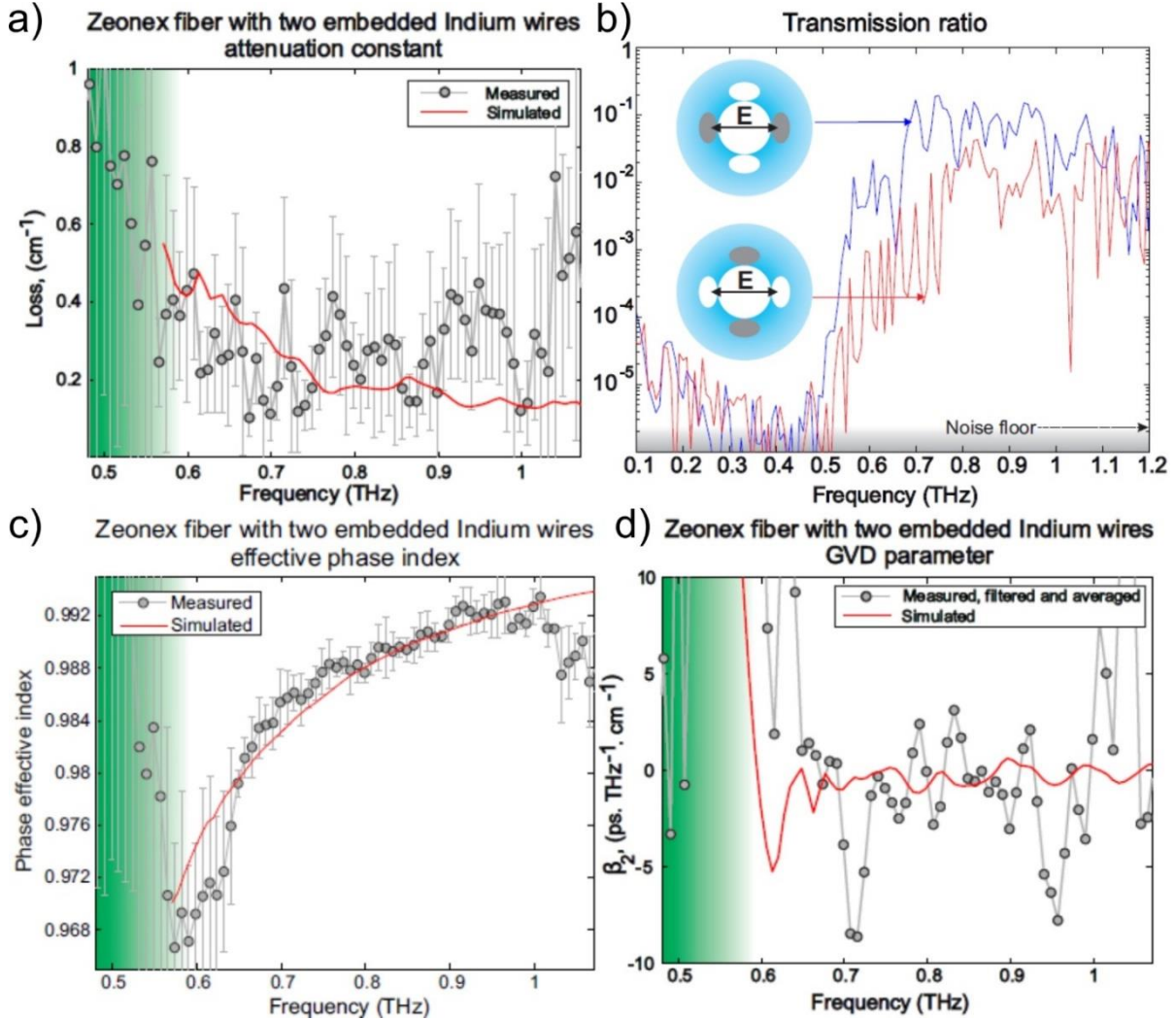



Figure 1.4 a) Loss coefficients as measured (grey) and as simulated (red line) for a two-wire fiber. b) Normalized transmission spectrum of 8 cm two-wire fiber with different wire plane orientation with respect to the electric field polarization as indicated. The indium wires are depicted as grey ellipses while the air region is the filled white space. c) Phase refractive indices as measured (grey) and as simulated (red line) for a two-wire fiber. d) The group velocity dispersion parameter determined from the measured data (grey) and as calculated from the simulation (red line) for a two-wire and fiber. Adapted from [61].


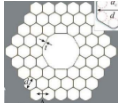
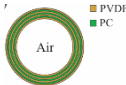
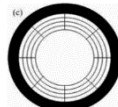
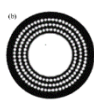
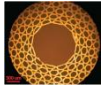

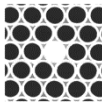

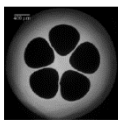
Transmission through the fibers has been measured using a standard free-space THz-TDS setup. The cutback method was used to characterize fiber propagation loss and modal effective refractive index. To obtain a modal field profile, a metal pinhole with a diameter of 0.8 mm was placed at the fiber output end and scanned across the fiber cross section. The experimentally obtained modal profiles agree well with the field distribution of the simulated HE_{11} -like mode. Figure 1.4 (a) shows comparison of the measured and simulated power absorption coefficients. The experimentally measured absorption loss (by power) is 0.3 cm^{-1} for the two-wire configurations. The simulated absorption loss has a trend of decreasing towards higher frequencies due to enhanced confinement in the air-filled fiber core. At lower frequencies, modal fields can have a significant presence in the lossy plastic cladding, thus leading to rapid increase in the modal propagation loss. Experimentally, this is manifested by the presence of a low frequency cut-off at $\sim 0.5 \text{ THz}$.


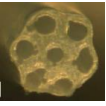
The effect of the two-wire orientation with respect to the excitation beam polarization has been investigated by rotating the fiber around its axis. The comparison of the transmission spectra is shown in Figure 1.4 (b). In both cases, the same low-frequency cut-off was observed, at around 0.5 THz . The transmitted power for the polarization perpendicular to the wire plane was reduced in comparison with the polarization parallel to the wire plane.

The effective refractive index is shown in Figure 1.4 (c), and its value is close to 1. The group velocity dispersion is calculated from the measured index data and is shown in Figure 1.4 (d). For the fiber with two-wires, GVD smaller than $5 \text{ ps}/(\text{THz}\cdot\text{cm})$ was found in the $0.65\text{--}1.0 \text{ THz}$ frequency range. It was further demonstrated that fibers with two-wires show generally lower losses and lower dispersions than fibers with four wires.

1.1.5 Terahertz waveguides examples

Waveguide type	Lowest observed losses, cm^{-1}	Remarks
 Pipe waveguide.	~ 0.02 (theoretical)	Material: Teflon, Frequency range: $0.35\text{--}0.55 \text{ THz}$ [42]

	Metal pipes with inner dielectric layer	~ 0.004	Material: Silver/Polyethylene coated, Frequency range: 1.2-2.0 THz [63]
	Hollow core photonic bandgap fiber	< 0.01 (theoretical)	Material: Teflon or high-density polyethylene, Frequency range: 0.85-1.05 THz [64]
	Ferroelectric hollow Bragg fiber	< 0.02 (theoretical), ~ 0.3 (experimental)	Material: PVDF and polycarbonate, Frequency range: 1.0-3.0 [38, 65]
	Cobweb structured hollow core Bragg fiber	$\sim 2 \times 10^{-5}$ (theoretical)	Material: high-density polyethylene, Frequency range: 0.3-4.0 THz [66]
	Hollow core microstructured fiber	~ 1.1	Material: PMMA, Frequency range: 0.8-1.4 THz [67]
	Kagome fiber	< 0.01 (theoretical), ~ 0.6 (experimental)	Material: Teflon or PMMA, Frequency range: 0.65-1.0 THz [68, 69]
	Solid-core subwavelength fiber	< 0.01	Material: polyethylene, Frequency range: 0.3-0.35 THz [34]
	Photonic crystal fiber	< 0.5	Material: high-density polyethylene, Frequency range: 0.1-2.0 THz [70]
	Polymeric photonic crystal fiber	< 0.1	Material: Topas, Frequency range: 0.3-0.65 THz [71]
	Microstructured fiber	< 1	Material: Zeonex Frequency range: 0.4-1.2 THz [62]

 <p>Porous-core dielectric fibers</p>	< 0.1	Material: PMMA, Frequency range: 0.2-0.35 THz [72, 73]
 <p>Porous-core subwavelength dielectric fiber</p>	< 0.1	Material: polyethylene, Frequency range: 0.1-0.3 THz [74]

1.2 Terahertz waveguides simulation

The ability to simulate terahertz wave propagation aids in the development novel waveguides and understanding the principles of their work. The finite element method (FEM) is a powerful computational technique for the simulation of electromagnetic waves propagation in terahertz waveguides [52]. Availability of commercial FEM software facilitates modelling of terahertz guided wave phenomena. Finite element method allows 2D frequency domain mode analysis and 3D time-domain electromagnetic wave propagation simulations of the waveguides. With the 3D simulation one can obtain loss, dispersion, and electric field distribution in the waveguide as the function frequency and waveguide length. In finite element method the spatial domain is divided into a finite number of subdomains, or elements, which can differ in size and shape. Finally, the field distribution and effective refractive index are computed for the structure, ensuring continuity at all boundaries between elements.

In [52] the authors demonstrated that FEM can be implemented for not only the simulation of the propagation and coupling into the waveguide but also for the optimization of the terahertz source geometry to ensure the optimal coupling. In [75] it was demonstrated that FEM can be efficiently used to calculate complex propagation characteristics of surface plasmons in metal coated silicon tubes. The FEM simulation explains the origin of surface plasmon modes and gives the conditions for their phase matching. In [76] the authors implemented their modification of the finite element method to achieve low-loss and relatively low dispersion guidance in a wide band of THz frequencies in hollow cylindrical metallic waveguides.

Finite-difference time-domain is another versatile technique that can be used to study the electromagnetic field propagation in terahertz waveguides of arbitrary shapes. However FDTD is

computationally very expensive. They require a gigantic amount of mesh cells because the simulation deals with lengths scaled from several nm to correctly describe THz field penetration into metals to many cm required to form stable modes in the waveguide. Therefore usually simplifications have to be made, such as neglecting surface roughness, bulk inhomogeneity, or replacing metals with perfect electric conductors [77]. In [78] the authors are implementing FDTD calculations to study waveguide structures and couplers. The ability of FDTD method to evaluate the evolution of the electromagnetic field in irregular shaped structures offered a possibility to optimize a whole set of matching ribbon-based components for single-mode propagation achieving low absorption and low bending loss guidance. Even more complex structure has been studied in [79]. The authors proposed a deep subwavelength terahertz waveguide based on the magnetic polariton guided in a narrow gap in magnetic metamaterial. Strong field confinement below the diffraction limit has been studied using FDTD for straight and bent waveguides, as well as waveguide splitters.

For a slab waveguide, or for a multilayered planar waveguide, or in the case of a perfectly symmetric circular geometry one can use the exact vectorial simulations in a transfer matrix formalism to calculate the waveguide mode parameters. Similar to frequency-domain FEM, transfer matrix theory allows to solve for the complex propagation constants. The transfer matrix method is based on simple continuity conditions for the electric field across boundaries between different media. In [80] ultra-broadband terahertz waveguide emitters are analyzed using the transfer matrix formalism. The model is able to predict the efficiency of different frequency generation of femtosecond optical pulses in five layer metal/cladding/core waveguide structure and their corresponding losses. The transfer matrix method has been applied to investigate metal-metal waveguides for terahertz quantum-cascade lasers [81]. The calculation results allowed the authors to optimize the choice of metal and its thickness to minimize losses in the waveguide. The circular symmetry and step-index refractive index profile of chalcogenide capillaries [41] dictate the modal field of a guided mode can be expressed as a linear combination of Bessel function. This allowed the authors to explain the experimental transmission spectra of anti-resonant guidance in such waveguides and accurately determine the thickness of the capillaries' walls.

1.3 Applications of foams in terahertz photonics

Plastic foam is an example of a dispersed media where open or closed-cell gas regions are uniformly dispersed in a solid polymeric matrix. Plastic foam can be produced and shaped into various forms by mechanical, chemical or physical processing techniques, see [82-85] for details. The different fabrication techniques result in foams of different densities. For example, higher density foams are used for mechanical protection, while lower density foams are used for thermal isolation.

Characterization of foam optical properties in the THz spectral range was first conducted by Zhao et al. [86], where they studied polystyrene foams. In their studies, the authors compared three samples of different densities. For all the samples they found very low refractive indices of 1.017 - 1.022 in the 0.1 - 4 THz spectral range. The extinction coefficient remained smaller than 1 cm^{-1} at frequencies lower than 2.5 THz for the three samples, and smaller than 1.5 cm^{-1} for frequencies below 4 THz for the best sample. THz characterization of the Polymethacrylimide foams reported in [87] showed the same kind of behavior - a low refractive index 1.0175 - 1.0321 and a low extinction coefficient (less than 2 cm^{-1} below 2 THz).

Because of the high porosity of foam, it is not surprising to find that there is a large difference in the values of the refractive indices of foam material and bulk material from which the foam is fabricated. For instance, the refractive index of bulk polystyrene in the THz spectral range is nearly constant and is close to 1.6, while as mentioned earlier, polystyrene foam has a refractive index close to one. Such low values of the foam refractive index can be explained within the effective medium approximation which describes propagation of electromagnetic waves in composite materials made of subwavelength particles / inclusions implanted into a host material [88, 89]. In particular, for THz waves, a typical wavelength is on the order of 300 microns and longer, while the thickness of polymer shells that encapsulate air in foams can be considerably smaller than 100 microns. When propagating through foam, THz will not scatter efficiently on the deeply subwavelength polymer boundaries of the gas pockets, thus explaining the low scattering loss. Moreover, relative presence of THz radiation inside of the polymer boundaries, as compared to the gas pockets, will be small, thus explaining a refractive index close to that of air and absorption losses which are only a small fraction of those of a bulk polymer material from which the foam is made [86, 87]. Ultimately, the THz extinction coefficient of foam is influenced both

by the foam microstructure (scattering loss) and the nature of the solid material of the foam (absorption loss) [90-93]. Therefore, for waveguide applications one has to choose foams made of low-absorbing solid materials; the foams should feature closed-cell porosity with a high content of low-loss gas (low density foams), and also the gas pockets and the solid shells confining the gas should have deeply subwavelength dimensions determined by the spectral range of interest [94].

Note that careful consideration should be given to the type of gas (blowing agent) used in the foam fabrication. For example, in their study, Zhao et al. [86] noted an absorption feature around 0.5 THz for the foam sample, made with HCFC 142 b gas as the blowing agent, and confirmed it to be caused by rotational transitions in the molecular gas. The two other samples were made with CO₂ and no absorption was detected in the studied region.

When solid material of a foam has low absorption loss (e.g., polystyrene with loss $\alpha = 1.00 \pm 0.12 \text{ cm}^{-1}$ at 0.5 THz [95, 96]), then foam scattering loss can become higher than foam absorption loss [86, 87]. Scattering loss becomes especially pronounced at higher frequencies when the scatterer (gas pocket) size becomes comparable to the wavelength of guided light. In fact, from the three samples used by Zhao et al. [86], the one with the largest average pore diameter $\sim 150 \text{ }\mu\text{m}$ had the highest extinction coefficient at frequencies above 2 THz. Therefore, in order to reduce the scattering, it is important to control the pore size and geometry.

As for the application of foams in THz frequency range I note the use of polystyrene foam as a substrate for imaging and for manufacturing of near-infrared dichroic filters [94, 97]. THz was also used for industrial non-destructive characterization of foams [98, 99] that allowed simultaneous monitoring of the chemical and structural information of the sample [99].

Surprisingly, no significant attention was given to foams as core materials for THz waveguiding. Although Mittleman et al. used polystyrene foam slabs to support the two-wire waveguide structure [30], the slabs were not used as a core or cladding material in those experiments. Most recently, our research group has demonstrated fabrication of 10 cm-long THz fibers from biodegradable silk foams that was used as a fiber core material [100].

1.4 Terahertz refractometers

Optical chemical and bio-sensors have attracted considerable attention in biochemistry and medicine where systems capable of highly sensitive, label-free and minimally invasive detection

are in high demand [101, 102]. Terahertz electromagnetic waves with a spectrum lying between far infrared and microwave regions offer unique properties that are not available at other wavelengths. THz radiation is nonionizing due to its low photonic energy and many substances are predicted to have a specific spectral response in the terahertz range.

Most of the current THz sensors are realized in the non-resonant configurations where sample is interrogated directly by the THz light. In resonant sensors, changes in the sample properties are measured indirectly by studying variations in the optical properties of a resonant structure coupled to a sample. In resonant sensing method one typically employs resonant spectral transmission characteristics or photonic band-gap effect of sensing devices. The sensors detect shifts of the resonant wavelength in response to resonant structure changes caused by the presence of the analyte. These sensors include thin-film micro-strip lines resonators [103], photonic crystal waveguides [104], metallized periodic groove structures integrated into parallel-plate waveguides [105], thin metallic meshes [106], planar double split-ring resonator arrays [107], resonant cavities integrated into parallel-plate waveguides [108], and dielectric pipe waveguides [109]. In the amplitude-based detection methodology one operates at a fixed wavelength and records changes in the amplitude of a signal, which are then reinterpreted in terms of changes in the analyte refractive index. Among the advantages of this type of sensors are low cost and ease of fabrication, since no precisely engineered resonant or photonic band-gap structure is required.

1.5 Novelty of the proposed waveguides

In this section I would like to explain how the proposed waveguides different from those developed earlier and mentioned in the literature review. I will emphasize the novelty of their design and state the new functionalities or conveniences that they bring.

The first waveguide that will be described in this thesis has a planar porous structure and consists of multiple layers of thin polyethylene film that are separated by low-loss air layers of comparable thickness. High porosity of the waveguide together with the low absorption of polyethylene makes this waveguide low-loss in the terahertz region. The lack of confinement in the direction perpendicular to polyethylene layers results in the absence of the low frequency cutoff enabling the broad bandwidth of the waveguide. So far multilayered dielectric waveguides in the terahertz range have been proposed only in the context of their anisotropic properties, and the first prototypes of wave plates have been demonstrated. In this thesis I will present the first thorough

investigation of the optical properties of such waveguides in the broad frequency range as a function of the waveguide geometry. Moreover, multilayered dielectric waveguides can be useful not only for low-loss THz wave delivery but also for sensing of biological and chemical specimens in the terahertz region by placing the recognition elements directly into the waveguide microstructure. The main advantage of the proposed planar porous waveguides is the convenient access to their optical mode, since the major portion of THz power launched into such a waveguide is confined within the air layers. Moreover, small spacing between the layers promotes rapid loading of the analyte into the waveguide due to strong capillary effect. The modal refractive index is easy to adjust by changing the air spacing between the layers, as well as the number of layers in the core.

Further along the text of the thesis several types of hybrid metal-wires/dielectric waveguides will be presented. Their structure is a combination of widely studied porous dielectric fibers and metal wires waveguides, yet it is the first attempt to combine these two types guiding structures. Previously reported composite metal-dielectric fibers are essentially hollow-core fibers not fully exploiting plasmonic guidance in a two metal-wire waveguide. Metal wires structure has been chosen as one of the most promising techniques of making cost efficient, low-loss, low-dispersion, and broadband waveguides in the terahertz range. And the porous dielectric cladding structure has been added to a two-wire waveguide to provide robust mechanical support in order to hold the metallic wires straight and parallel to each other, to optically separate the core region from the environment, and to provide encapsulation for the dry gas in the vicinity of the wires. In such a fiber design, a significant fraction of the modal power is propagating in the air-filled core, which reduces the modal absorption losses as well as the modal group velocity dispersion compared to an empty porous fiber of the same geometry (without metal wires).

Then I describe an alternative approach that allows mechanical support and encapsulation of the metal wires. Having a large fraction of power guided inside of dry low-loss gas is beneficial for reduction of the modal propagation loss. Foam is inherently highly porous, its pores are filled with gas and the pores can be sealed during fabrication. For the aforementioned reasons, foam is a good candidate for guiding of THz waves. To the best of my knowledge, no significant attention was given to foams as core materials for THz waveguiding. Polystyrene foam slabs have been used to support the two-wire waveguide structure before but they were not used as a core or cladding material. In this thesis I will describe demonstrate that foam can be utilized as cladding material

for two-wire waveguides providing mechanical stability, ease of manipulation, and insensitivity to the variations in the environment.

Finally, hybrid metal-wire/dielectric fibers described can also be useful for sensing in the terahertz region by placing the recognition elements directly into the fiber microstructure. Introduction of even lossless analytes into the fiber core leads to significant changes in the modal losses, which is used as a transduction mechanism. With a refractive index resolution on the order of $\sim 10^{-3}$ RIU, the composite fiber-based sensor is capable of identifying various gaseous analytes and aerosols or measuring the concentration of dust particles in the air. From the comparison of sensor resolutions it follows that the proposed device combines both the sensitivity comparable to that of the best demonstrated sensors while being cost effective and easy to manufacture.

I would like to make a small comment of the potential for future commercial exploitation of the THz field. I note that the prices of terahertz systems are steadily decreasing, whereas their variety and availability are booming. At low frequency THz region solid state oscillators, frequency multipliers and amplifiers are offering an efficient solution to reduce the cost of terahertz systems. At higher THz frequencies optical-to-THz down conversion and high temperature quantum cascade lasers are the two most intensively used technique with the former having the variations including usage of photoconductive antennas, photodiodes, and nonlinear optics crystals.

CHAPTER 2 METHODOLOGY

2.1 Numerical modelling

To numerically study the propagation in THz waveguides I primarily employ commercially available, finite element (FEM) software COMSOL Multiphysics. I import cross sections of waveguides and fibers of interest and then utilize two-dimensional (2D) simulation to solve for the complex refractive indices and field distribution over a cross section to obtain a complete modal structure of a waveguide or a fiber. Optical waveguides modes are governed by the time-independent Helmholtz equation that has the complex effective refractive index as a parameter. The software splits the cross section of a waveguide into a set of finite elements, usually triangles that closely approximate the boundaries of the waveguide structure. Thus, a mesh of triangular finite elements is created, discretizing the whole cross section of the waveguide. Then, the equation is solved for each element giving the solution for the field inside each node of the mesh and creating the global matrix system for the entire waveguide under study. Finally, the field distribution and effective refractive index are computed for the whole cross section, ensuring continuity at all boundaries between mesh nodes. The accuracy of the solution increases with the number of elements, as does the computation intensity, thus a balance between the precision and duration of the simulation must be found. When computing waveguides whose structures possess symmetry, it might be useful to exploit this property as it will reduce the number of discrete elements needed to achieve a given level of accuracy. For all the simulations presented in this thesis, I have also used perfectly matched layers (PML), artificial absorbing boundary conditions surrounding the main computational domain. The usage of PML eliminates the spurious solutions that are often generated by numerical mode solvers.

To take into consideration the dispersive properties of the materials, I use the frequency dependent complex refractive index for dielectric materials and frequency dependent relative permittivity and conductivity of metal in the THz spectral range modeled using the Drude formula. For metals I use the parameters derived from the literature. Whereas, for dielectrics, there is a strong discrepancy between the material parameters in the THz spectral range reported by different research groups, likely due to different manufacturing technologies of the same material by various

companies. Therefore, where possible, I utilize the material parameters measured in our laboratory for the simulation.

I am using the semi-analytical theoretical model to explain the transmission in terahertz waveguides. To reduce the complexity of the solution, I consider all the modes of the waveguides individually, obtaining the superposition of their respective fields at the output of the waveguide. As the modes propagate they gain frequency dependent phase factors and lose power due to absorption in the waveguide material which is also a function of frequency. The distribution of the transverse E-field components $\vec{E}_{output} = (E_{output}^x, E_{output}^y)$ at the output facet of a waveguide of length L_w is modeled as the coherent superposition of the N guided modes:

$$\vec{E}_{output}(x, y, \omega) = \sum_{m=1}^N C_m \cdot \vec{E}_m(x, y, \omega) \cdot \exp\left(i \frac{\omega}{c} \cdot n_{eff,m} \cdot L_w\right) \cdot \exp\left(-\frac{\alpha_m L_w}{2}\right) \quad (2.1)$$

where $\vec{E}_{output} = (E_{output}^x, E_{output}^y)$ stands for the transverse field components of the m-th guided mode, x-axis and y-axis correspond to the horizontal and vertical directions in the subsequent figures. The variables α_m and $n_{eff,m}$ denote respectively the power loss coefficient and the real part of the effective refractive index of the m-th mode at a given frequency ω . The lowest order mode has the smallest value of the effective refractive index. The total intensity profile in the waveguide will vary during propagation, because the different $n_{eff,m}$ values of different modes lead to varying relative optical phases, moreover losses of different modes might vary drastically.

The variable C_m refers to the normalized amplitude coupling coefficients computed from the overlap integral of the respective flux distributions of the m-th mode with that of the Gaussian beam of the source. Specifically, the definition of C_m is based on the continuity of the transverse field components across the input interface (i.e. cross-section of the subwavelength waveguide) between the incident beam and the excited fiber modes [110]:

$$C_m = \frac{1}{4} \int_{wc} dx dy \left(\mathbf{E}_m^*(x, y) \times \mathbf{H}_{input}(x, y) + \mathbf{E}_{input}(x, y) \times \mathbf{H}_m^*(x, y) \right) \times \\ \times \frac{1}{\sqrt{\frac{1}{2} \text{Re} \int_{wc} dx dy \left(\mathbf{E}_m^*(x, y) \times \mathbf{H}_m(x, y) \right)}} \cdot \frac{1}{\sqrt{\frac{1}{2} \text{Re} \int_{wc} dx dy \left(\mathbf{E}_{input}^*(x, y) \times \mathbf{H}_{input}(x, y) \right)}} \quad (2.2)$$

To model the field structure of the source, I assume a Gaussian beam whose fields are normalized to carry power P :

$$\vec{E}_{Input}(x, y) = \vec{n}_x \cdot \sqrt{\frac{2P}{\pi\sigma^2}} \cdot \exp\left[-\frac{x^2}{2\sigma^2}\right] \cdot \exp\left[-\frac{y^2}{2\sigma^2}\right] \quad (2.3)$$

$$\vec{H}_{Input}(x, y) = \vec{n}_y \cdot \frac{1}{\sqrt{\mu_0 / \epsilon_0}} \cdot \sqrt{\frac{2P}{\pi\sigma^2}} \cdot \exp\left[-\frac{x^2}{2\sigma^2}\right] \cdot \exp\left[-\frac{y^2}{2\sigma^2}\right] \quad (2.4)$$

where the Gaussian beam waist parameter σ is related to the full-width at half-maximum by field as $FWHM = 2\sigma\sqrt{2 \cdot \ln 2}$, \vec{n}_x and \vec{n}_y are unit vectors, and $\sqrt{\mu_0 / \epsilon_0}$ is the intrinsic impedance of vacuum. The frequency dependence of the beam waist was measured independently and then fitted by a linear function of the input wavelength with a result $\sigma \approx 2.5 \cdot \lambda$. This model was subsequently used in the following simulations. To address the change of the experimental setup used for the characterization of planar waveguides (cylindrical lenses were added to the system to reshape the terahertz beam) in the corresponding simulation, the Gaussian beam was replaced by a y-polarized 2D Gaussian beam polarized along the y-direction and uniform in x-direction

$$\vec{E}_{Input}(x, y) = \vec{n}_x \cdot \sqrt{\frac{2P}{\pi\sigma^2}} \cdot \exp\left[-\frac{y^2}{2\sigma^2}\right] \quad (2.5)$$

$$\vec{H}_{Input}(x, y) = \vec{n}_y \cdot \frac{1}{\sqrt{\mu_0 / \epsilon_0}} \cdot \sqrt{\frac{2P}{\pi\sigma^2}} \cdot \exp\left[-\frac{y^2}{2\sigma^2}\right] \quad (2.6)$$

2.2 Experimental setup

All the measurements in our experiments were obtained using a modified terahertz time-domain spectroscopy (THz-TDS) setup. This setup consists of a frequency doubled femtosecond fiber laser (MenloSystems C-fiber laser) used as the pump source and two identical GaAs dipole antennae used as a THz emitter, as well as a detector yielding a spectrum range of 0.1 to 3.0 THz. However, because of the lower dynamic range and increased material losses in the waveguide at higher frequencies, I only considered the spectrum range of 0.1 to 1.5 THz in the following sections. In the photoconductive antenna, a fs pulse laser is focused on the antenna gap, exciting the substrate which has a subpicosecond carrier lifetime. The electrons are accelerated by the bias voltage applied between the electrodes, producing THz pulses. The identical photoconductive

antenna serves as a detector. THz pulses hitting the detector antenna induce a voltage across the antenna gap, which can be probed by measuring the current when a fs probe pulse excites free carriers in the detector gap.

Sampling in time-domain gives amplitude and phase frequency spectra. The THz electric field is measured point-by-point in the time-domain by using a field detector. The Fourier transform of the time signal gives a complex frequency spectrum yielding amplitude and phase information. The absorption is retrieved using amplitude information whereas the refractive index can be evaluated using phase information.

In contrast to the standard arrangement of most THz-TDS setups, where the configuration of parabolic mirrors is static, a parabolic mirror is mounted on the translation rails. This arrangement allows for the measurement of waveguides up to 45 cm long. Figure 2.1 illustrates the experimental setup where the fiber was fixed by apertures and placed between the two parabolic mirrors. In the case of fiber measurement, its input facet was fixed by an aperture to minimize the uncertainty in the fiber position. Both the input and output ends of the fiber were placed at the focal points of the parabolic mirrors.

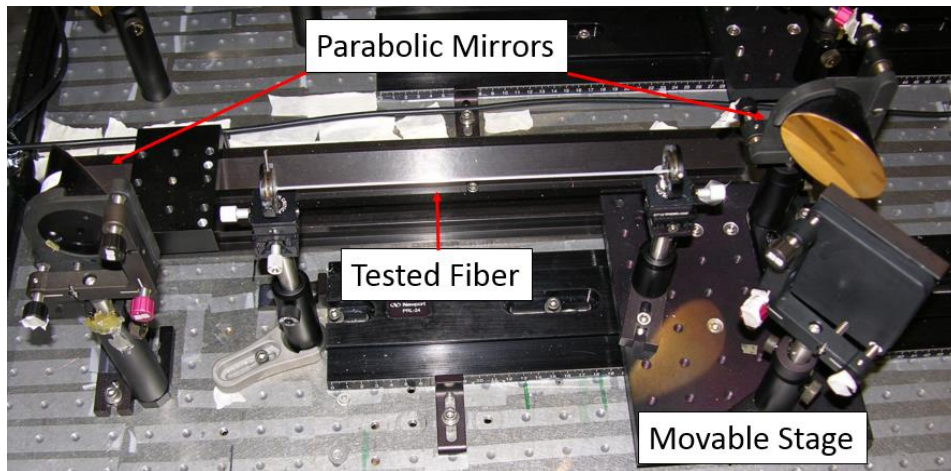


Figure 2.1. Experimental setup with the fiber mounted in the apertures.

In order to provide efficient coupling into the planar waveguide, it was placed between the focal lines of the two Teflon cylindrical lenses. The cylindrical lenses change the transverse profile of the Gaussian beam from the source by reshaping it into the beam uniform in the direction of the waveguide layers and Gaussian in the perpendicular direction which is then launched into the planar waveguide core. The metal slit before the waveguide input facet is used to avoid propagation along the upper and lower surfaces of the waveguide.

Several methods have been employed to measure the optical properties of terahertz waveguides. Using the first technique, one compares the two pulses. The first one being a sample pulse which propagates through the entire optical system with all the mirrors, lenses and the waveguide included. For the second measurement, one excludes the waveguide keeping the rest of the optical hardware intact. The transmission and dispersion can then be calculated based on these two measurements. While providing a general overview of the waveguide optical characteristics this method does not allow discriminating different sources of the losses, for example coupling from free-space into the waveguide, absorption in the waveguide structure and coupling into the air at the output facet of the waveguide.

For the characterization of the hybrid metal-wire/dielectric fibers it was the most important to compare their transmission with the all-dielectric fibers of the same design. Then in order to understand the modal structure of the hybrid fibers it was crucial to compare the transmission for different orientations of the incoming THz light polarization. Thus, a series of experiments has been conducted in which I studied the optical properties of the proposed fibers with and without metal wires in their structure for different polarization of THz radiation

Another technique is the cut-back method. The absorption coefficient is calculated by comparing the transmission through the waveguide segments of different lengths. The input facet of the fiber is fixed during the measurement and the fiber is repeatedly shortened by cutting its output end. While having some issues with the accuracy of waveguide positioning between the subsequent cuts, the cutback method eliminates the waveguide coupling efficiency from losses calculation.

For the single mode propagation in the waveguide the relation between the input and the output electric field can be expressed as [111]:

$$E_{out}(\omega) = E_{ref}(\omega) \cdot T_1 \cdot T_2 \cdot C^2 \cdot \exp(-\alpha_{eff} L / 2) \cdot \exp(-i\beta_{eff} L) \quad (2.7)$$

where $E_{ref}(\omega)$ and $E_{out}(\omega)$ are the complex electric field at frequency ω at the entrance and the exit of the waveguide, T_1 and T_2 are the total transmission coefficients at the input and output faces of the waveguide, C is the coupling coefficient between the field distribution of the waveguide mode and that of the free-space propagating THz radiation, the same for both faces of the waveguide, L is the length of the waveguide, α_{eff} is the absorption coefficient of the propagating

mode, and $\beta_{eff} = n_{eff} \cdot 2\pi / \lambda = n_{eff} \cdot \omega / c$ is its propagation constant, and n_{eff} is its effective refractive index.

Applying Equation (2.7) for two different lengths of the waveguide and dividing the two equation one by another we can get rid of the coefficients T_1 , T_2 and C , assuming that the alignment does not change during the measurement:

$$\frac{E_{out1}(\omega)}{E_{out2}(\omega)} = \exp(-\alpha_{eff}(L_1 - L_2)/2) \cdot \exp(-i\beta_{eff}(L_1 - L_2)) \quad (2.8)$$

Then, the propagation constant of the mode and the effective material loss can be extracted from the Equation (2.8).

2.3 Fiber fabrication

All the microstructured cladding structures described in my thesis were fabricated in our laboratory using fiber drawing technique. Particularly, microstructured preforms corresponding to the desired cladding geometries were first fabricated by machine controlled (CNC) drilling of the polyethylene rods. Waveguide preforms are the oversized version of the desired fiber geometry, which are prepared for drawing in a draw tower. The resolution of the preform's details is limited by the smallest drill bit size available. When heated in the furnace of the draw tower the molten preform stretches into a fiber. The diameter of the fiber is controlled by adjusting the drawing temperature and pulling strength. During the drawing process, the size of the holes (in the fiber cladding) was controlled using overpressure. The drawing technique allows us to fabricate very long fibers at the rate of many meters per day. Finally, metallic wires were inserted into the drawn microstructured claddings to obtain hybrid two-wire fibers. The diameter of the copper wires was chosen to match that of the fiber holes in order to reduce the potential misalignment inside the fiber. Using this method, 20 cm-long hybrid fibers were manufactured and later used in the measurements. The length of the resulting fibers was mainly limited by the limitations related to metal wire insertion. The force necessary to insert a longer wire and push it through the fiber's microstructure was often resulting in wire bending, which in its turn leads to the non-uniformity of the fiber cross section resulting in the increased losses.

CHAPTER 3 ARTICLE 1: PLANAR POROUS THZ WAVEGUIDES FOR LOW-LOSS GUIDANCE AND SENSING APPLICATIONS

This chapter is based on the paper “Planar porous THz waveguides for low-loss guidance and sensing applications,” published in IEEE Transactions on THz Science and Technology in 2013. I am the primarily author of this article, and my co-authors were Anna Mazhorova and Maksim Skorobogatiy. My role in preparing this article included the design of the experiment, analysis of the experimental data, performing numerical simulations, and development of the theoretical model for the THz guidance in planar porous waveguides.

In this chapter, planar porous dielectric waveguides featuring periodic sequence of deeply subwavelength air/dielectric bi-layers are proposed, fabricated and characterized in view of their potential applications as low-loss waveguides and sensors in the THz spectral range. The waveguide design maximizes the fraction of power guided in the air to reduce waveguide loss due to material absorption, as well as to provide a conveniently accessible microfluidic channels for sensor measurements. The choice of the geometrical parameters of the waveguide has been dictated by the necessity of dielectric layers thickness being significantly smaller than the operational wavelength. On the other hand, 50 μm is the minimal thickness of the polyethylene film at which we could ensure that it can be properly stretched to maintain uniform separation between the layers.

3.1 Introduction

The main complexity in designing terahertz waveguides is the fact that almost all materials are highly absorbent in the terahertz region [31]. Since the lowest absorption loss occurs in dry air, an efficient waveguide design must maximize the fraction of power guided in the air. Different types of THz waveguides and fibers have been proposed based on this concept. The simplest subwavelength fiber [32-34], features dielectric core that is much smaller than the wavelength of guided light. As a result, a high fraction of modal power is guided outside of the lossy material and in the low-loss gaseous cladding. Another type of low-loss fibers features porous core region with the size of the individual pores much smaller than the wavelength of light [32, 33]. As a result, guided light is concentrated mostly in the low-loss gas-filled pores inside the core and in the gaseous cladding. Porous fibers, generally, feature higher confinement in the core region and are less prone to bending losses and influence of the environment compared to simple rod-in-the-air

subwavelength fibers [32, 35]. Another important type of the low-loss waveguides feature hollow gas-filled core surrounded by a structured cladding serving as a reflector. The main challenge in the design of such waveguides is to ensure high reflection at the core-cladding interface. Different hollow-core structures have been investigated including metalized bores [35-37], periodic dielectric multilayers [38], as well as thin-walled dielectric pipes [39,41,42]. Other types of the THz waveguide are parallel plate waveguides [43] and slit waveguides [44] remarkable for their low transmission losses and high mode confinement. Metal wire, can be used to transport terahertz pulses with virtually no dispersion and low attenuation [49].

In this paper we explore a novel design of a planar porous low-loss waveguide for 0.1-1.5 THz frequency range. The waveguide structure consists of multiple layers of thin (25 - 50 μm) polyethylene film that are separated by low-loss air layers of comparable thickness. We believe that waveguides described in this paper can be useful not only for low-loss THz wave delivery but also for sensing of biological and chemical specimens in the terahertz region by placing the recognition elements directly into the waveguide microstructure similarly to what has been recently demonstrated in [112].

The main advantage of the proposed planar porous waveguides is the convenient access to their optical mode, since the major portion of THz power launched into such a waveguide is confined within the air layers. Moreover, small spacing between the layers promotes rapid loading of the analyte into the waveguide due to strong capillary effect (< 1 s filling of a 10 cm long waveguide with an analyte). The modal refractive index of porous waveguide is smaller compared to pure polymer and it is easy to adjust by changing the air spacing between the layers, as well as the number of layers in the core. The porous waveguide exhibits considerably smaller transmission losses than a bulk material. For completeness we note that planar multilayered materials have been recently studied in a broader context of birefringent anisotropic materials for THz devices [47].

3.2 Waveguide design

The photograph of a planar porous multilayer waveguide and its metal holder is presented in the Figure 3.1 (a). The waveguide has been fabricated using commercial 50 μm thick polyethylene films. The layers were stacked together and separated using spacers in the form of a plastic tape placed along the waveguide edges. The layers and the spacers were held together by metal holders that also allowed some tension control over the whole structure, thus, resulting in a

porous core with well-defined and consistent $75\ \mu\text{m}$ air gaps between the individual polyethylene layers. The thickness of the spacers has been measured with the optical microscope to be $75\ \mu\text{m}$ (see Figure 3.1 (b)), the tension of the polyethylene layers has been high enough to maintain the uniform thickness of the air layers. The overall width of a THz waveguide is $3.3\ \text{cm}$ and its length is $11\ \text{cm}$. The number of polyethylene layers used in our experiments varied from 1 to 10, with the maximal core thickness of $1.2\ \text{mm}$ (10 layers). The influence of the metal borders of the waveguide on its optical properties will be discussed later in section 3.8.

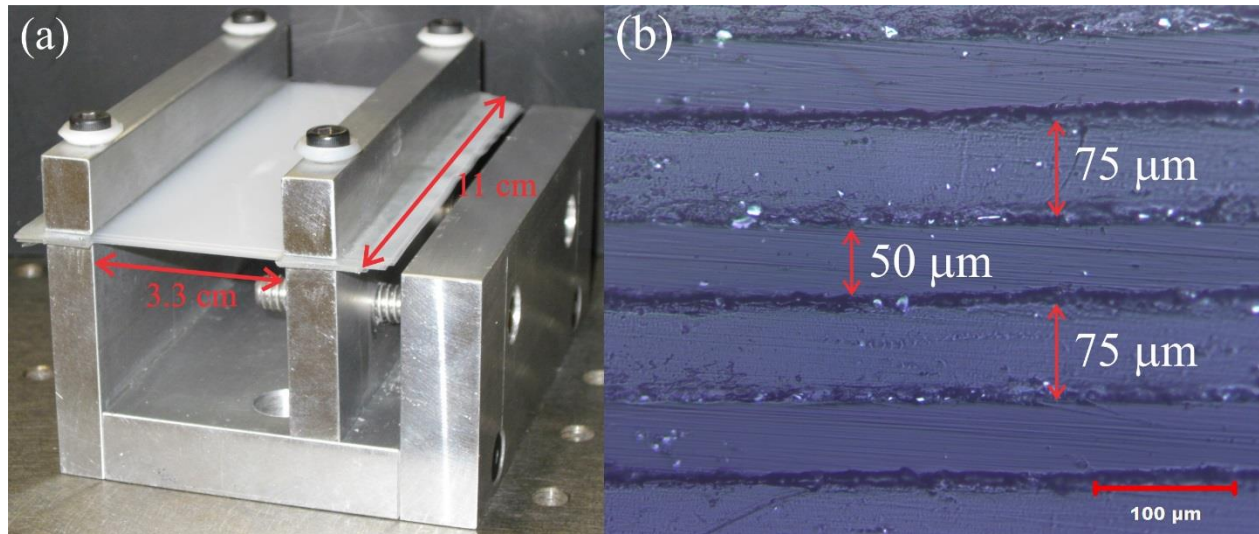


Figure 3.1 (a) Photograph of the planar porous multilayer waveguide fabricated from polyethylene and its metal holder, (b) Microscope image of the waveguide cross-section (in the place where the PE layers are separated by the spacers), the thickness of the polyethylene layers is $50\ \mu\text{m}$, while the thickness of spacers is $75\ \mu\text{m}$.

As the major portion of the THz light propagating in such planar porous waveguides is confined within the low-loss air layers, the relatively high absorption loss of Polyethylene films are effectively mitigated. Moreover, the waveguide optical properties are very sensitive to the real and imaginary parts of the permittivity of the separating (air) layers, thus, making it possible to use changes in the waveguide transmission spectrum for characterizing of the specimens placed inside of the waveguide structure (such as gases and liquids).

3.3 Fundamental mode of the waveguide

The multilayer porous waveguides features a broader spectral region of single mode operation compared to the fully solid slab waveguide of the same size. The criterion for a single mode operation of a planar slab waveguide is [110]:

$$k \cdot d \cdot \sqrt{n_2^2 - n_1^2} < \pi, \quad (3.1)$$

where n_2 is the refractive index of the core material, which for most materials is larger than $n_2 > 1.45$, and n_1 is the refractive index of the cladding material, which in our case equals to $n_1 = 1$, d is the thickness of the slab waveguide. Thus, for single mode propagation for most practical materials the single mode operation criterion is $d < \lambda/2$. On the other hand, the waist size of the Gaussian beam of the source depends on the radiation wavelength. The theory predicts and the conducted experiments confirm that the diameter of the Gaussian beam used in our experiments is directly proportional to the operation wavelength. Particularly, in our THz setup we have measured that beam FWHM is about $2.5 \cdot \lambda$. For high coupling efficiency the waveguide width should be comparable to the waist of the source beam, and hence, $d \sim 2.5 \cdot \lambda$, which contradicts the above mentioned criterion for single mode propagation in a solid slab waveguide. Thus, in a single slab waveguide single mode operation usually comes at a price of a very low excitation efficiency of the fundamental core mode.

In a stark contrast with solid slab waveguides, the multilayer porous waveguide can be designed to be arbitrarily large in size and still guide only a single mode. Particularly, in the porous waveguides where higher refractive index (solid) layers of refractive index n_2 are separated with lower refractive index (air) layers n_1 (assumed to be of the same material as the cladding), then single mode operation condition becomes [110]:

$$k \cdot d \cdot \sqrt{n_2^2 - n_1^2} \sqrt{\delta_2} < \pi, \quad (3.2)$$

where $\delta_2 = d_{solid} / (d_{solid} + d_{air})$ is the relative size of the solid layers in the solid/air bilayer and d is the total height of the waveguide. This expression is derived in the limit when both the solid and air layers are deeply subwavelength. For the transverse electric field distribution of the fundamental mode of the porous waveguide see Figure 3.2. For the single mode criterion in terms of the waveguide size we then get:

$$d < \lambda / \left(2\sqrt{n_2^2 - n_1^2} \sqrt{\delta_2} \right) \quad (3.3)$$

Thus, by choosing a small enough relative size of the higher-refractive-index layers we can increase the transverse size of the waveguide to the required lever while preserving its single mode guiding regime.

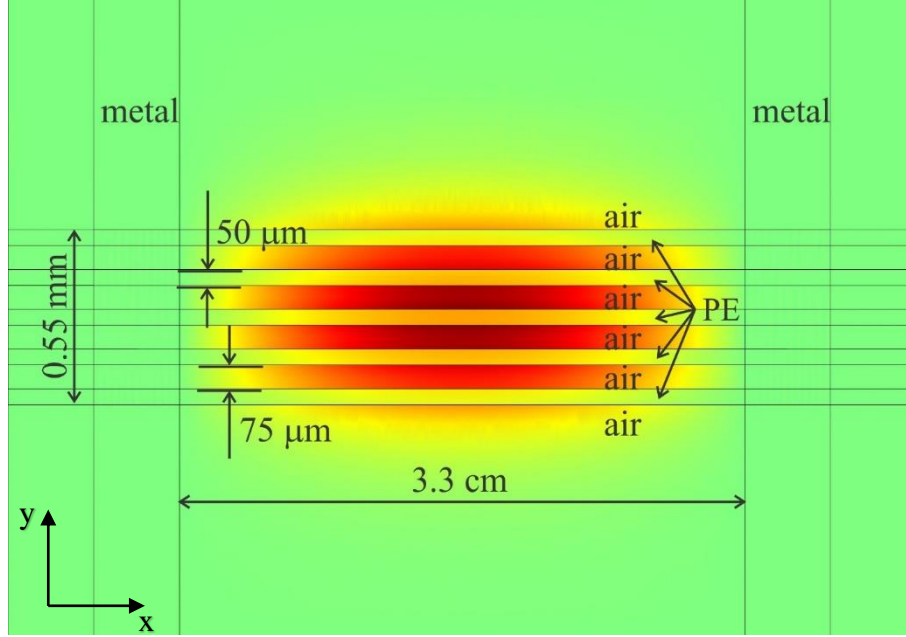


Figure 3.2 Transverse electric field distribution of the fundamental mode of the porous waveguide.

3.4 Details of the numerical modelling of the modal fields

In the following sections we explain the transmission features of planar porous waveguides using semi-analytical theoretical model. In what follows the distribution of the transverse E-field components $\vec{E}_{output} = (E_{output}^x, E_{output}^y)$ at the output facet of a waveguide of length L_w is modeled as the coherent superposition of the N guided modes:

$$\vec{E}_{output}(x, y, \omega) = \sum_{m=1}^N C_m \cdot \vec{E}_m(x, y, \omega) \cdot \exp\left(i \frac{\omega}{c} \cdot n_{eff,m} \cdot L_w\right) \cdot \exp\left(-\frac{\alpha_m L_w}{2}\right) \quad (3.4)$$

where $\vec{E}_{output} = (E_{output}^x, E_{output}^y)$ stands for the transverse field components of the m -th guided mode, x -axis and y -axis correspond to the horizontal and vertical directions in the Figure 3.2 and the

subsequent figures. The variables α_m and $n_{eff,m}$ denote respectively the power loss coefficient and the real effective index of the m-th mode at a given frequency ω . The variable C_m refers to the normalized amplitude coupling coefficients computed from the overlap integral of the respective flux distributions of the m-th mode with that of the 2D Gaussian beam of the source. Specifically, the definition of C_m is based on the continuity of the transverse field components across the input interface (i.e. cross-section of the subwavelength waveguide) between the incident beam and the excited fiber modes [110]:

$$C_m = \frac{1}{4} \int_{wc} dx dy \left(\mathbf{E}_m^*(x, y) \times \mathbf{H}_{Input}(x, y) + \mathbf{E}_{Input}(x, y) \times \mathbf{H}_m^*(x, y) \right) \times \\ \times \frac{1}{\sqrt{\frac{1}{2} \text{Re} \int_{wc} dx dy \left(\mathbf{E}_m^*(x, y) \times \mathbf{H}_m(x, y) \right)}} \cdot \frac{1}{\sqrt{\frac{1}{2} \text{Re} \int_{wc} dx dy \left(\mathbf{E}_{Input}^*(x, y) \times \mathbf{H}_{Input}(x, y) \right)}} \quad (3.5)$$

To model the field structure of the source, we assume a y-polarized 2D Gaussian beam along the y-direction and uniform in x-direction whose fields are normalized to carry power P:

$$\vec{E}_{Input}(x, y) = \vec{n}_x \cdot \sqrt{\frac{2P}{\pi\sigma^2}} \cdot \exp\left[-\frac{y^2}{2\sigma^2}\right] \quad (3.6)$$

$$\vec{H}_{Input}(x, y) = \vec{n}_y \cdot \frac{1}{\sqrt{\mu_0 / \epsilon_0}} \cdot \sqrt{\frac{2P}{\pi\sigma^2}} \cdot \exp\left[-\frac{y^2}{2\sigma^2}\right] \quad (3.7)$$

where the Gaussian beam waist parameter σ is related to the full-width at half-maximum by field as $FWHM = 2\sigma\sqrt{2 \cdot \ln 2}$, \vec{n}_x and \vec{n}_y are unit vectors, and $\sqrt{\mu_0 / \epsilon_0}$ is the intrinsic impedance of vacuum. The frequency dependence of the beam waist was measured independently and then fitted by a linear function of the input wavelength with a result $\sigma \approx 2.5 \cdot \lambda$. This model was subsequently used in the following simulations.

3.5 Measurement setup

All the data in our experiments was acquired using a modified THz-TDS (Time-Domain Spectroscopy) setup. The setup consists of a frequency-doubled femtosecond fiber laser (MenloSystems C-fiber laser) used as a pump source and identical GaAs dipole antennae used as source and detector yielding a spectrum range ~0.1 to 1.5 THz.

In contrast with a standard arrangement of most THz-TDS setups where the configuration of parabolic mirrors is static, our setup has mirrors mounted on the translation rails. This flexible geometry allows measurement of the waveguides up to 45 cm in length without any realignment. Figure 3.3 illustrates the experimental setup where the planar waveguide is placed between the focal lines of the two Teflon cylindrical lenses. The cylindrical lenses change the transverse profile of the Gaussian beam from the source by reshaping it into the beam uniform in the direction of the waveguide layers and Gaussian in the perpendicular direction, which is then launched into the planar waveguide core. The metal slit before the waveguide input facet is used to avoid propagation along the upper and lower surfaces of the waveguide. The width of the slit is 1.5 mm, which is higher than the major part of the studied wavelength range, thus, the diffraction effects can be significant only for frequencies below 0.2 THz. Slit's dimension was adjusted experimentally so that the spectra measured with and without it are practically the same.

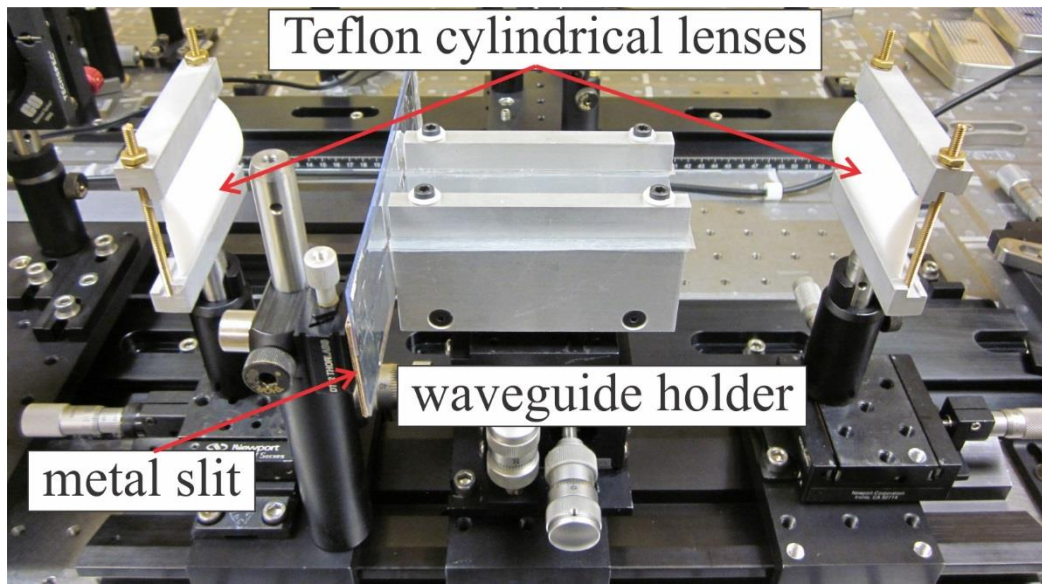


Figure 3.3 Experimental THz-TDS setup with the waveguide fixed between two cylindrical Teflon lenses.

3.6 Polyethylene refractive index and absorption losses

In order to model the optical properties of the waveguide, first, we have measured the transmission and absorption through the commercial polyethylene (LDPE) bulk material used in the waveguide fabrication. Characterization of refractive index and absorption losses was performed with a THz-time domain spectroscopy (TDS) setup using thick polymer slabs with

parallel interfaces. The sample was prepared by cutting and polishing a 1.5 cm thick slice of the PE rod.

The refractive index and absorption losses of polyethylene were retrieved by fitting the predictions of a transfer matrix model to the experimental transmission data [113]. The determined refractive index is largely constant between 0.10 and 1.00 THz and equal to $n_{PE} = 1.514$. Power absorption losses in cm^{-1} of polyethylene increase quadratically as a function of frequency, and for simplicity it can be fitted as $\alpha_{PE, \text{slabs}} [\text{cm}^{-1}] \approx 0.28 \cdot f^2 [\text{THz}]$ (see Figure 3.4), where f is the frequency in THz. The absorption losses rapidly increase with frequency, therefore, the propagation length (defined at the 1/e of original intensity) in bulk plastic is about 3 meters for 0.1 THz frequency and only 3 cm for 1 THz.

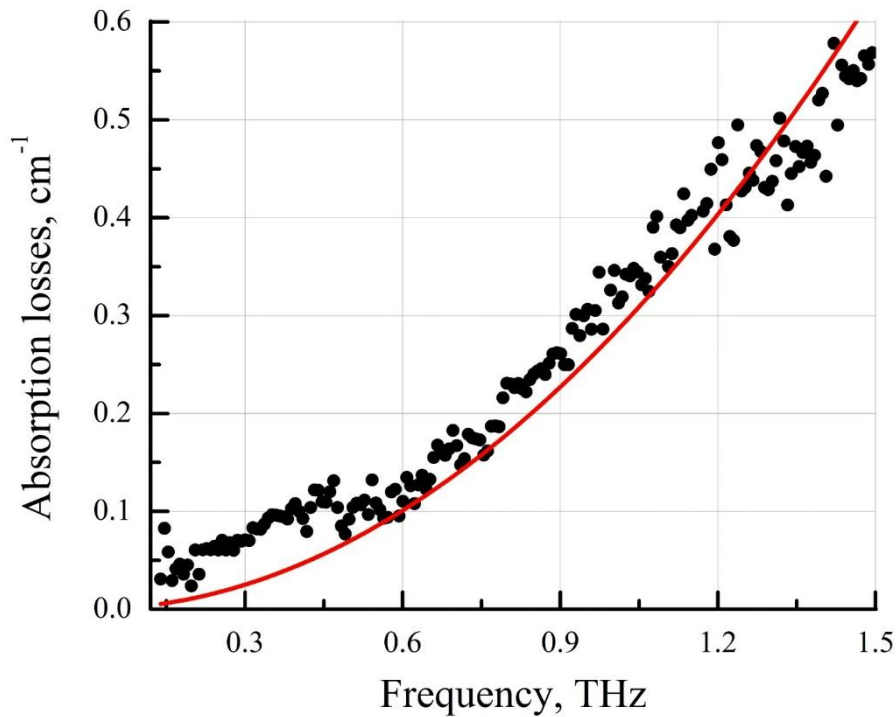


Figure 3.4 Absorption losses of the bulk polyethylene. Red line – quadratic fitting curve.

Note that polyethylene losses measured using bulk samples (polished slabs from the large diameter cylindrical rods) are typically consistently smaller than the losses of polyethylene films extruded from the same material. We believe that this can be explained by the difference in the surface roughness of polished slabs and films. From the experiments previously conducted in our group we found that losses of thin films can be 2-4 times larger than those of the polished slabs

made of the same material. Further studies are necessary to understand this discrepancy. From numerical simulations that follow we find that the best fit with the experimental data is achieved when absorption losses of the polyethylene films are taken as $\alpha_{PE,films}[cm^{-1}] \approx 0.89 \cdot f^2[THz]$.

3.7 Waveguide transmission and dispersion measurements

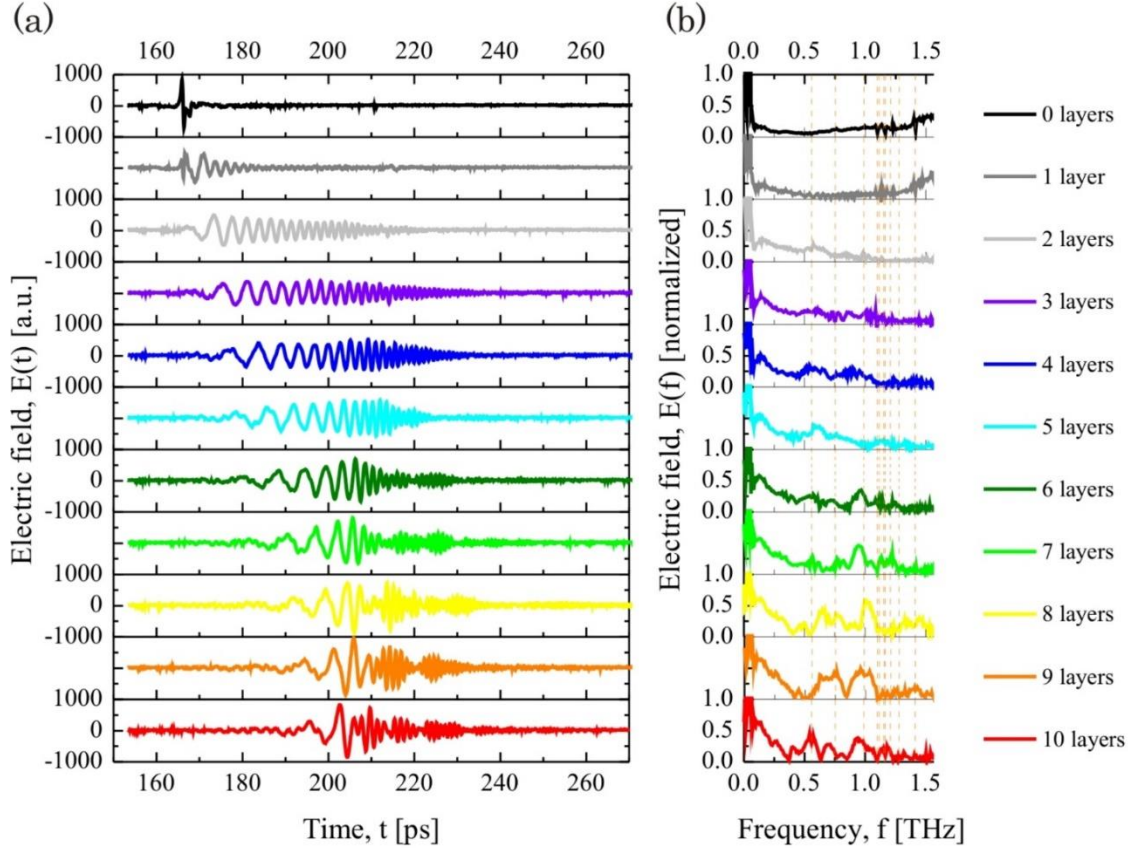


Figure 3.5 Experimentally measured electric field (a) in time domain and (b) in frequency domain at the output of the waveguide for different number of layers in the waveguide core. Black line corresponds to the absence of the waveguide.

In Figure 3.5 we present experimentally measured electric field at the output of the waveguides having different number of layers in the core. Interestingly, we note that increasing the number of layers also increases the bandwidth of the waveguides, from 0.15 – 0.6 THz for a one layer waveguide to 0.15 – 1.5 THz for a ten layer waveguide. Regardless of the number of layers all the spectra exhibit small oscillations in transmission (see Figure 3.5 (b)). Also there are some pronounced dips in the transmission spectra, with their number and depths depending on the number of layers in the waveguide. Thus, there is just one transmission peak for waveguides having

1 to 3 layers, two transmission peaks for waveguides having 4 to 6 layers and three peaks for the waveguides with the number of layers larger than 7. As we will see in the upcoming sections, spectral dips signify the onset of multimode guidance for waveguides with larger core sizes (larger number of layers in the core).

Experimentally measured electric field in time domain at the output of the waveguide (see Figure 3.5 (a)) allows direct measurement of the waveguide dispersion. The dispersion is proportional to the increase of the pulse duration and inversely proportional to the pulse bandwidth and the length of the waveguide. However, it is somewhat difficult to define exactly the starting and finishing points of the pulse, leading to high relative error in the dispersion estimation. The approximate dispersion values extracted from the experimental data don't exceed 1 ps/(THz•cm) which is significantly lower than typical dispersion values for slab waveguides of the comparable dimensions.

Small temporal spreading of the short terahertz pulse is important to maintain high signal-to-noise ratio when transmitting over appreciable distances. Dispersion of the fundamental core mode of the infinite waveguide can be estimated analytically. For a waveguide with size d , having a cladding refractive index n_1 , and a porous core made of the two layers with the refractive indices n_2 and n_1 , and the relative size of the solid layers in the solid/air bilayer δ_2 , the dispersion is [110]:

$$D \simeq \frac{1}{c} \frac{\Delta \varepsilon_{porous}}{4n_1 \omega} \gamma (1 - \xi \gamma) (3 - 4\xi \gamma) + O\left(\left(\frac{\omega}{\omega_{porous}}\right)^5\right) \quad (3.8)$$

where

$$\begin{aligned} \Delta \varepsilon_{porous} &= (n_2^2 - n_1^2) \cdot \delta_2 \\ \omega_{porous} &= \frac{c}{d} \frac{1}{\sqrt{\Delta \varepsilon_{porous}}} \\ \xi &= \frac{1}{3} + \frac{\Delta \varepsilon_{porous}}{16 \cdot n_1^2} \\ \gamma &= \frac{\omega^2}{(\omega_{porous})^2 + \xi \omega^2} \end{aligned} \quad (3.9)$$

Dispersion of the fundamental mode of the waveguide has been also computed using finite element simulation. Effective refractive index of the fundamental mode $n_{eff}(\omega)$ has been obtained in .COMSOL Multiphysics FEM software and, then, dispersion has been computed:

$$D = \frac{1}{c} \frac{\partial^2 (n_{eff}(\omega) \cdot \omega)}{\partial \omega^2} \quad (3.10)$$

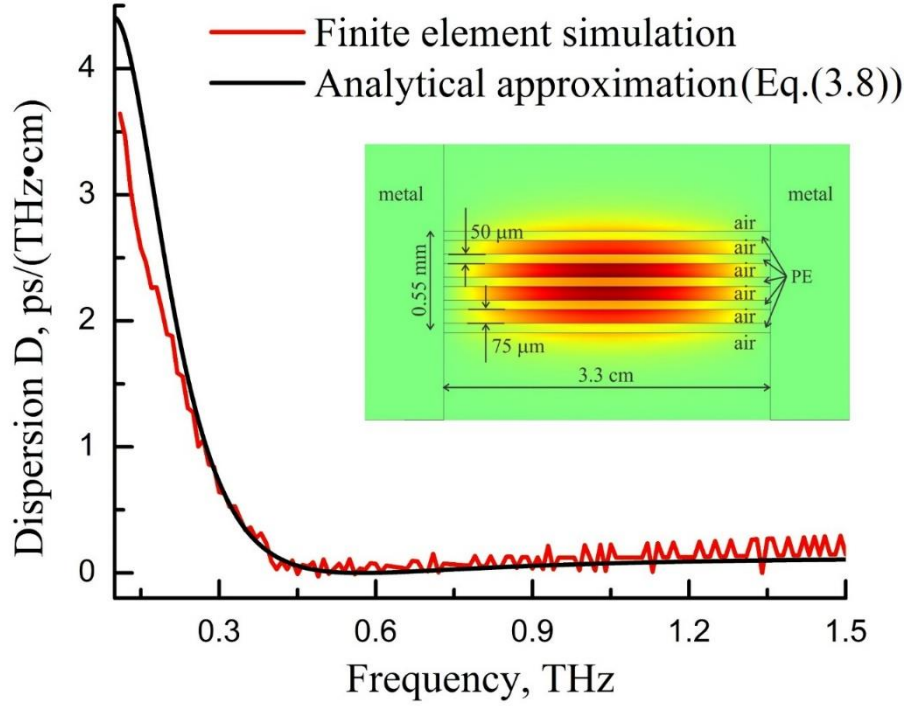


Figure 3.6 Dispersion of the fundamental mode of a porous waveguide; comparison between exact simulation and analytical approximation. Black line – analytically calculated dispersion (see Equation 3.8, red line – dispersion computed using finite element method. Layer width 50 μm , spacer width 75 μm , overall waveguide size 0.55 mm, 5 PE layers.

Comparison between waveguide dispersion obtained using two different approaches is presented in Figure 3.6 for the waveguide with 5 PE layers and overall thickness 0.55 mm. The Figure 3.6 shows an excellent match between the analytical and simulated results except for the low frequency region, where it becomes difficult to compute the waveguide mode in FEM software due to strong mode delocalization.

3.8 Fitting experimental transmission data with a theoretical model

We can now derive an expression for the intensity of the transmitted field as measured by the detector placed at the output facet of a waveguide in the absence of scattering losses:

$$\begin{aligned}
 T(\omega) &= \iint_{\text{waveguide}} \left| \vec{E}_{\text{output}}(x, y, \omega) \right| \cdot dx dy = \\
 &= \iint_{\text{waveguide}} \left| \sum_{m=1}^N C_m \vec{E}_m(x, y, \omega) \cdot \exp\left(i \frac{\omega n_{\text{eff},m} L_w}{c}\right) \cdot \exp\left(-\frac{\alpha_m L_m}{2}\right) \right|
 \end{aligned} \tag{3.11}$$

To study numerically the propagation in the planar porous waveguides we imported its cross-section into COMSOL Multiphysics FEM software and then solved for the complex effective refractive indices and field profiles. Coupling coefficients were computed for each mode as overlap integrals between the modal fields and the fields of a 2D Gaussian beam. Relative transmission through the waveguide was calculated at the waveguide center using Equation 3.11 and dividing it by the reference spectrum at waveguide input end.

In the horizontal direction the waveguide core is limited by the metal walls leading to the quantization of the modal wave vector in the transverse direction which is also equivalent to the appearance of the numerous side propagating modes. The nature of the side modes is easy to understand. We first consider an infinite slab waveguide that supports a single mode with refractive index n_0 . Note that direction of the mode wave vector \vec{k} can be anywhere in the plane of the waveguide core as long as both of its components satisfy the dispersion relation:

$$k_x^2 + k_z^2 = n_0^2 (\omega/c)^2 \tag{3.12}$$

When confining the mode in the x direction with metallic boundaries, this forces the transverse wave vector component to be quantized:

$$k_{x,p} \approx \frac{\pi(p-1)}{W} \tag{3.13}$$

which is equivalent to the quantization of the propagation directions of the same fundamental mode of a waveguide. W in (3.13) is the width of the waveguide and $p=1,2,3,\dots$ is the side mode number. Side modes are thus, nothing else as the same fundamental mode propagation at different angles with respect to the waveguide direction. In Eq. (3.13) the modal index $p=1$ corresponds to

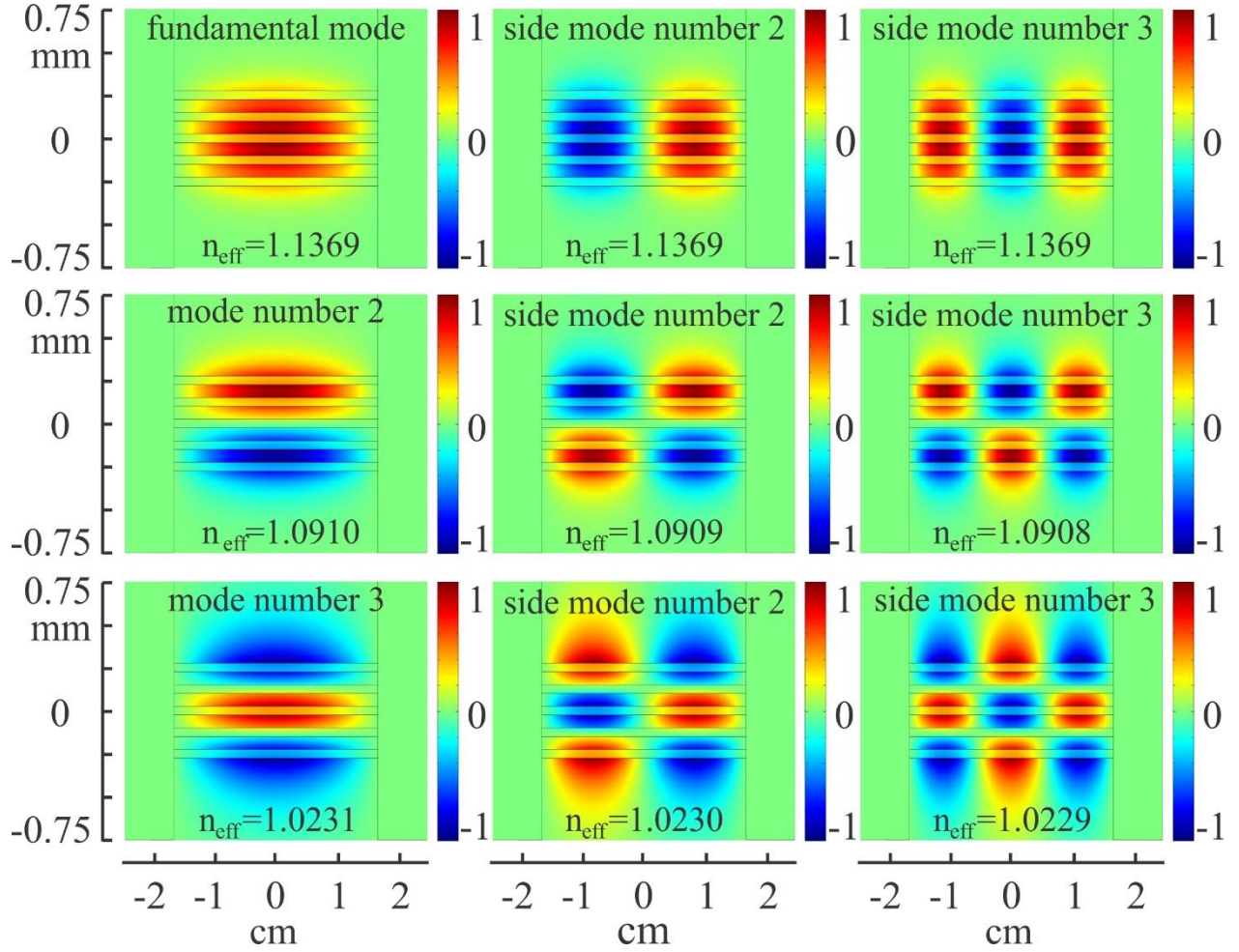


Figure 3.7 Transverse electric field distributions of the lower order modes of the waveguide. The modes in the second and third columns are defined as the side modes of the fundamental (top left) and higher order modes (other modes of the first column) in the text of the paper.

the mode propagating along the waveguide direction, and its refractive index is typically very close to that of the mode of an infinite planar waveguide. Refractive index of the side modes can be easily derived from the original dispersion relation (3.12) and the quantization condition (3.13) as:

$$\begin{aligned}
 k_{x,p}^2 + k_{z,p}^2 &= n_0^2 \left(\frac{\omega}{c} \right)^2 \Rightarrow \\
 \Rightarrow n_p &= \frac{k_{z,p} c}{\omega} = \sqrt{n_0^2 - \left(\frac{c k_{x,p}}{\omega} \right)^2} = \sqrt{n_0^2 - \left(\frac{\lambda(p-1)}{2W} \right)^2}
 \end{aligned} \tag{3.14}$$

where p is the side mode number, and W is width of the waveguide. We have verified that a very good agreement between analytical expression for the side mode dispersion relation (3.14) and

results of exact Comsol simulations are observed. Moreover, from the modal field structure of the 2D Gaussian beam and the field structure of the side modes (see Figure 3.7) it is clear that there is a simple approximate relation between the coupling coefficients from the Gaussian beam into the side mode of the p 's order. Particularly:

$$C_p = \begin{cases} C_1 / p & ; \quad p = 2n + 1 \\ 0 & ; \quad p = 2n \end{cases}, \quad (3.15)$$

where C_1 is the coupling coefficient into the fundamental mode of a metal bounded waveguide. We have verified that this simple analytical relation is in very good correspondence with the results of an exact Comsol simulation.

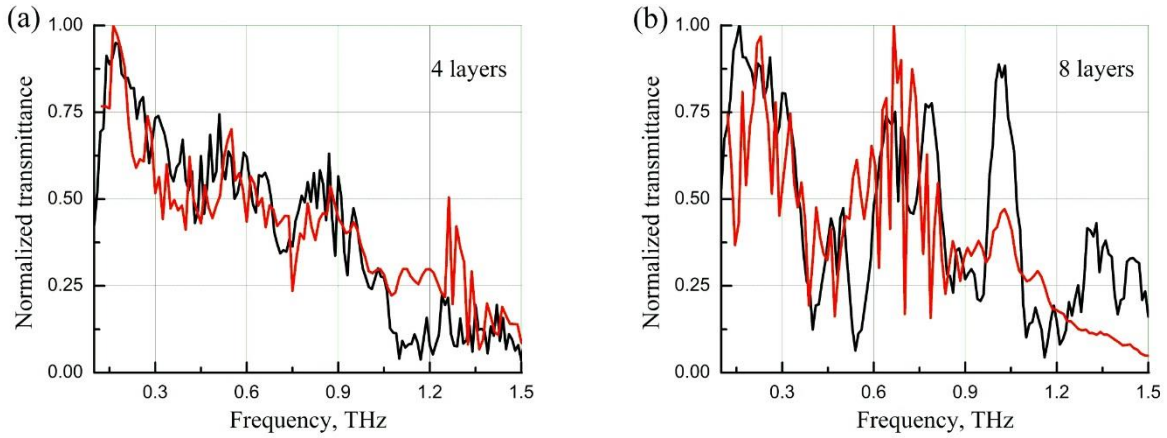


Figure 3.8 Black line – normalized experimental transmittance, red line – theoretical normalized transmittance (a) 4 layers waveguide, 11 cm length, (b) 8 layers waveguide, 11 cm length

Comparison of the numerical simulations of spectral transmission through the 11 cm long waveguide to the experimental data is depicted in Figure 3.8 for several waveguides having different number of layers in the core region. The presence of small oscillations in the transmission curves can be clearly attributed to the presence of a large number of side modes corresponding to the same mode of an infinite planar waveguide. At the same time, the presence of more pronounced dips in the transmission spectrum can be unambiguously explained by appearance of the higher-order waveguide modes and their destructive interference with the fundamental mode of a waveguide in the vicinity of their cutoff frequencies due to large mismatch in their effective

refractive indices. Overall, we observe a good comparison between experimental and numerical results.

3.9 Conclusion

Planar porous waveguides featuring a periodic sequence of the subwavelength material layers separated with air regions are proposed as waveguides for THz radiation. A large fraction of the modal fields in these waveguides is guided in the low-loss air region, thus effectively reducing the waveguide transmission losses. Convenient access to the modal fields in the air regions and on the waveguide surface makes them useful for sensing of biological and chemical specimens in the THz region. The transmission and absorption properties of such waveguides have been investigated both experimentally using THz-TDS spectroscopy and theoretically using finite element software. Good agreement between experimental data and theoretical results has been achieved.

CHAPTER 4 ARTICLE 2: TWO-WIRE TERAHERTZ FIBERS WITH POROUS DIELECTRIC SUPPORT

This chapter is based on my paper “Two-wire Terahertz fibers with porous dielectric support,” published in Optics Express in 2013. There are no other contributors to this article besides me and my research supervisor. Therefore, my role in this article includes all the aspects of the novel fiber design starting from the initial idea, through the preliminary simulations and fiber geometry optimization to the resulting fiber characterization and analysis.

In this chapter, a novel plasmonic THz fiber is described that features two metallic wires that are held in place by the porous dielectric cladding functioning as a mechanical support. This design is more convenient for practical applications than a classic two metal wire THz waveguide as it allows direct manipulations of the fiber without the risk of perturbing its core-guided mode. Not surprisingly, optical properties of such fibers are inferior to those of a classic two-wire waveguide due to the presence of lossy dielectric near an inter-wire gap. At the same time, composite fibers outperform porous fibers of the same geometry both in bandwidth of operation and in lower dispersion. Finally, by increasing cladding porosity one can consistently improve optical properties of the composite fibers.

4.1 Introduction

The main complexity in designing terahertz waveguides is the fact that almost all materials are highly absorbent in the terahertz region [31]. Since the lowest absorption loss occurs in dry air, an efficient waveguide design must maximize the fraction of power guided in the air. Different types of THz waveguides and fibers have been proposed based on this concept. The simplest subwavelength fiber [32-34] features dielectric core that is much smaller than the wavelength of guided light. As a result, a high fraction of modal power is guided outside of the lossy material and in the low-loss gaseous cladding. Another type of the low-loss fibers includes fibers featuring porous core region with the size of the individual pores much smaller than the wavelength of light [32, 33]. Consequently, guided light has a strong presence in the low-loss gas-filled pores inside the core. High modal confinement in the core makes such fibers less prone to bending losses and less sensitive to the environment compared to the simple rod-in-the-air subwavelength fibers [32, 35]. Another important type of the low-loss fibers includes fibers featuring gas-filled core

surrounded by a structured cladding serving as a reflector. The main challenge in the design of such fibers is to ensure high reflection at the core-cladding interface. Different hollow-core structures have been investigated including metalized bores [35-37], periodic dielectric multilayers [38], as well as thin-walled dielectric pipes [39,41,42]. Among other types of the THz waveguide, we note parallel plate waveguides [43] and slit waveguides [44], which are known for their low transmission losses and high mode confinement.

Metal wire, can be used to transport terahertz pulses with virtually no dispersion and low attenuation [49]. However, it is difficult to realize efficient coupling into the wire-bound mode. This is because the fundamental mode of a single wire is radially polarized, thus, commonly used photoconductive antennas that tend to produce linearly polarized THz light cannot be used directly for efficient excitation of the wire mode. In addition, high bending losses of a single wire waveguide limit its practical applications. Thus, even a slight bending of the wire can lead to considerable increase in the modal transmission loss, e.g. from 0.03 cm^{-1} for a straight wire to 0.05 cm^{-1} for a slightly bend one (bending radius of 90 cm, [15]).

Metal wire, can be used to transport terahertz pulses with virtually no dispersion and low attenuation [14]. However, it is difficult to realise efficient coupling into the wire-bound mode. This is because the fundamental mode of a single wire is radially polarized, thus, commonly used photoconductive antennas that tend to produce linearly polarized THz light cannot be used directly for efficient excitation of the wire mode. In addition, high bending losses of a single wire waveguide limit its practical applications. Thus, even a slight bending of the wire can lead to considerable increase in the modal transmission loss, e.g. from 0.03 cm^{-1} for a straight wire to 0.05 cm^{-1} for a slightly bend one (bending radius of 90 cm, [50]).

The two-wire waveguides [30] combine low loss performance and high excitation efficiency. Particularly, field distribution in the fundamental transverse-electromagnetic (TEM) mode of a two-wire waveguide (see Figure 4.1) has the same symmetry as that of an electromagnetic wave emitted by a simple THz dipole source (photoconductive antenna) when the wave is polarised along the line joining the two wires. Thus, one expects high excitation efficiencies of the fundamental mode of a two-wire waveguide when using standard dipole terahertz sources. Moreover, efficient confinement of the modal energy between the two wires, as opposed to highly delocalised Sommerfeld wave on a single wire, makes two-wire waveguides less

prone to the bending losses. Thus, for the same bending radius, bending loss of a single wire waveguide can be more than 5 times higher than that of a two-wire waveguide [30]. Additionally, absorption losses, and group velocity dispersion (GVD) of the fundamental mode of a two-wire waveguide are extremely low (see the simulation results in Figure 4.2).

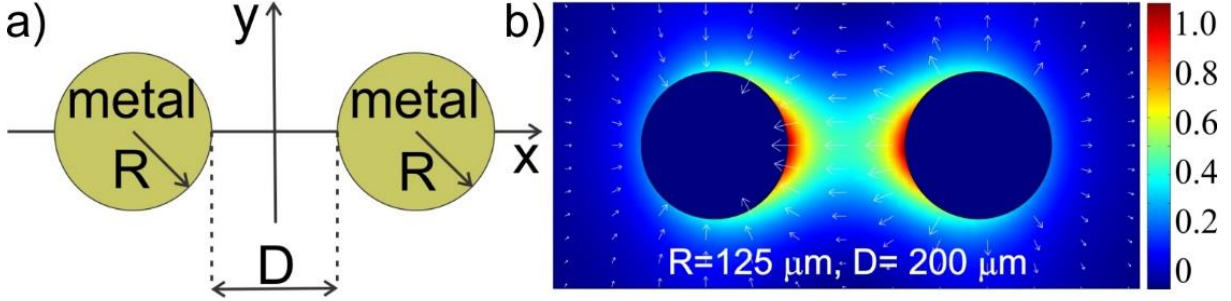


Figure 4.1 a) Schematic of a classic two-wire waveguide. b) Longitudinal flux distribution for the TEM mode of a two-wire waveguide. Arrows show vectorial distribution of the corresponding transverse electric field.

While having outstanding optical properties, a classic two-wire waveguide is inconvenient in practical applications. Thus, in a typical experiment the two wires have to be aligned and kept straight and parallel to each other with high precision. This requires bulky holders and cumbersome coupling setups. Moreover, the fiber core is not encapsulated into a protective cladding, thus leaving the core (space between wires) exposed to the environment.

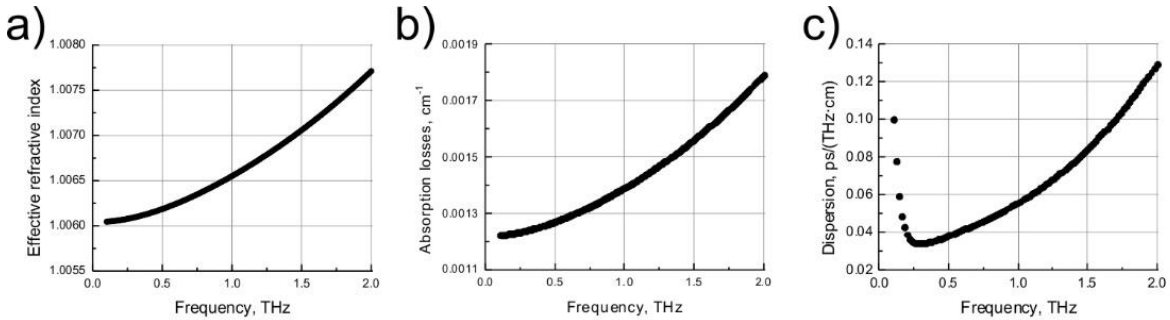


Figure 4.2 a) Effective refractive index, b) absorption losses and c) group velocity dispersion of the fundamental mode of a two metal wire waveguide shown in Figure 4.1.

In this paper, we explore several practical designs of the two-wire waveguides for THz guidance. Particularly, we aim at designing two-wire waveguides that are more convenient to manipulate mechanically without disturbing the structure of the guided mode, while retaining as much as possible the outstanding optical properties of a classic two-wire waveguide. The proposed waveguide structure consists of a porous polyethylene fiber and two metal wires that are positioned

inside of a porous cladding. In its simplest implementation, a polyethylene fiber has three interconnected circular holes, among which the central hole is empty and the two peripheral holes are filled with the metal wires. Designs that are more complex feature a larger number of holes or a web of thin bridges in the air that are arranged within the fiber outer jacket. The metal wires are placed into two fiber holes with an inter-hole separation comparable to the wire diameter. In all these designs, a significant fraction of the modal power is propagating in the air-filled porous core, which reduces the modal absorption losses as well as the modal group velocity dispersion. Finally, we believe that fibers described in this paper can be useful not only for low-loss THz wave delivery but also for sensing of biological and chemical specimens in the terahertz region by placing the recognition elements directly into the fiber microstructure similarly to what has been recently demonstrated in [112].

Several experimental studies have been reported so far that studied propagation of THz pulses in composite metal-dielectric air-core fibers. Thus, in [114, 115] we have reported a polyethylene fiber featuring three interconnected holes and two small copper wires of 250 μm diameter (see Figure 4.4). The wires had a small 200 μm air gap between them, which served as a fiber core. Strong polarisation sensitivity of a three-hole composite fiber was confirmed. Moreover, we have clearly observed significant degradation of the composite fiber optical properties compared to those of a classic two-wire waveguide. Our preliminary experimental work has prompted this theoretical study where we quantify in a systematic manner the impact of porous plastic cladding on the properties of a two-wire composite waveguide.

Most recently in [61], another research team has reported a metal-dielectric composite waveguide featuring two large indium wires placed into a large hollow plastic tube. The inter-wire separation in that work was $\sim 2\text{mm}$, which is 10 times larger than in our work [114, 115]. Although the two waveguides in [114, 115] and in [61] might appear similar, their guiding mechanisms are significantly different. Thus, the small core fiber in [114, 115] shows significant polarisation sensitivity and modal refractive index larger than that of air, which signifies plasmonic guidance. In contrast, the large core fiber [61] shows low polarisation sensitivity and modal refractive index smaller than that of air, which is typical for the ARROW type modes of a plastic tube modified by the presence of metallic inclusions. In fact, one can demonstrate that there is a fundamental connection between the two fibers in [114, 115] and [61]. Particularly, by shrinking the size of a

large fiber [61] by a factor of 15, one can change its guidance regime from ARROW-like to plasmonic-like reported in [114, 115].

In this paper, we concentrate on the plasmonic guidance regime of a two-wire composite fiber. As a departure point, we detail outstanding optical properties of a classic two-wire waveguide. Then, we add porous plastic cladding in order to improve waveguide handling and investigate the impact of cladding on the properties of a resultant plasmonic waveguide. Finally, we show that one can mitigate the negative impact of the plastic cladding on the optical properties of a composite waveguide by increasing cladding porosity.

4.2 Classic two-wire waveguide

Before we present the study of composite fibers, we would like to address the issue of coupling efficiency into a classic two-wire waveguide. From our experiments, we observe that this coupling is a sensitive function of the excitation wavelength. As it is well known, the coupling efficiency into a classic two-wire waveguide achieves its maximal value at the wavelength that is comparable to the inter-wire separation, while the coupling efficiency stays relatively low for the wavelengths that are significantly smaller or larger than the optimal one. For a detailed discussion see for example [57], where the authors used the mode-matching technique and a full-wave FEM numerical simulations to study this issue. Ultimately, the frequency dependent coupling efficiency limits practically usable bandwidth in such waveguides. Moreover, coupling efficiency into two-wire waveguides depends strongly on several geometric parameters such as position of the THz beam focal point, the width of the wires and the distance between them. For the completeness of presentation, we first study numerically the influence of each of these parameters on the waveguide excitation efficiency.

Modes of the waveguides and fibers studied in this work were computed using COMSOL Multiphysics FEM mode solver. The frequency dependent relative permittivity and conductivity of metal in the THz spectral range is modeled using the Drude formula:

$$\varepsilon(\omega) = 1 - \frac{\omega_p^2}{\omega^2 + i\omega\Gamma_{THz}} \approx -\frac{\omega_p^2}{\Gamma^2} + i \cdot \frac{\sigma}{\omega \cdot \varepsilon_0} \quad ; \quad \sigma_{THz} \approx \frac{\varepsilon_0 \omega_p^2}{\Gamma}, \quad (4.1)$$

where ε_0 is the free-space permittivity, ω is the angular frequency, ω_p is the angular plasma frequency, and Γ is the electron scattering rate. In our simulations we assume copper as a metal,

and we use the following values of the parameters: $\omega_p = 2\pi \cdot 1.969 \cdot 10^{15} \text{ Hz}$, $\Gamma = 2\pi \cdot 4.775 \cdot 10^{12} \text{ Hz}$ (derived from [116-118]). In the THz frequency range the Drude model is especially simple as it predicts frequency independent real part of the relative permittivity $\varepsilon_r = -1.7 \cdot 10^5$, and frequency independent conductivity $\sigma = 4.5 \cdot 10^7 \text{ S/m}$. We note that the choice of metal does not play a significant role at terahertz frequencies, since there is almost no field present inside metal wires due to extremely low skin depths in THz range.

Coupling efficiency into a two-wire waveguide (defined as a fraction of the coupled power to the power in the excitation beam) was computed similarly to our prior work [33] assuming as an excitation source a Gaussian THz beam with a frequency-dependent beam diameter $d_0 \approx 2.5 \cdot \lambda$. Efficient coupling of the Gaussian beam into the fundamental mode of a two-wire waveguide requires a linear polarization of the THz beam with electric field directed along the line connecting the two wires. As modal power in a two-wire waveguide is mainly confined between the wires, we expect the highest coupling efficiency when the Gaussian beam diameter is comparable to the size of the inter-wire gap.

In Figure 4.3, we present excitation efficiency of the fundamental mode of a two-wire waveguide using Gaussian beam as a source. We consider effect of the various geometric parameters on the coupling efficiency, including misalignment of the THz beam relative to the position of the wires, as well as choice of the wire radius and size of the inter-wire gap.

First, we study excitation of the fundamental TEM mode of a two-wire waveguide using Gaussian beam with the focal point displaced from the mid-point between the two wires (the point of maximal coupling efficiency). From Figure 4.3 (a) we see that displacement of the beam focal point along the OX axis by 100 μm leads to 20% decrease in the TEM excitation efficiency in the whole THz range, while displacement by 200 μm leads to 50% drop in the TEM excitation efficiency. The effect of displacement of the Gaussian beam focal point along the OY axis is much less pronounced [see Figure 4.3 (b)]. Thus, displacement of the beam focal point by 100 μm from the waveguide center leads to only 5% decrease in the TEM excitation efficiency. Remembering that the inter-wire gap size is 200 μm , we conclude that coupling efficiency is only moderately sensitive to the errors in the positioning of the Gaussian beam.

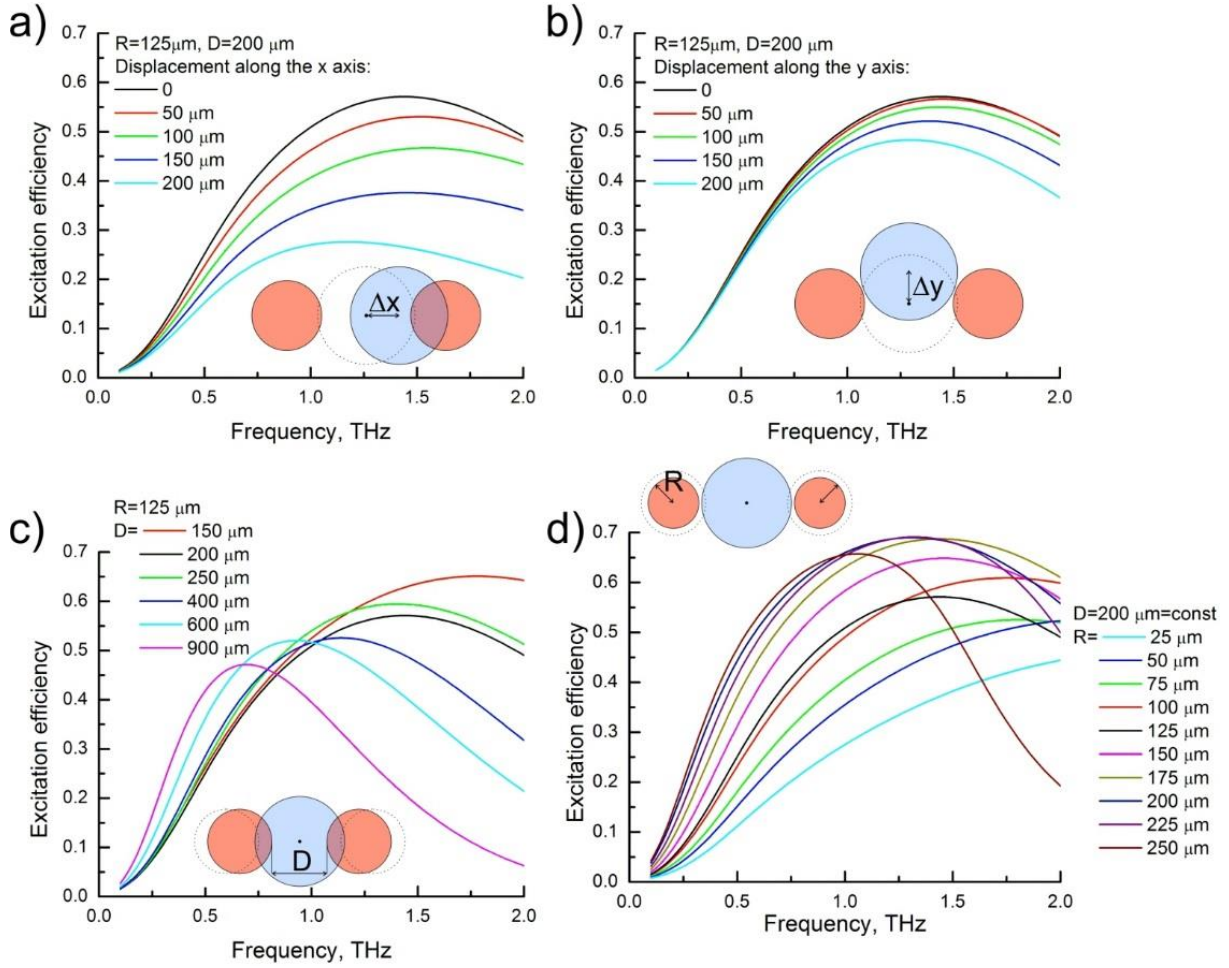


Figure 4.3 Excitation efficiency of the fundamental mode of a classic two-wire waveguide using Gaussian beam with a frequency-dependent beam diameter ω as an excitation source. Dependence of the excitation efficiency on various geometrical parameters, such as: a) displacement along the x axis from the core center; b) displacement along the y axis from the core center; c) inter-wire gap size; d) wire radius

We now examine excitation of the TEM mode using a perfectly centered Gaussian beam while varying distance between the two wires. From Figure 4.3 (c) we find that the TEM mode is excited most efficiently when the Gaussian beam waist is comparable to the size of the inter-wire gap. The excitation efficiency remains high 40 – 70% in the whole THz frequency range 0.5 – 1.5 THz when the inter-wire distance is 150 – 400 μm . Finally, for a fixed 200 μm gap between the two wires, in Figure 4.3 (d) we plot excitation efficiency as a function of the wire radii. For small values of the radius the excitation efficiency increases with the radius until reaching its maximal value at $R=200 \mu\text{m}$. Further increase of the wire radius leads to a monotonous decrease of the coupling efficiency.

4.3 Composite fiber featuring two metal wires in a three-hole porous cladding

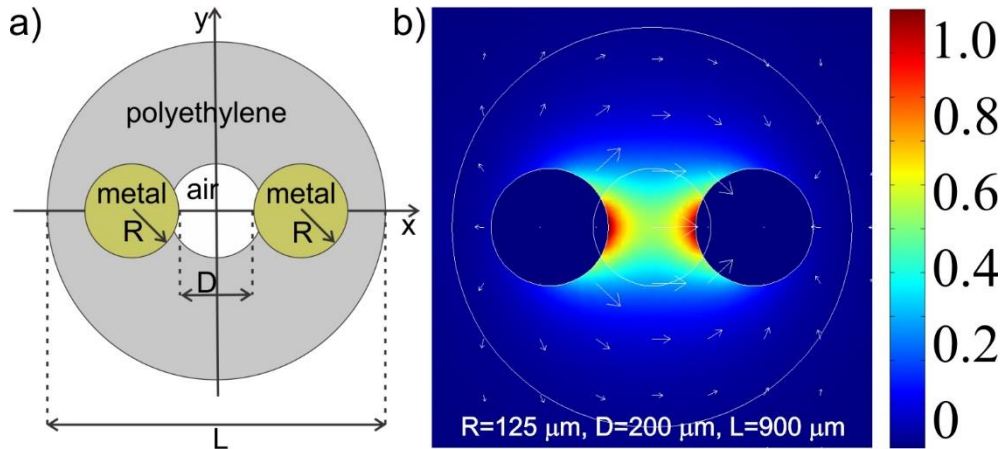


Figure 4.4 a) Schematic of a composite fiber featuring two metal wires in a three-hole cladding. b) Longitudinal flux distribution of a typical guided mode presents a mixture of the plasmonic mode guided by the metal wires and a TIR mode guided by the porous fiber cladding.

Presently, there are no fibers operating in the THz frequency range that are low-loss, low-dispersion, and broadband at the same time. The two-wire waveguides open a possibility for making practical THz fibers since they offer low-loss, low-dispersion transmission and good coupling efficiency to standard photoconductive antennas. Strong optical performance of the two-wire waveguides is a direct consequence of the modal confinement predominantly in the low-loss, low-dispersion dry gas between the two wires. At the same time, practical two-wire waveguides require some form of a robust mechanical support or overcladding in order to hold the metallic wires straight and parallel to each other, to optically separate the core region from the environment, and to provide encapsulation for the dry gas in the vicinity of the wires. We propose using porous polyethylene fibers that were demonstrated to exhibit excellent guiding characteristics at low frequencies [119-121] to provide a convenient packaging solution for the two-wire waveguides. In their simplest implementation such fibers can contain three adjacent holes with the two of them occupied by the metal wires, while the central one kept empty and used to guide a larger portion of the THz radiation (see Figure 4.4).

Naturally, the wave guiding in such fibers is most efficient for the light polarized parallel to the line connecting the wires. A typical modal pattern represents the mixture of a plasmonic mode guided by the two wires, and a TIR (total internal reflection) mode guided by the fiber plastic cladding (see Figure 4.4). For the perpendicularly polarized light, efficient excitation of the

plasmonic mode is not possible, and the fiber guides largely as a porous TIR fiber studied earlier [119]. In this work, we therefore concentrate only on the parallel polarisation.

The modal dispersion relations, the absorption losses, and the excitation efficiencies of the various modes of a composite two-wire fiber are presented in Figure 4.5 in black color. In our simulations we used 1.514 as a frequency independent refractive index of polyethylene with frequency dependent material loss $\alpha [cm^{-1}] = 0.28 \cdot f^2$ (operation frequency f is in THz).

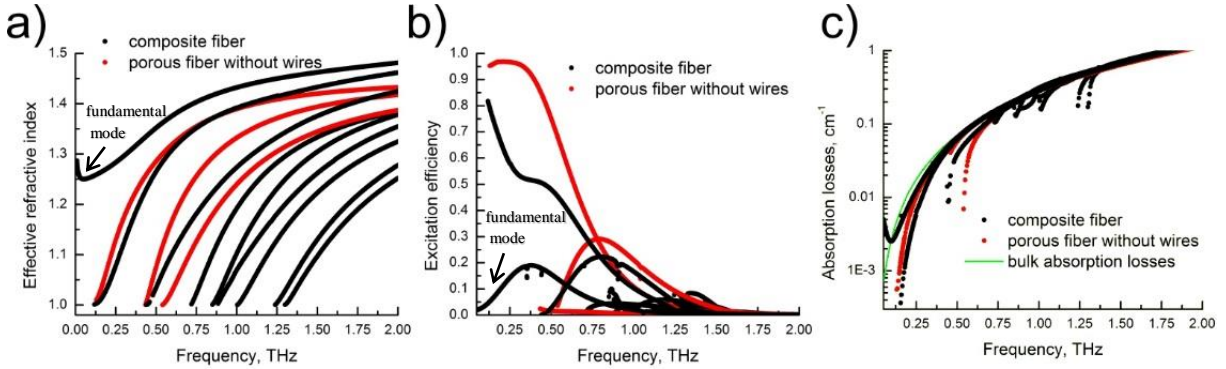


Figure 4.5 . Black color: the effective refractive indices, absorption losses and excitation efficiencies for the various modes of a composite two-wire fiber shown in Figure 4.4. Red color: various optical properties of the modes of a corresponding porous cladding (no metal wires).

The presence of porous polyethylene cladding significantly complicates the fiber modal structure. In order to distinguish predominantly plasmonic modes from the modes of a porous cladding, in Figure 4.5 we also present (in red color) optical properties of the modes of a porous cladding alone (no wires). Note that among the modes of a composite fiber, there is one that has no corresponding analogue among the modes of a porous cladding, which is especially evident at lower frequencies < 0.25 THz. In what follows, we call this mode a “fundamental plasmonic mode”. Note that addition of porous cladding shifts the frequency of maximal excitation efficiency of the fundamental plasmonic mode from 1.5 THz in a classic two-wire waveguide to a much lower frequency of ~ 0.4 THz in a composite fiber.

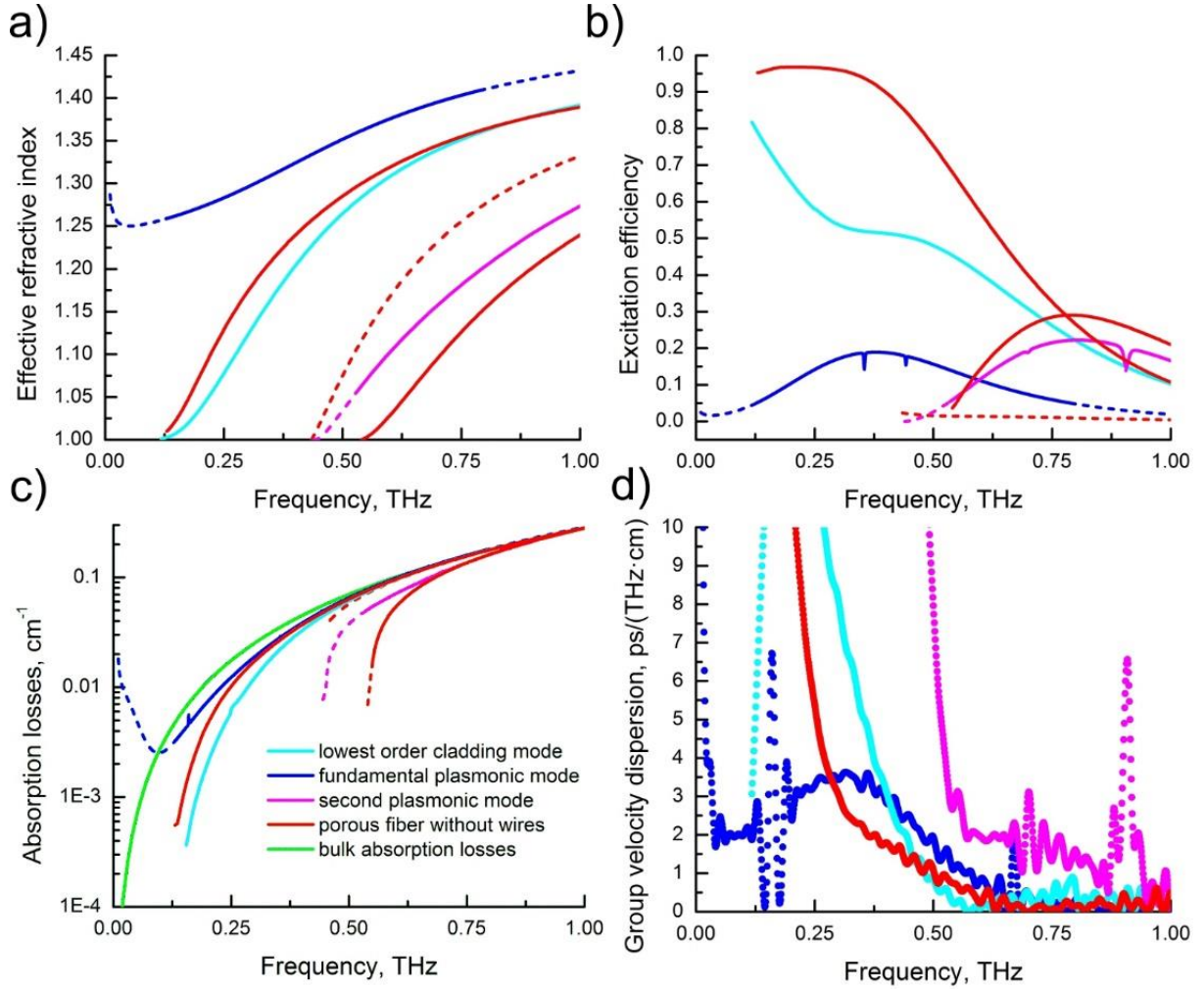


Figure 4.6 a) Effective refractive indices, b) excitation efficiencies, c) absorption losses and d) group velocity dispersion for the various modes of a composite two-wire fiber shown in Figure 4.4. Dips in the excitation efficiency versus frequency graph correspond to the frequencies of anticrossing between the plasmonic modes and the fiber cladding modes.

We now consider in more details the modes of a 3-hole composite fiber depicted in Figure 4.4. In Figure 4.6 we present again the effective refractive indices, the absorption losses and the excitation efficiencies of the composite fiber modes, however, this time we concentrate on the sub – 1 THz frequency range. Moreover, solid colors in Figure 4.6 define frequency ranges where modal excitation efficiency is higher than 5%, while dashed curves define spectral regions with less than 5% coupling efficiency from the Gaussian beam. In these simulations, we assume that the fiber center coincides with the focal point of a Gaussian beam.

First, we concentrate on the fundamental plasmonic mode of a composite fiber. Optical properties of this mode are presented in Figure 4.6 in blue color. Coupling efficiency into the fundamental plasmonic mode varies between 5% – 20% in the 0.13 – 0.79 THz frequency range. As shown in Figure 4.7, at lower frequencies 0.1 – 0.4 THz, electric field of the mode is mostly oriented along the line connecting the two wires, and the corresponding modal power is concentrated in the air-filled central hole. This results in modal losses that can be considerably smaller than the bulk absorption loss of polyethylene.

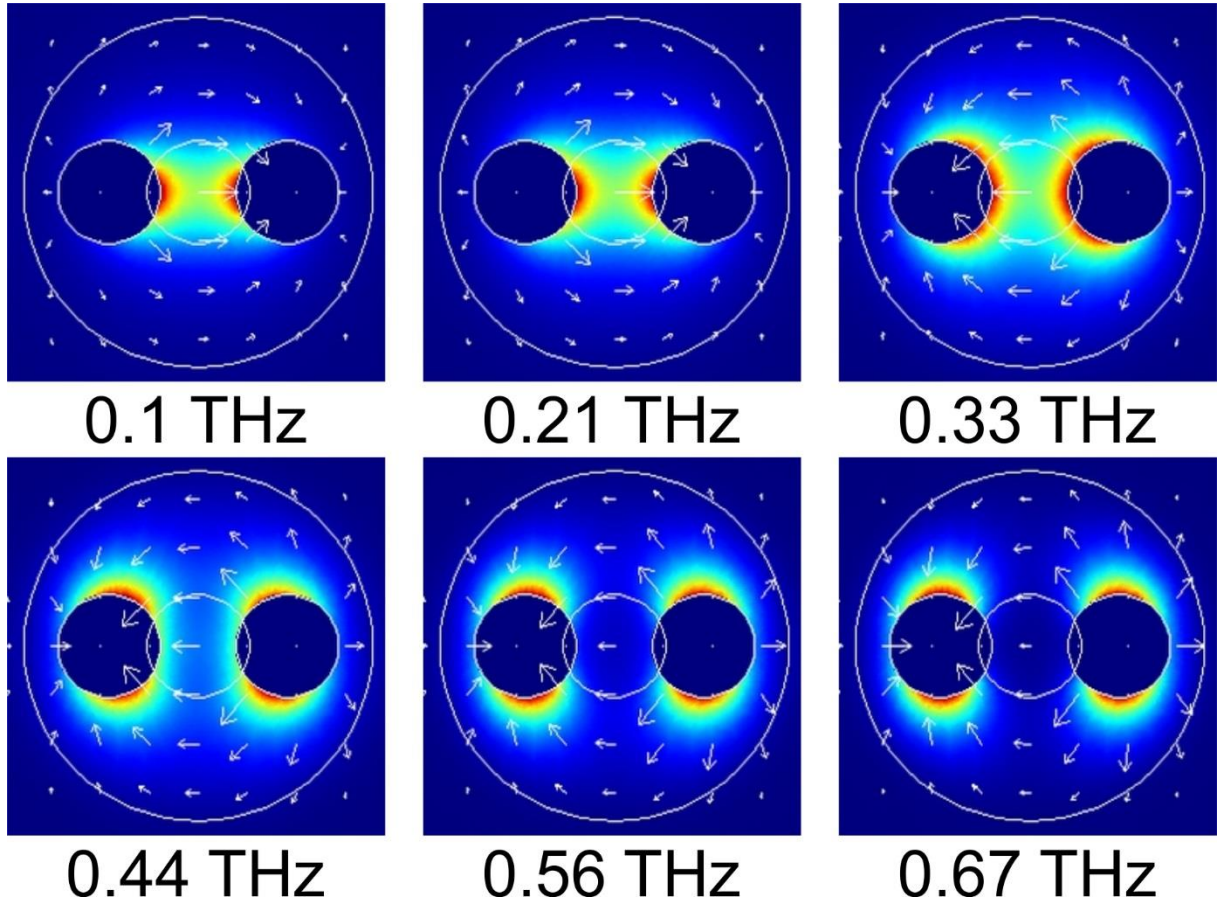


Figure 4.7 Longitudinal flux distribution of the fundamental plasmonic mode of a composite fiber at various operation frequencies. The flux is normalized at its maximal value at each frequency.

At higher frequencies (> 0.4 THz) the modal power is displaced away from the central air hole (see Figure 4.7) and into the polyethylene cladding surrounding the wires. Consequently, at higher frequencies absorption loss of the fundamental plasmonic mode approaches the bulk absorption loss of polyethylene. Furthermore, from the modal dispersion relation presented in

Figure 4.6 it follows that the group velocity dispersion of the fundamental plasmonic mode is $\sim 2 - 3 \text{ ps}/(\text{THz}\cdot\text{cm})$, which is much higher than that of a fundamental mode of a classic two-wire waveguide ($\sim 0.1 \text{ ps}/(\text{THz}\cdot\text{cm})$). The reason for the relatively high value of the group velocity dispersion of the fundamental plasmonic mode of a composite fiber is in the rapid change of the modal confinement pattern in the 0.1 - 0.8 THz range from mostly air at lower frequencies to both air and polyethylene at higher frequencies. At the same time, at lower frequencies ($< 0.3 \text{ THz}$), fundamental plasmonic mode of a composite fiber has a much smaller group velocity dispersion when compared to the $\sim 10 \text{ ps}/(\text{THz}\cdot\text{cm})$ dispersion of the fundamental mode of the corresponding porous fiber (without metal wires).

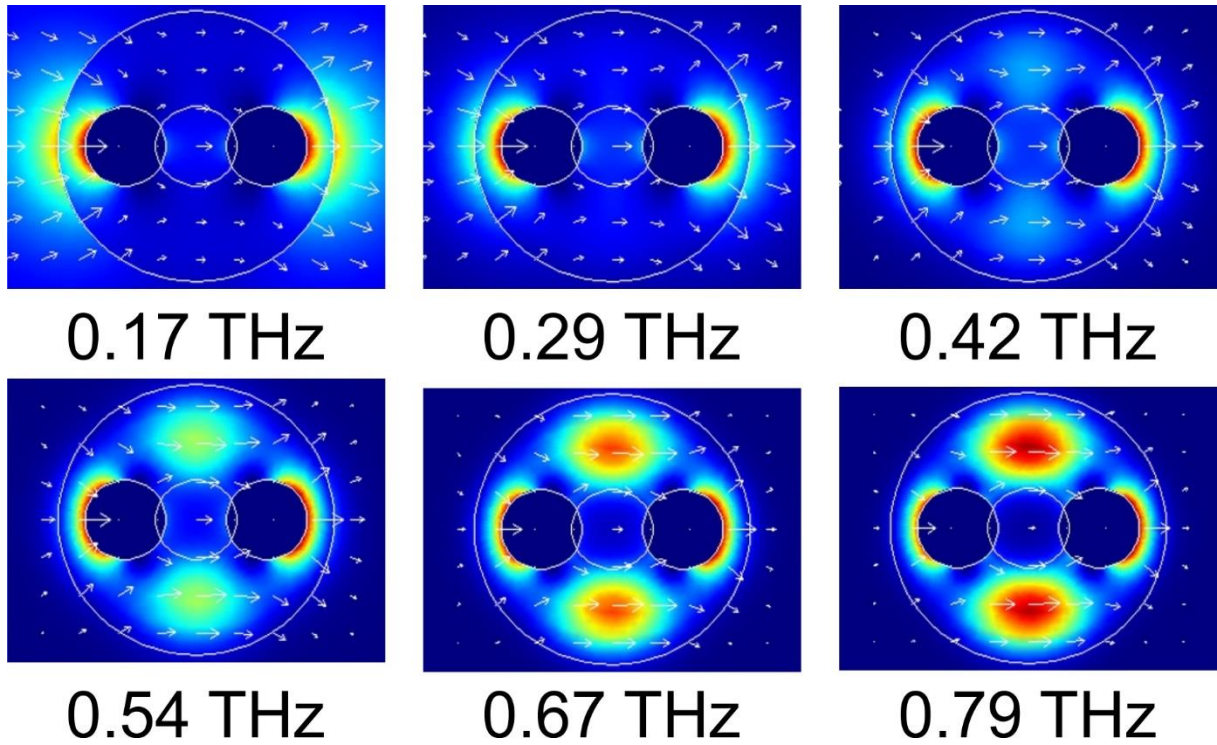


Figure 4.8 Longitudinal flux distribution of the lowest order cladding mode of a composite fiber at various frequencies. The flux is normalized at its maximal value at each frequency.

We now consider the lowest order cladding mode of a composite fiber in the 0.12 – 1.00 THz frequency range (cyan color in Figure 4.6). At lower frequencies ($< 0.3 \text{ THz}$) when operation wavelength is larger or comparable to the fiber size, the lowest order cladding mode has a strong presence outside of the fiber (see Figure 4.8). At higher frequencies, the modal fields tend to confine inside of the fiber cladding, thus resulting in the mode absorption losses similar to the bulk

absorption losses of the cladding material. Note that the lowest order cladding mode of a composite fiber is in fact a hybrid mode that has a significant plasmon contribution. For this particular mode, the plasmon is propagating at the plastic/metal interface with almost no energy found in the central air hole.

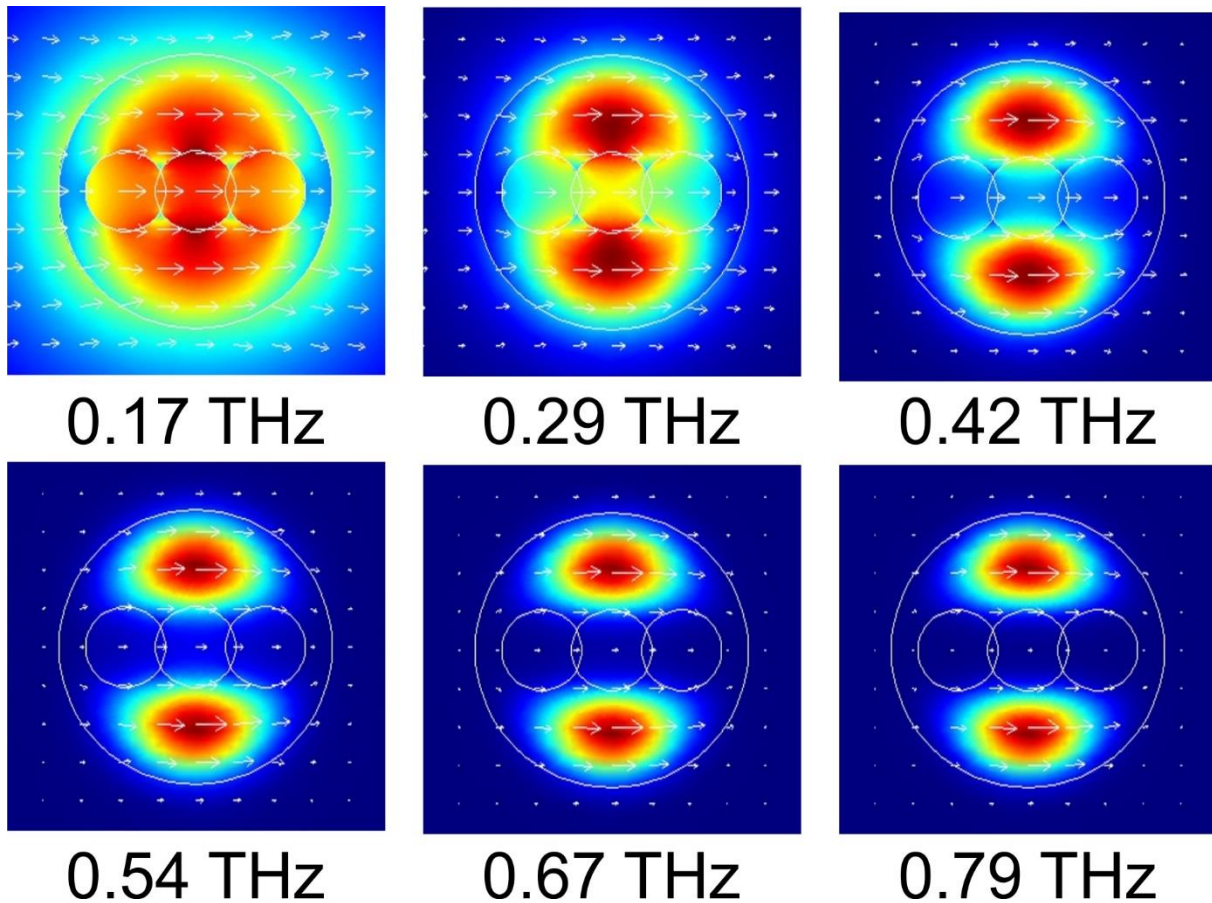


Figure 4.9 Longitudinal flux distribution of the fundamental mode of a porous fiber (same cross section as in Figure 4.4, however, without metal wires). The flux is normalized at its maximal value at each frequency.

It is interesting to compare cladding modes of a composite fiber with the modes of a porous fiber of the same cross section, however, without the metallic wires. Optical properties of the modes of a porous fiber are presented in Figure 4.6 in red color. We note that in the broad frequency range 0.13 – 1.0 THz, optical properties of the fundamental mode of a porous fiber are quite similar to those of the lowest order cladding mode of a composite fiber. At the same time, the corresponding field distributions are somewhat different at low frequencies. Thus, below 0.5 THz (see, for example, Figure 4.9, 0.17 THz), field distribution of the fundamental mode of a porous fiber shows

significant presence in the air cladding outside of the fiber, as well as in the air holes inside of a plastic cladding. In contrast, lowest order cladding mode of a composite fiber (see Figure 4.8, 0.17THz), shows no field presence in the central air hole between the two metal wires, while having significant field concentration in the air region outside of the fiber. At higher frequencies (Figure 4.8 and Figure 4.9, $> 0.5\text{THz}$) field distributions of the two modes become very similar to each other and feature strong light localisation in the plastic fiber cladding. Consequently, optical properties of the two modes also become very similar at higher frequencies.

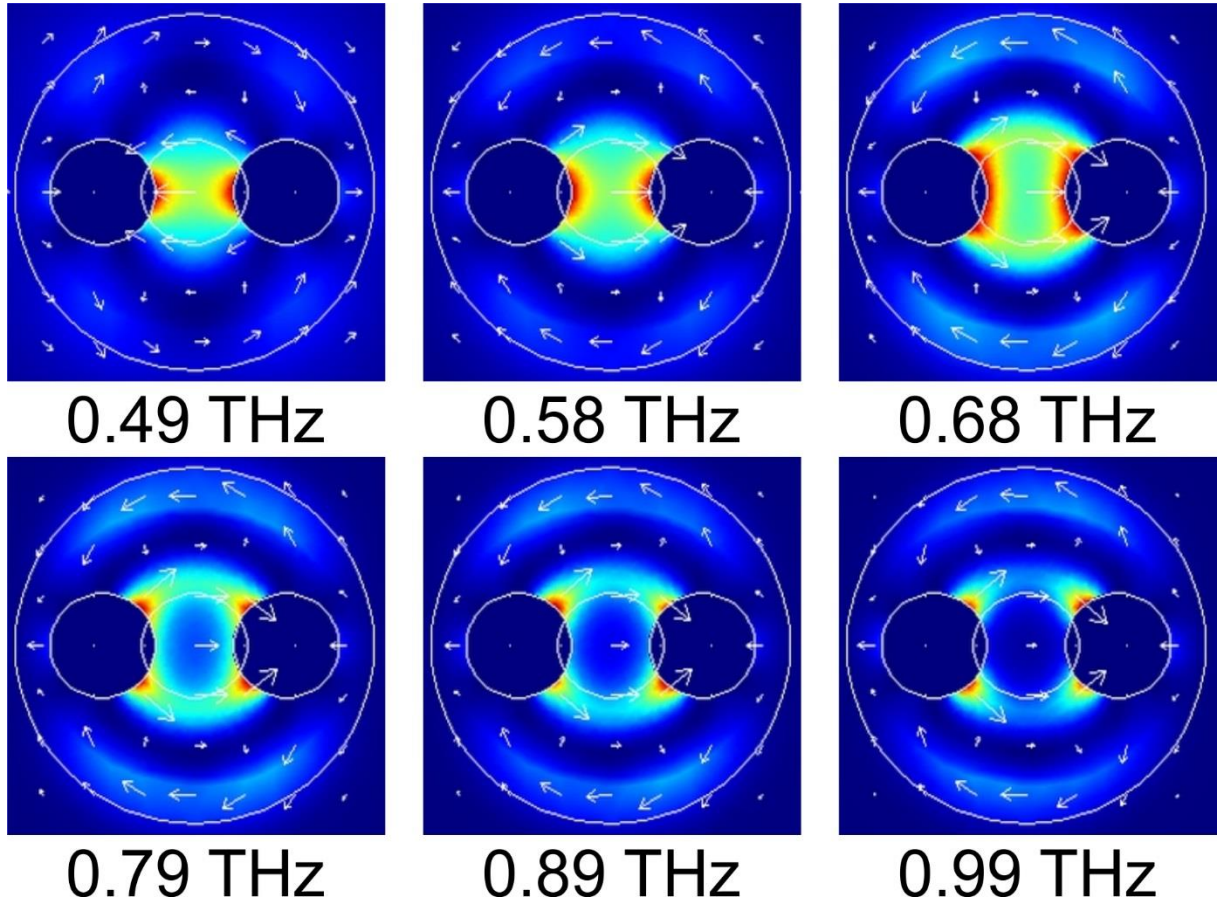


Figure 4.10 Longitudinal flux distribution of the second plasmonic mode of a composite fiber. The flux is normalized at its maximal value at each frequency.

Finally, we consider the second order cladding mode of a composite fiber, which is presented in Figure 4.6 in magenta color in the frequency range of 0.54 – 1.0 THz. From the corresponding field distributions showed in Figure 4.10 it follows that the second order cladding mode is, in fact, a hybrid mode that has a significant plasmon contribution. Moreover, at lower frequencies (0.5 – 0.7 THz) the plasmon is propagating at the air/metal interface with a significant

amount of energy concentrated in the central air hole between the two wires. In what follows we call this mode the second plasmonic mode as it can be used for low loss guidance of THz light within the central air hole of a composite fiber.

At higher frequencies (> 0.7 THz), the second plasmonic mode leaves the central air hole, while localising in the vicinity of the metal/plastic/air junctions (see, for example, Figure 4.10, 0.79 THz). This results in significant energy transfer into the cladding, and, consequently, modal absorption losses of this mode become comparable to the bulk absorption losses of a polyethylene cladding. In the 0.5 – 0.9 THz spectral range, the second order plasmonic mode has relatively low group velocity dispersion $\sim 1 - 2$ ps/(THz·cm), which is even smaller than that of the fundamental plasmonic mode.

It is now timely to highlight the main differences in the optical properties of the modes of a two-wire composite fiber and the modes of a corresponding porous fiber without metal wires. Firstly, from Figure 4.6 we note that the fundamental plasmonic mode of a composite fiber extends into very low frequencies (< 0.1 THz), while being well confined within the fiber (see Figure 4.7). This can be of advantage when compared to the fundamental mode of a porous fiber, which at low frequencies is highly delocalised in the air cladding outside of the fiber (see Figure 4.9). In practical terms it means that at very low frequencies, the fundamental plasmonic mode of a composite fiber is still suitable for guiding THz light due to its strong confinement in the core and, consequently, low sensitivity to bending, imperfections on the fiber surface, as well as perturbations in the environment. At the same time, at very low frequencies, fundamental mode of a porous fiber is largely found outside of the fiber core, which makes it highly sensitive to perturbations in the environment, as well as bending and fiber surface quality.

Secondly, cladding modes of a composite fiber tend to have lower absorption losses than the corresponding modes of a porous fiber without wires. This is mostly due to enhanced expulsion of the modal fields from the lossy plastic cladding near the metal wires.

Finally, we conclude that the fundamental mode of a classic two-wire waveguide can still be recognised in the modal structure of a composite two-wire fiber. In this case, however, the pure plasmonic mode is hybridised with the modes of a plastic cladding, thus, leading to increased modal losses and increased modal group velocity dispersion compared to those of the fundamental mode of a two-wire waveguide. At the same time, predominantly “plasmonic” modes of a composite

fiber, while exhibiting comparable absorption losses, possess significantly lower group velocity dispersion than the modes of a corresponding porous fiber. Therefore, under the restricted launch conditions, when mostly plasmonic modes of the composite fiber are excited, we believe that such fibers can outperform both in loss and in the effective group velocity dispersion the corresponding porous fibers without metal wires.

4.4 The influence of porosity on the fiber optical properties

In the previous section, we have observed that absorption losses of the modes of a three-hole composite fiber were quite smaller than the bulk absorption losses of a plastic cladding. This is a direct consequence of the modal localisation in the fiber central air hole and in the air region outside of the fiber. At the same time, losses and group velocity dispersion of the modes of a three-hole composite fiber were still much higher than those of a classic two-wire waveguide. This is due to the fact that many modes of a composite fiber bear strong resemblance to the modes of a porous three-hole plastic fiber without wires.

As we saw in our prior work [119-121], group velocity dispersion of the modes of a porous fiber can be quite large especially in the spectral region where modal guidance mechanism changes from low confinement (subwavelength guidance) to strong confinement in the dielectric cladding. As demonstrated in [110] this transition happens in the vicinity of the following characteristic frequency:

$$\nu_0 \approx \frac{c}{2\pi R_f \sqrt{(1-f)(\epsilon_c - \epsilon_a)}}, \quad (4.2)$$

where c is the speed of light in vacuum, R_f is the fiber radius, ϵ_c and ϵ_a are the relative permittivities of the cladding material and air respectively, and f is the fiber porosity defined as a ratio of the total area taken by the holes to the total area of the fiber cross section. In order to keep the influence of plastic cladding to the minimum both in terms of the material absorption loss and in terms of the group velocity dispersion, we need to ensure that the operation frequency range of a two-wire waveguide corresponds to the subwavelength guidance regime of a porous cladding. For example, for a composite fiber of 1 mm diameter made of polyethylene, from Equation 4.2 it follows that in order for the fiber cladding to operate in the low confinement (subwavelength) regime at 1 THz, porosities of 99.3% are required.

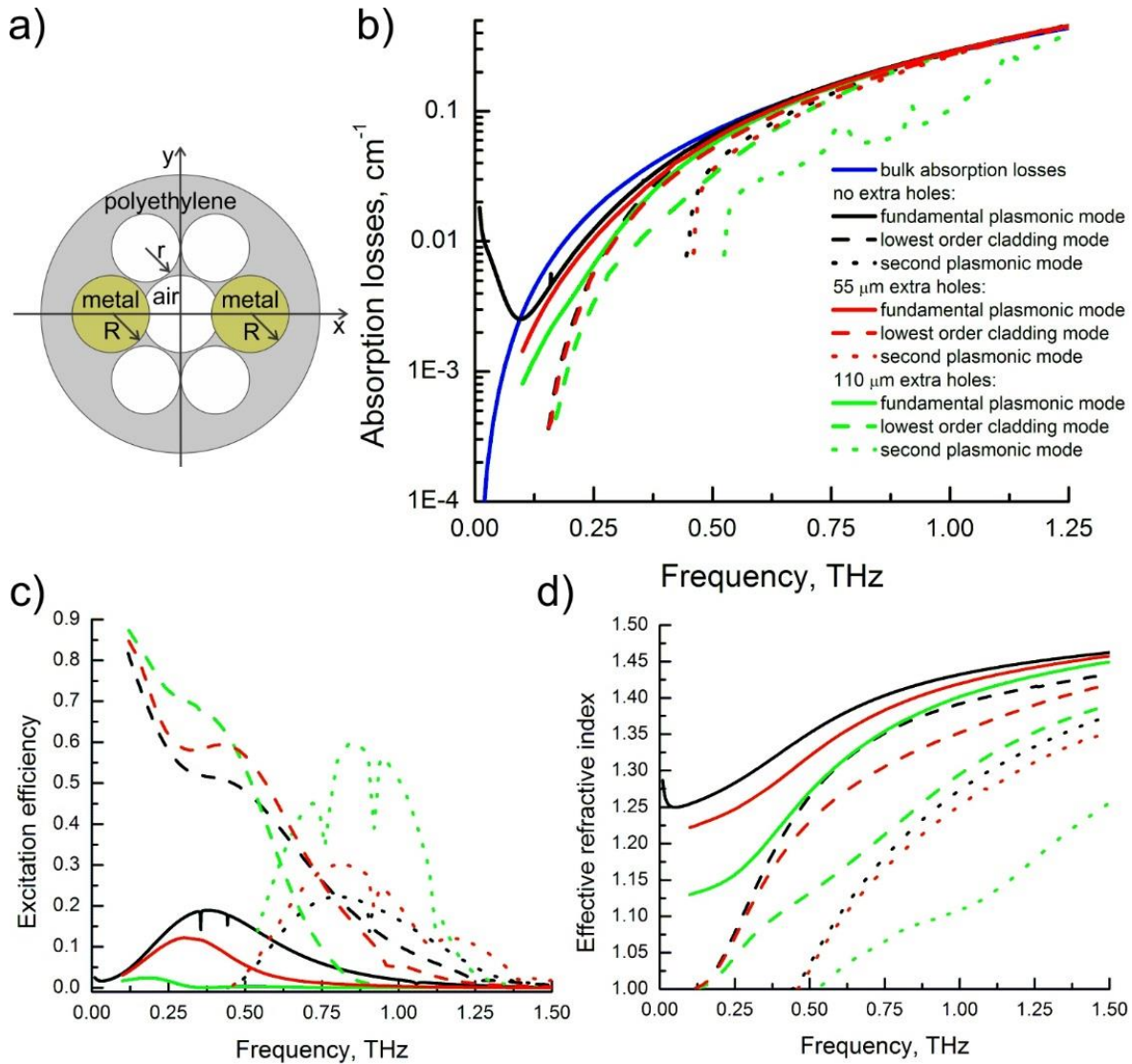


Figure 4.11 a) Schematic of a seven-hole fiber with overlapping holes. b) Absorption losses, c) excitation efficiencies, and d) effective refractive index of the various modes of the seven-hole fiber with overlapping holes.

Although in practice, such high porosities are challenging to achieve, it is clear that increasing porosity of the composite fiber cladding should consistently improve the fiber optical properties. To demonstrate this point we introduce four air holes into the cladding of our three-hole fiber [see Figure 4.11 (a)], and study the effect of increasing porosity on the fiber optical properties. Porosity is controlled by changing the radii of the cladding holes from 0 (three-hole fiber of the previous section) to 110 μm . The positions of the cladding holes are chosen in such a way that when the holes radii are 110 μm , the smallest thickness of all the material bridges between two small holes, between any small hole and the core hole, and between any metal wire and the closest

small holes is $10\text{ }\mu\text{m}$. In Figure 4.11 we present the effective refractive indices, the absorption losses and the excitation efficiencies of several modes of a composite fiber for various values of the holes radii. First, we observe that when increasing fiber porosity the excitation efficiency of the fundamental plasmonic mode reduces quickly from 20% in the three-hole fiber to below 4% in the 7-hole fiber with cladding hole radii of $r = 110\text{ }\mu\text{m}$.

At the same time, excitation efficiency of the second plasmonic mode increases significantly when using fibers of higher porosities, from the maximum of $\sim 20\%$ in the three hole fiber to the maximum of 60% in the 7-hole fiber ($r = 110\text{ }\mu\text{m}$). Additionally, we confirm that both the modal effective refractive index and modal losses decrease significantly at higher porosities. Modal distributions of the principal modes are shown in Figure 4.12 for $r = 110\text{ }\mu\text{m}$.

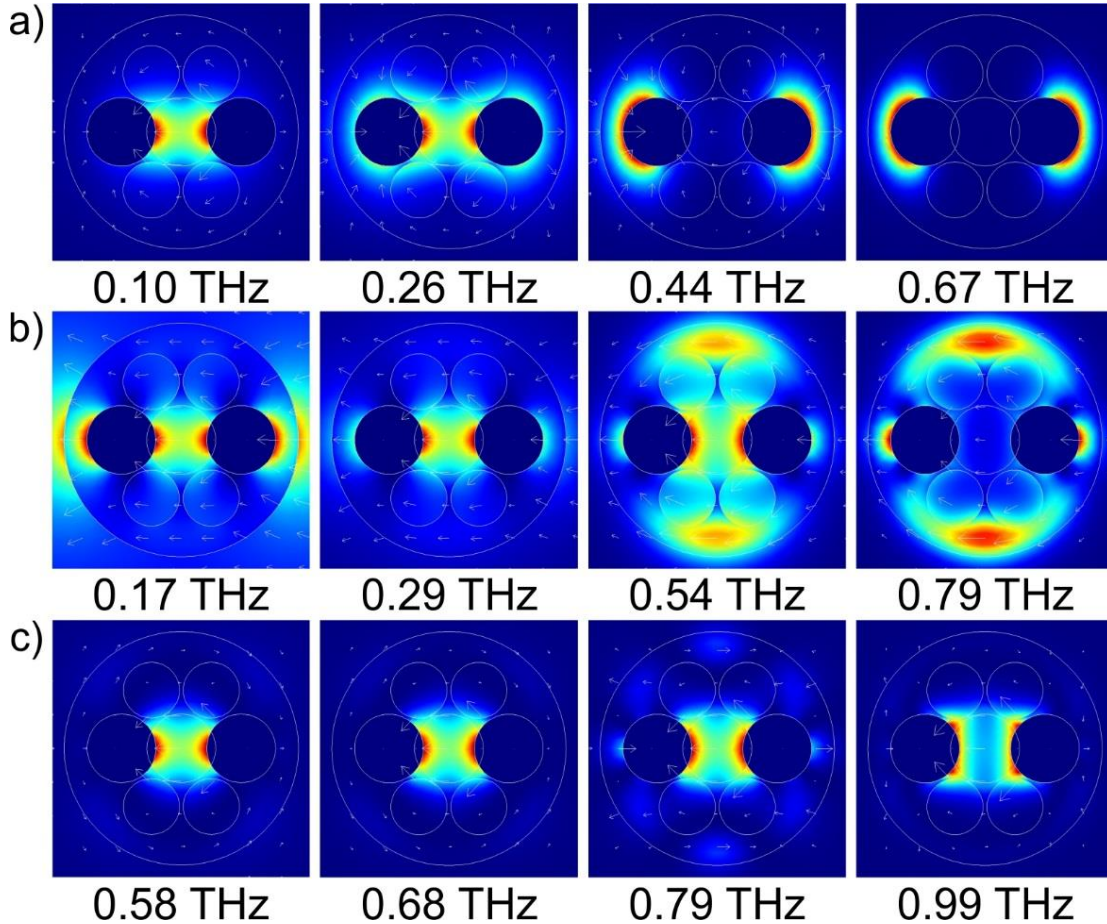


Figure 4.12. Longitudinal flux distribution for the modes of a composite seven-hole fiber with overlapping holes and $r = 110\text{ }\mu\text{m}$. a) Fundamental plasmonic mode, b) lowest order cladding mode, c) second plasmonic mode. The flux is normalized at its maximal value at each frequency.

4.5 Composite fiber featuring two metal wires in a seven-hole porous cladding

Next, we study a simple seven-hole fiber with non-overlapping air holes placed in the vertices of an equilateral triangular lattice [see Figure 4.13 (a)]. The metal wires are placed in the two opposing holes of the fiber, thus forcing THz light to be guided predominantly in the central air hole [see Figure 4.13 (b)]. The modal structure and the modal properties of such a waveguide are very similar to those of a seven-hole fiber with overlapping holes studied in the previous section. At the same time, as seen from the modal field distribution in Figure 4.13 (b), in the fiber with non-overlapping holes, some part of the modal fields is unavoidably guided in the plastic bridges. In this respect, design presented in the previous section is advantageous as there metal wires face directly the air core region [see Figure 4.11 (a)]. Nevertheless, we have decided to present the fibers with non-overlapping holes as they are definitely easier to fabricate than the fiber with overlapping holes.

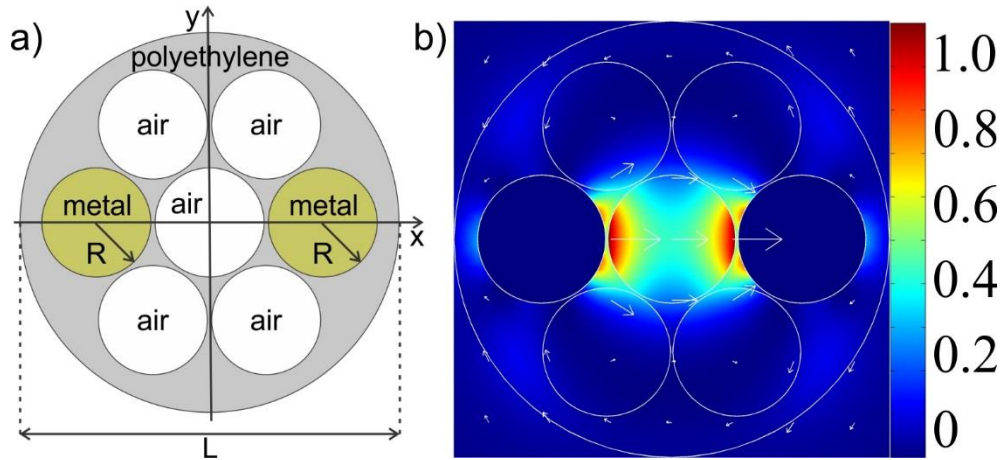


Figure 4.13 a) Schematic of a seven-hole fiber with two metal wires. b) Longitudinal flux distribution for a typical guided mode of a composite fiber presents a mixture of the plasmonic mode guided by the metal wires and a TIR mode guided by the fiber cladding.

In order to decrease the number of cladding modes, thickness of the outer cladding has to be minimized. This thickness is defined as the smallest distance between the fiber outer surface and the boundary of the internal air holes. From our experience with plastic porous fibers and capillaries [41, 119], outer cladding thickness larger than 50 μm is sufficient to mechanically protect the inner structure of the fiber. In our calculations, the smallest bridge size between any two air holes is taken to be 10 μm , which can be readily realised in practice as demonstrated in our prior experiments with suspended core fibers [33]. The outer diameter of the seven-hole fiber is

870 μm , the wire diameter is the same as before and equal to 250 μm , and the air hole diameter is equal to the wire diameter.

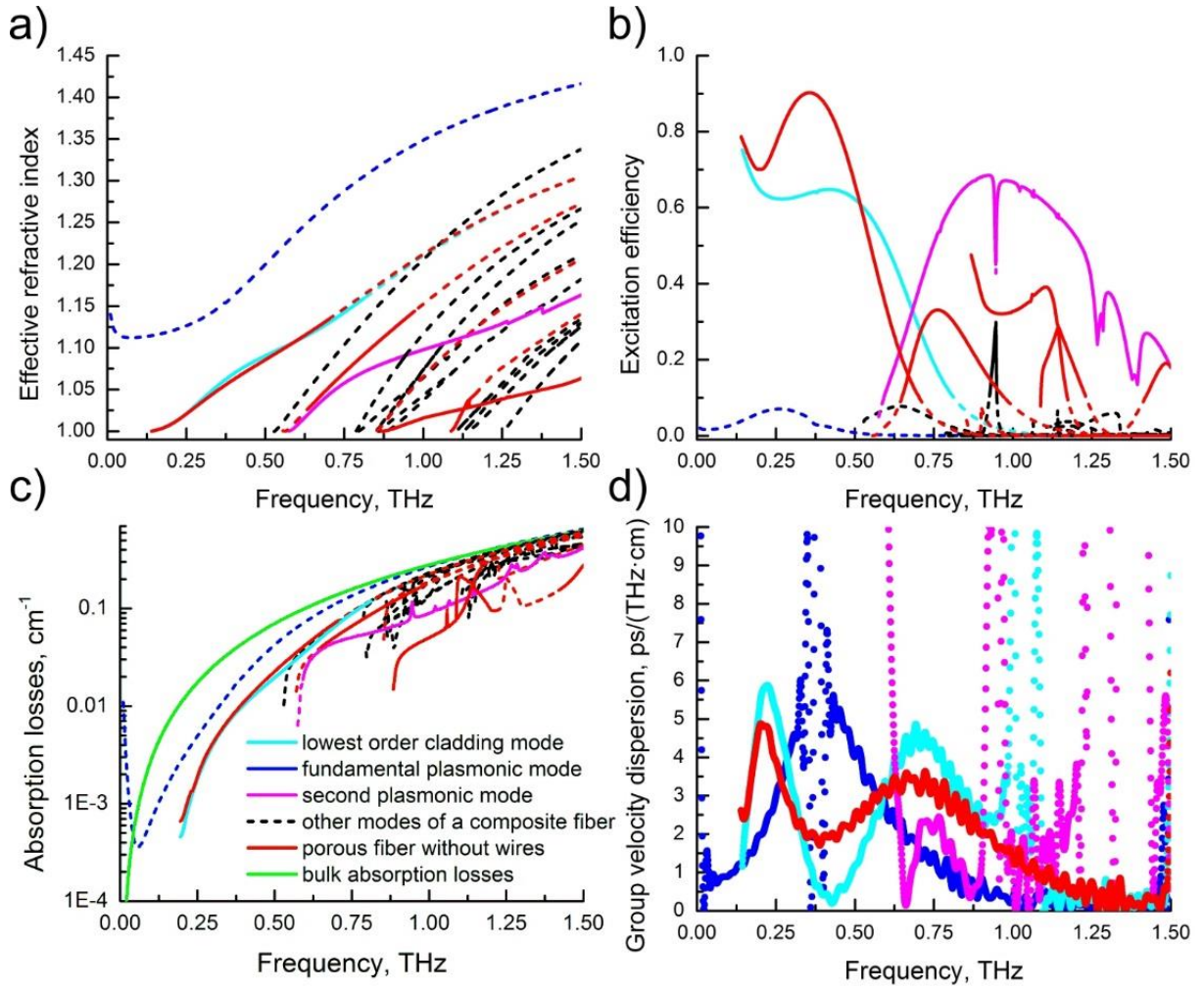


Figure 4.14 a) Effective refractive indices, b) excitation efficiencies, c) absorption losses and d) group velocity dispersion for the various modes of a seven-hole composite fiber shown in Figure 4.13. Solid lines define frequency ranges where the modal excitation efficiency is higher than 10%.

In Figure 4.14 we present dispersion relations, absorption losses, coupling efficiencies, and group velocity dispersion of the modes of a seven-hole composite fiber shown in Figure 4.13 (a). First, we observe that at lower frequencies (< 1.0 THz) modal structure of a seven-hole composite fiber is similar to that of a three-hole composite fiber (see Figure 4.6). Thus, we distinguish the “fundamental plasmonic mode” (blue color in Figure 4.14), which has a strong presence in the central air hole at frequencies below 0.4 THz [see Figure 4.15 (a)]. Unfortunately, coupling to this mode is quite inefficient and is below 10% in the whole THz range. Next, we note that optical

properties of the lowest order cladding mode (cyan color in Figure 4.14) resemble closely those of the corresponding mode of a three-hole fiber. The major difference between the two modes is observed at lower frequencies < 0.3 THz where modal field presence in the air regions is more pronounced in a seven-hole fiber due to higher porosity of its plastic cladding (compare Figure 4.15 (b) and Figure 4.8). Finally, when comparing optical properties of the second plasmonic mode of the two fibers, we note that excitation efficiency of this mode in a seven-hole fiber is relatively high (20-70%) in a broad spectral range 0.59 THz-1.7 THz, while the maximal excitation efficiency of this mode in a three-hole fiber is only 20% at 0.8 THz. Moreover, as seen from Figure 4.15 (c) and Figure 4.10, at higher frequencies, modal field of the second plasmonic mode of a seven-hole fiber has a much stronger presence in the central air hole when compared to the three-hole fiber. This, again, can be explained by the higher porosity of the seven-hole fiber. Finally, from Figure 4.14 we observe that even at higher frequencies ~ 1 THz transmission losses of a seven-hole fiber is significantly smaller (3-5 times) than the bulk absorption loss of a cladding material, while the fiber effective group velocity dispersion stays in the ~ 1 -4 ps/(THz·cm) range.

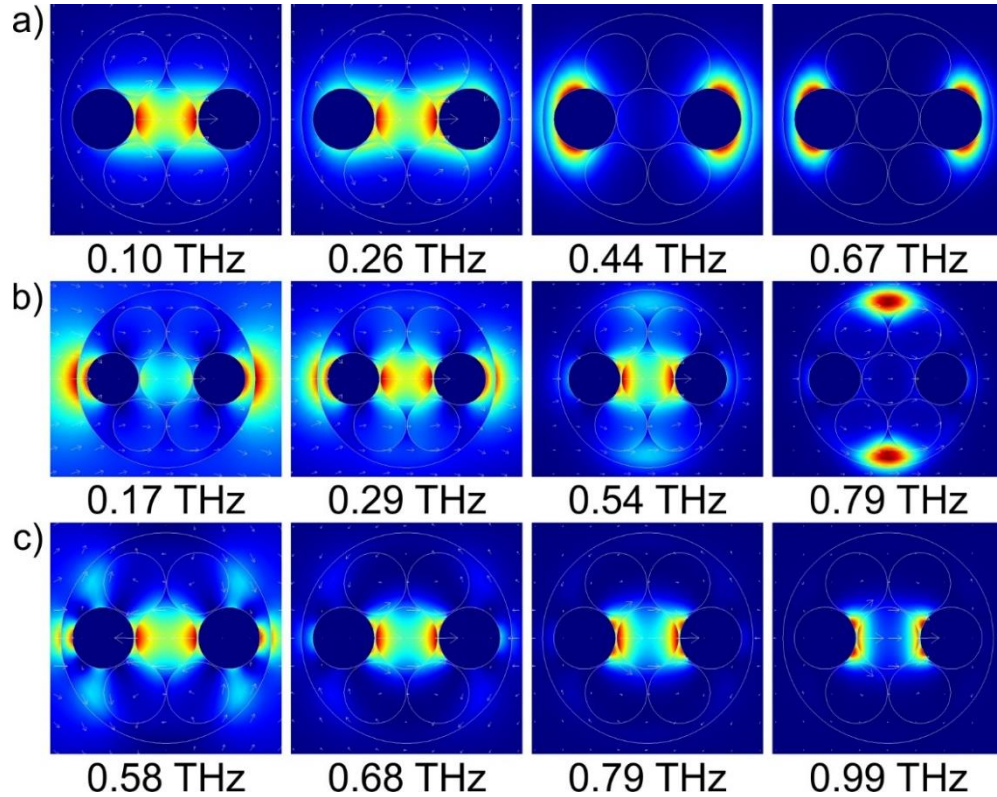


Figure 4.15. Longitudinal flux distribution for the modes of a seven-hole composite fiber
a) fundamental plasmonic mode, b) lowest order cladding mode, c) second plasmonic mode. The flux is normalized at its maximal value at each frequency.

When comparing optical properties of the two seven-hole fibers with overlapping and non-overlapping holes, we note that modal structure and modal optical properties of the two fibers are very similar (compare Figure 4.11 and Figure 4.14). In a seven-hole fiber with overlapping holes, plasmonic mode is less concentrated in the plastic bridges than in a seven-hole fiber with non-overlapping holes. From comparison of Figure 4.11 and Figure 4.14 it might appear that a seven-hole fiber with non-overlapping holes somewhat outperforms the fiber with overlapping holes. This is not quite correct as it is difficult to compare exactly the performance of the two fibers as not only the wire separation but also the core size and the cladding porosity should be comparable in the two fibers. For example, in the figures above, the size of the hollow core was the same in the two fibers, however the inter-wire distance in the fiber with overlapping holes was somewhat smaller than that in the fiber with non-overlapping holes. This pushed the mode into cladding more effectively in the fiber with overlapping holes, thus resulting in somewhat higher losses. Although a fair comparison between the two fibers is challenging, it is obvious that a seven-hole fiber with overlapping holes is clearly preferable, as plasmonic modes in such fibers have smaller presence in the plastic bridges.

4.6 Conclusion

A novel type of practical THz fibers is proposed that combines low-loss, low-dispersion and efficient excitation properties of the classic two-wire waveguides together with mechanical robustness, and ease of manipulation of the porous dielectric fibers. We then show that while optical properties of composite fibers are inferior to those of a classic two-wire waveguide, at the same time, composite fibers outperform porous fibers of the same geometry both in bandwidth of operation and in lower dispersion. Finally, we demonstrated that by increasing porosity of the fiber dielectric cladding its optical properties could be consistently improved.

Particularly, using the finite element method we first ascertained that a classic two-wire waveguide features very low loss ($< 0.01 \text{ cm}^{-1}$) and very low group velocity dispersion ($< 0.1 \text{ ps}/(\text{THz}\cdot\text{cm})$) in the whole THz spectral range. We then studied coupling efficiency into such a waveguide as a function of various geometrical parameters and concluded that for an optimised waveguide, excitation efficiency of the fundamental mode can be relatively high ($> 50\%$) in the broad frequency range $\sim 1 \text{ THz}$. Moreover, we confirmed that this excitation efficiency has

a weak dependence on the misalignment in the position of a Gaussian excitation beam that was considered as the excitation source.

Next, we proposed using porous polyethylene cladding as a mechanical support for the two metal wires in order to provide a practical packaging solution for the classical two-wire waveguide. In their simplest implementation, resultant composite fibers feature three adjacent air holes placed in a plastic cladding. Two peripheral holes are occupied by the metal wires, while the central one is used to guide the THz light. We then concluded that in a three-hole fiber the lowest order modes could be classified as either plasmonic modes or the modes of a porous cladding. This identification is possible when comparing field distributions and dispersion relations of the composite fiber modes with those of a corresponding porous fiber without metal wires, as well as with those of a classic two-wire waveguide.

Notably, the fundamental plasmonic mode of a composite fiber extends into very low frequencies (< 0.1 THz), while being well confined within the fiber. Both the fundamental and second plasmonic modes have reasonable excitation efficiencies of $> 10\%$ in the broad frequency range $0.25 - 1.25$ THz, while having relatively low group velocity dispersion of $1-3$ ps/(THz·cm) and absorption losses that are, generally, $1.5-3$ times smaller than the bulk absorption loss of a polyethylene cladding in the broad THz range $0.1 - 0.6$ THz.

Similarly, the lowest order cladding mode of a composite fiber has, generally, lower absorption losses compared to those of the fundamental mode of the corresponding porous fiber without wires. At the same time, group velocity dispersion of this mode at low frequencies < 0.3 THz can be as high as 10 ps/(THz·cm), which is typical for porous fibers. Finally, coupling into the lowest order cladding mode of a composite fiber is quite efficient at lower frequencies < 1.0 THz and could be consistently above 50% .

We, therefore, conclude that composite three-hole fiber can somewhat outperform the corresponding porous fiber without wires, in terms of the bandwidth, absorption losses and lower group velocity dispersion if a restricted launch condition is used in order to preferentially excite the fiber plasmonic modes.

Finally, we demonstrated that the optical properties of a composite fiber could be consistently improved by further increasing the porosity of the fiber cladding. As an example, we considered a seven-hole composite fiber and demonstrated that such a fiber can have absorption

losses that are at least $\sim 3 - 5$ times smaller than those of the bulk polyethylene in the broad THz frequency range $0.1 - 1.2$ THz. Moreover, coupling efficiency into some plasmonic modes of such fibers was significantly improved (above 50% in the $0.75 - 1.25$ THz range), thus enabling low-loss light transmission with low group velocity dispersion of < 3 ps/(THz·cm). In this case of higher cladding porosity, the seven-hole composite fiber can clearly outperform the corresponding porous fiber both in the overall bandwidth and in the lower group velocity dispersion.

In order to consistently improve the optical properties of a composite two-wire fiber one has to further increase porosity of its plastic cladding. The composite fibers presented here have simple geometries, which are easy to fabricate. At the same time, it appears that more complex structures offering higher porosities have to be investigated in order to approach the outstanding low-loss, low-dispersion performance of the classic two-wire waveguides.

CHAPTER 5 ARTICLE 3: HYBRID METAL WIRE-DIELECTRIC TERAHERTZ WAVEGUIDES: CHALLENGES AND OPPORTUNITIES [INVITED]

This chapter is based on my paper “Hybrid metal wire-dielectric terahertz waveguides: challenges and opportunities [invited],” published in Journal of the Optical Society of America in 2014. I am the primary author of this article, which has been written in co-authorship with Hichem Guerboukha and Maksim Skorobogatiy. My role in this article includes all the aspects of the waveguide characterization. I am responsible for the initial idea, the experimental characterization and the theoretical analysis of the proposed structures.

The content of this article partly coincides with the material of Chapters 4 and 6, however the novel findings are included in this chapter, mainly concerning the experimental investigation of the proposed two-wire waveguides and hybrid metal/dielectric fibers. In this chapter, I show that polystyrene foam can be used as an optical cladding for a classic two-wire THz waveguide. The importance of this demonstration is that it shows a way of making practical THz waveguides that profit from the outstanding guidance properties of a two-wire waveguide, while also showing mechanical stability, ease of manipulation, and insensitivity to the variations in the environment. I have recently obtained all the results presented in this section.

In this chapter I evaluate recent experimental and theoretical progress in the development of hybrid metal / dielectric waveguides used for practical low-loss and low-dispersion delivery of terahertz radiation. Waveguides considered in this review utilize plasmonic modes guided in the air gap between two parallel wires. The two parallel wires are, in turn, encapsulated inside of a low-loss, low-refractive index micro or nano-structured cladding that provides mechanical stability and isolation from the environment. I describe two alternative techniques that may be used to encapsulate the two-wire waveguides while minimizing the negative impact of dielectric cladding on the optical properties of the waveguide. The first technique uses low-density foam as a cladding material, while the other uses air-filled microstructured plastic claddings to support metallic wires. Additionally, I offer a detailed analysis of the modal properties of the hybrid metal/dielectric waveguides, compare them with the properties of a classic two-wire waveguide, and present several strategies for the improvement of hybrid waveguide performance. Using resonant dependence of the confinement properties of some hybrid plasmonic modes also allows us to propose their use in

THz refractometry. Finally, I demonstrate that hybrid metal/dielectric porous waveguides can have a very large operational bandwidth while supporting tightly confined, air-bound modes both at high and low frequencies. This is possible as, at higher frequencies, hybrid fibers can support ARROW-like low-loss air-bound modes while changing their guidance mechanism to plasmonic confinement in the inter-wire air gap at lower frequencies.

5.1 Introduction

The main complexity with designing terahertz waveguides is the fact that for propagation distances of $\sim 1\text{m}$ almost all materials are highly absorbent in the terahertz spectral range [31]. Moreover, group velocity dispersion of many standard waveguides is high enough to result in significant THz pulse broadening over even modest propagation distances of $\sim 10\text{ cm}$.

In fact, the lowest loss materials in THz spectral range are dry gases. Therefore, one of the ways to reduce waveguide absorption loss is to maximize the fraction of light guided in the gas phase. Different types of THz waveguides and fibers have been proposed based on this concept. The simplest of such waveguide is a subwavelength fiber [32-34] that features dielectric core that is much smaller than the wavelength of guided light. As a result, a high fraction of modal power is guided outside of the lossy material and in the low-loss gaseous cladding. Another type of the low-loss fibers includes fibers featuring porous core region with the size of the individual pores much smaller than the wavelength of light [32, 33]. Consequently, guided light has a strong presence in the low-loss gas-filled pores inside the core. Higher modal confinement in the core makes such fibers less prone to bending losses and less sensitive to the environment compared to the simple rod-in-the-air subwavelength fibers [32, 35]. Subwavelength and porous fibers, however, can have significant group velocity dispersions as these fibers usually operate in the frequency range where modal confinement changes rapidly from weak at lower frequencies (high modal presence in the cladding) to strong at higher frequencies (high modal presence in the core).

Another important type of the low-loss THz waveguides includes fibers featuring gas-filled hollow core surrounded with a structured cladding serving as a reflector. The main challenge in the design of such fibers is to ensure high reflection at the core-cladding interface. Different hollow-core structures have been investigated including metalized bores [35-37], periodic dielectric multilayers [38], as well as thin-walled dielectric pipes [39,41,42]. These fibers, however, have a tendency of having a large core size that can easily be 10 times larger than the wavelength of guided

light. This is necessary in order to reduce modal absorption losses in the reflector structure. Moreover, hollow core waveguides that use photonic crystal cladding usually tend to have large outer diameters (over 1 cm) as they need to contain enough layers for efficient modal confinement.

Among other types of the THz waveguides, we note air-filled parallel plate waveguides [43] and slit waveguides [44], which are known for their low losses and strong confinement. An obvious disadvantage of such waveguides is a somewhat inconvenient form factor.

In the following sections we review another promising approach towards designing of low-loss, low-dispersion THz waveguides. These hybrid metal/dielectric waveguides use plasmonic mode guided in the gap between two parallel wires that are, in turn, encapsulated inside a low-loss, low-refractive index micro-structured cladding that provides mechanical stability and isolation from the environment.

In this review paper we first present a short history of the two-wire THz waveguides. we then describe several promising techniques that can be used to encapsulate the two-wire waveguides, while minimizing the negative impact of dielectric cladding on the waveguide optical properties. Particularly, we detail the use of low density foams and microstructured plastic claddings as two enabling materials for the two-wire waveguide encapsulation. We then present a detailed analysis of the modal properties of the hybrid metal/dielectric waveguides, compare them with the properties of a classic two-wire waveguide, and then present several strategies for the improvement of hybrid waveguide performance. Additionally, we detail an intriguing resonant property of some hybrid plasmonic modes of metal / dielectric waveguides that manifests itself in the strong frequency dependent change in the modal confinement from dielectric-bound to air-bound. We then discuss how this property can be used to construct THz refractometers. Finally, we demonstrate that hybrid metal/dielectric porous waveguides can have a very large operational bandwidth, while supporting tightly confined, air-bound modes both at high and low frequencies. This is possible as at higher frequencies, hybrid fibers can support ARROW-like low-loss air-bound modes, while changing their guidance mechanism to plasmonic confinement in the inter-wire air gap at lower frequencies.

5.2 Metallic wire-based THz waveguides operating using plasmonic modes

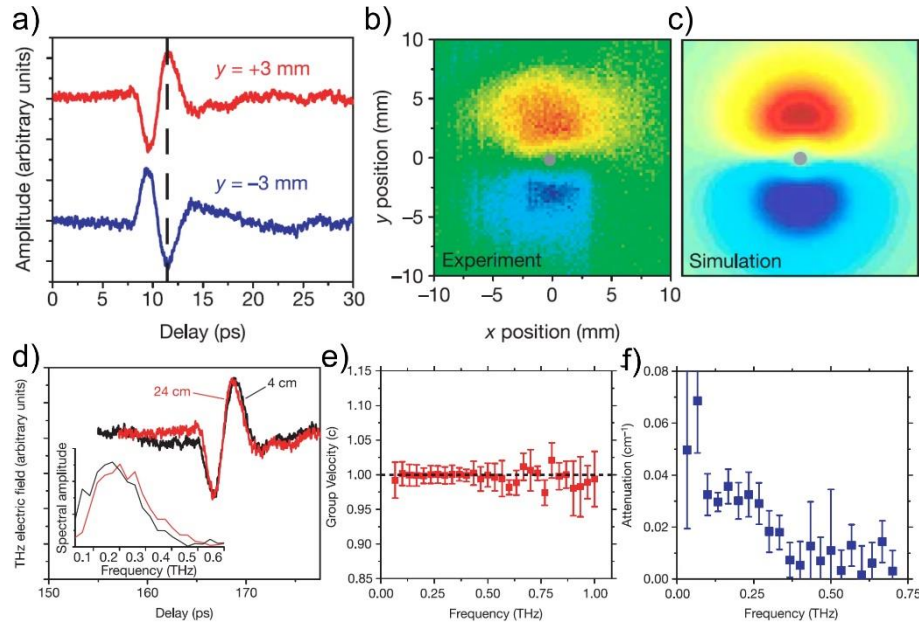


Figure 5.1. a) Time-domain electric field waveforms detected with the receiver 3mm above and 3mm below the waveguide. b) Spatial profile of the electric field obtained by moving the THz receiver in a plane perpendicular to the waveguide axis. c) The simulated spatial profile of the electric field propagating along the wire. d) THz waveforms measured after 4 cm (black) and 24 cm (red) of propagation distance along the wire. e) Group velocity of the propagating mode as a function of frequency. f) The electric field amplitude attenuation coefficient of the propagating mode as a function of frequency. Adapted by permission from Macmillan Publishers Ltd © 2004.

THz guidance with metal wires was first demonstrated by Mittleman et al. in [49]. In principle, a single metal wire can be used to transport terahertz pulses with virtually no dispersion and low attenuation (see Figure 5.1). In practice, however, it is difficult to realize efficient excitation of the guided mode of a single wire waveguide. This is because the fundamental mode of a single wire is radially polarized (angular momentum $m=0$), while commonly used photoconductive antennas tend to produce linearly polarized THz light ($m=1$). Because of this symmetry mismatch, direct excitation of the guided mode on a single wire is problematic. Furthermore, high bending losses of a single wire waveguide limit its practical applications. Even a slight bending of the wire can lead to considerable increase in the modal transmission loss, e.g. from 0.03 cm^{-1} for a straight wire to 0.05 cm^{-1} for a slightly bent one (bending radius of 90 cm, [50]).

To overcome difficulties with modal excitation, Deibel et al. [51] used a radially symmetric photoconductive antenna instead of a linear dipole antenna, and demonstrated coupling efficiencies in excess of 50%. Van der Valk et al. [53] then studied the effect of thin dielectric coatings (deposited on metal wires) on propagation properties of the guided plasmonic mode. Their measurements demonstrated strong distortion of THz pulses even when nondispersive dielectric materials were used in the layer. At the same time, in [122] it was demonstrated that coating the wire with a thin layer of dielectric improves confinement of the THz pulse in the vicinity of the wire due to significant presence of the modal field in the dielectric layer. It was argued that this effect can be potentially exploited for sensitive detection of changes in physical properties of thin dielectric layers. At the same time, from these experiments one can also conclude that outstanding THz guiding properties of a single standing metal wire (low-loss, low-dispersion) can be compromised if the wire surface is not pristine. Later, Cao et al. [54] introduced a novel approach for coupling THz pulses onto the guided mode of a single metal wire using grooves inscribed directly on the wire surface. Adjustment of the groove number, groove geometrical parameters, and inter-groove separation allows controlling bandwidth and center frequency of the excited THz pulse. Finally, conical (tapered) metal wires have been proposed [55] for superfocusing of a THz wave.

Recently, an efficient solution to the coupling problem has been proposed in [30], where Mittleman et al. suggested using two-wire waveguides that support linearly polarized low-loss and low-dispersion plasmonic modes. Compared to complicated coupling schemes or utilization of specialized THz antennas, two metal wire waveguides can be directly excited with linearly polarized field patterns emitted by the majority of THz sources.

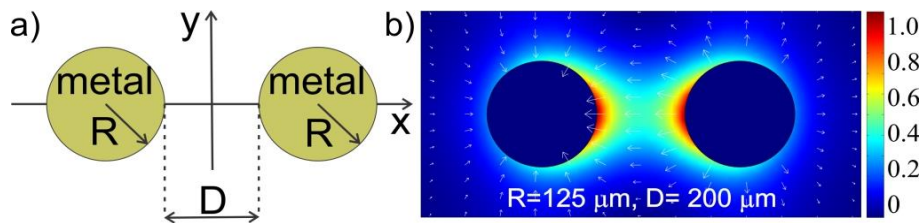


Figure 5.2. a) Schematic of a two-wire waveguide. b) Longitudinal flux distribution for the TEM mode of a two-wire waveguide. Arrows show vectorial distribution of the modal transverse electric field.

Indeed, field distribution in the fundamental TEM mode of a two-wire waveguide (see Figure 5.2) has the same symmetry as that of a wave emitted by a simple THz dipole photoconductive antenna when the wave is polarized along the line joining the two wires. Thus, one expects high excitation efficiencies of the fundamental mode of a two-wire waveguide when using standard dipole terahertz sources. Moreover, efficient confinement of the modal energy between the two wires, as opposed to a highly delocalized Sommerfeld wave on a single wire, makes two-wire waveguides less prone to bending losses. For example, in [30] it was demonstrated that for the same bending radius, bending loss of a two-wire waveguide was 5 times smaller than bending loss of a single wire waveguide. Additionally, absorption losses and group velocity dispersion of the fundamental mode of a two-wire waveguide are extremely low (see Figure 5.3). Finally, the confinement of the modal power in a small area between the metal wires opens possibilities for various guidance, sensing and even non-linear THz photonics applications.

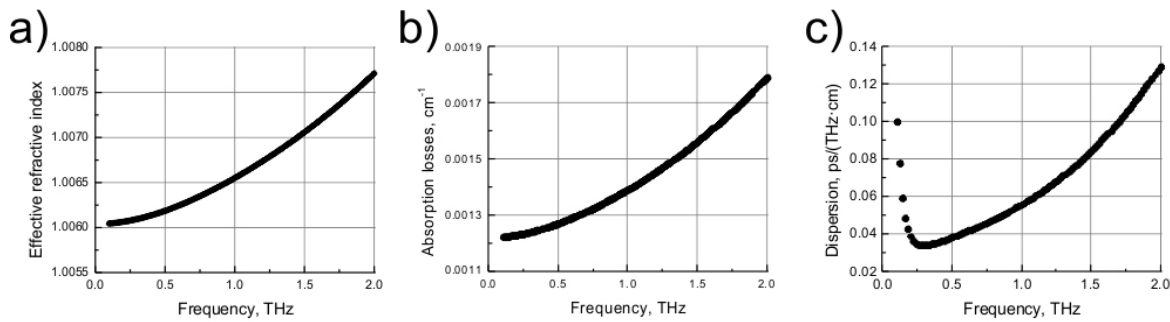


Figure 5.3. a) Effective refractive index, b) absorption losses, and c) group velocity dispersion of the fundamental mode of a two metal wire waveguide shown in Figure 5.2.

Coupling efficiency into a two-wire waveguide is a sensitive function of the excitation wavelength. It has been established that, the coupling efficiency achieves its maximal value at the wavelength that is comparable to the inter-wire separation, while the coupling efficiency stays relatively low for the wavelengths that are significantly smaller or larger than the optimal one. For a detailed discussion, see for example [56-58, 123], where the authors use a mode-matching technique and a full-wave FEM numerical simulation to study this issue. Ultimately, it is the frequency dependent coupling efficiency that limits practically usable bandwidth in such waveguides. Furthermore, as demonstrated in [123], coupling efficiency into two-wire waveguides depends strongly on various geometric parameters such as position of the THz beam focal point, the width of the wires, and the inter-wire distance (see Figure 5.4).

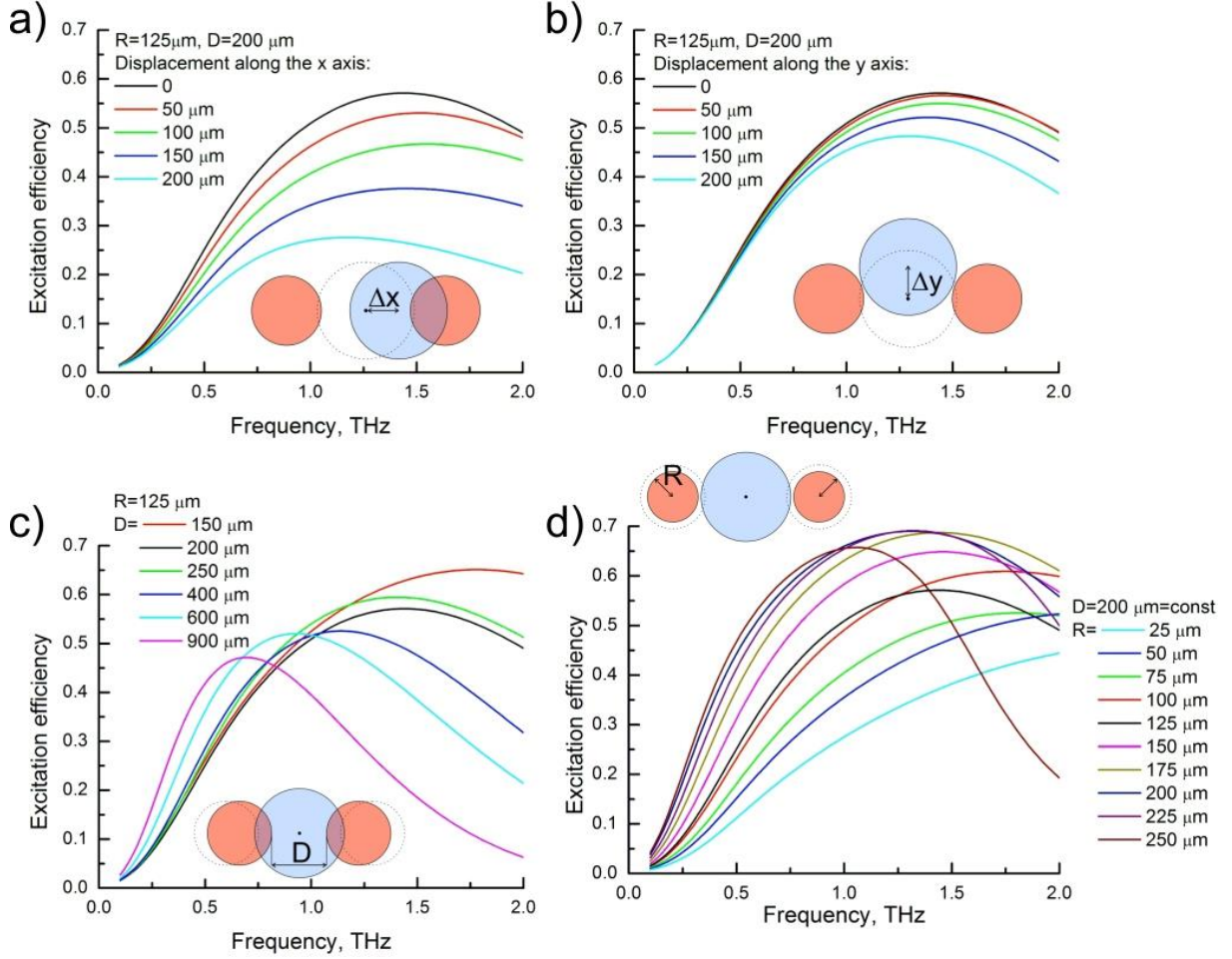


Figure 5.4. Excitation efficiency of the fundamental mode of a two-wire waveguide using diffraction limited Gaussian beam as an excitation source. Dependence of the excitation efficiency on various geometrical parameters, such as: a) displacement along the x axis from the core center, b) displacement along the y axis from the core center, c) inter-wire gap size, and d) wire radius.

Further improvement of the excitation efficiency of a TEM mode in a two-wire waveguide using realistic THz beams (non diffraction limited) as a source is possible by employing Y-shaped waveguide couplers, as shown in [58]. In this work, the authors used four wires adiabatically merging into a two-wire waveguide. The simulation results show an increased coupling efficiency for the two-wire waveguides without a significant effect on the overall group velocity dispersion or losses.

In [59] the authors have studied potential of the two-wire waveguides for application in chip-to-chip interconnects at operation frequencies up to 100 THz. The authors have shown that a two-wire waveguide with a wire radius of 10-20 μm and the inter-wire separation distance of 50-

100 μm can be used to interconnect chips placed several mm apart. Such interconnects were then achieved using standard wire bonding techniques with a loss of less than 1.7 dB/mm.

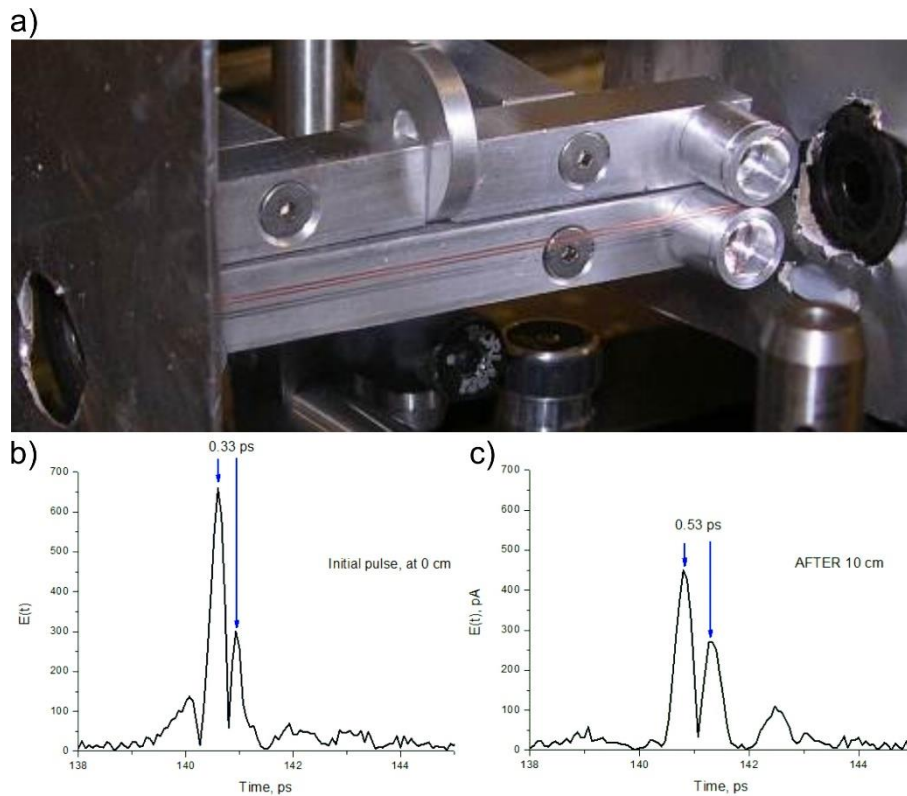


Figure 5.5. a) A two-wire THz waveguide made in our research group. b) THz waveform at the input of the waveguide. c) THz pulse transmitted through a 10 cm-long waveguide.

While having outstanding optical properties, the classic two-wire waveguide is inconvenient in practical applications. Indeed, in a typical experiment (see Figure 5.5) the two wires have to be aligned and kept straight and parallel to each other with high precision. This requires bulky holders and coupling setups. Moreover, the fiber core is not encapsulated into a protective cladding, thus leaving the core (space between wires) exposed to the environment.

The first attempt to demonstrate practical two wire waveguides was reported in [30]. There the authors used a ~ 10 cm-long piece of a standard TV antenna cable that is comprised of two metal wires encapsulated into a plastic jacket and separated with a plastic divider (Figure 5.6). The authors have managed to transmit a THz signal, however, the received pulse was considerably distorted and attenuated. In the same paper, the authors have also demonstrated that traditional bulky metal holders can be partially substituted by foam holders that are highly transparent to THz radiation.

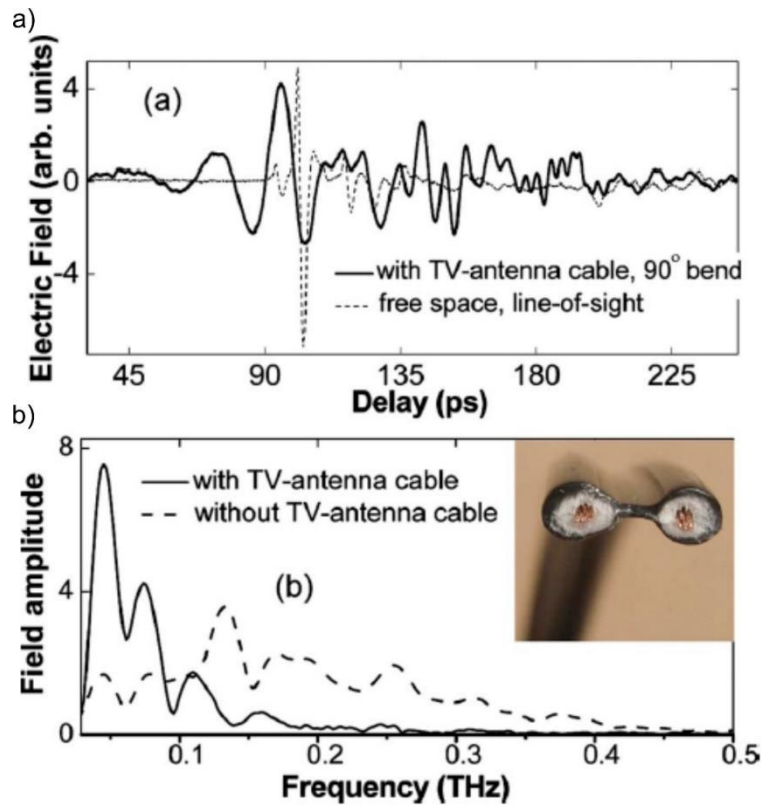


Figure 5.6. a) THz pulse transmitted through a 9.5 cm length of commercially available TV twin-lead antenna cable, with THz emitter and receiver at 90° to one another (solid curve); for comparison in dotted curve free-space THz transmission along a direct line-of-sight between the transmitter and receiver separated by the same 9.5 cm spacing, with no waveguide or optics in between. b) Amplitude spectra for the two THz waveforms.

5.3 Two-wire THz fibers with dielectric foam cladding

In what follows, we show that polystyrene foam can be used as an optical cladding for a classic two-wire THz waveguide. The importance of this demonstration is that it shows a way of making practical THz waveguides that profit from the outstanding guidance properties of a two-wire waveguide, while also showing mechanical stability, ease of manipulation, and insensitivity to the variations in the environment. All the results presented in this section were recently obtained by our group.

As discussed earlier, having a large fraction of power guided inside of dry low-loss gas is beneficial for reduction of the modal propagation loss. Foam is inherently highly porous, its pores are filled with gas and the pores can be sealed during fabrication. Importantly, a large number of

foam products made from various base materials are commercially available. For the aforementioned reasons, foam is a good candidate for guiding of THz waves.

Plastic foam is an example of a dispersed media where open or closed-cell gas regions are uniformly dispersed in a solid polymeric matrix. Plastic foam can be produced and shaped into various forms by mechanical, chemical or physical processing techniques. The review of these methods is beyond the scope of this paper and we refer the reader to [82-85] for details. The different fabrication techniques result in foams of different densities. For example, higher density foams are used for mechanical protection, while lower density foams are used for thermal isolation.

Characterization of foam optical properties in the THz spectral range was first conducted by Zhao et al. [86], where they studied polystyrene foams. In their studies, the authors compared three samples of different densities. For all the samples they found very low refractive indices of 1.017 - 1.022 in the 0.1 - 4 THz spectral range. The extinction coefficient remained smaller than 1 cm^{-1} at frequencies lower than 2.5 THz for the three samples, and smaller than 1.5 cm^{-1} for frequencies below 4 THz for the best sample. THz characterization of the Polymethacrylimide foams reported in [87] showed the same kind of behavior - a low refractive index 1.0175 - 1.0321 and a low extinction coefficient (less than 2 cm^{-1} below 2 THz).

Because of the high porosity of foam, it is not surprising to find that there is a large difference in the values of the refractive indices of foam material and bulk material from which the foam is fabricated. For instance, the refractive index of bulk polystyrene in the THz spectral range is nearly constant and is close to 1.6, while as mentioned earlier, polystyrene foam has a refractive index close to one. Such low values of the foam refractive index can be explained within the effective medium approximation which describes propagation of electromagnetic waves in composite materials made of subwavelength particles / inclusions implanted into a host material [88, 89]. In particular, for THz waves, a typical wavelength is on the order of 300 microns and longer, while the thickness of polymer shells that encapsulate air in foams can be considerably smaller than 100 microns. When propagating through foam, THz will not scatter efficiently on the deeply subwavelength polymer boundaries of the gas pockets, thus explaining the low scattering loss. Moreover, relative presence of THz radiation inside of the polymer boundaries, as compared to the gas pockets, will be small, thus explaining a refractive index close to that of air and absorption losses which are only a small fraction of those of a bulk polymer material from which

the foam is made [86, 87]. Ultimately, the THz extinction coefficient of foam is influenced both by the foam microstructure (scattering loss) and the nature of the solid material of the foam (absorption loss) [90-93]. Therefore, for waveguide applications one has to choose foams made of low-absorbing solid materials; the foams should feature closed-cell porosity with a high content of low-loss gas (low density foams), and also the gas pockets and the solid shells confining the gas should have deeply subwavelength dimensions determined by the spectral range of interest [94].

Note that careful consideration should be given to the type of gas (blowing agent) used in the foam fabrication. For example, in their study, Zhao et al. [86] noted an absorption feature around 0.5 THz for the foam sample, made with HCFC 142 b gas as the blowing agent, and confirmed it to be caused by rotational transitions in the molecular gas. The two other samples were made with CO₂ and no absorption was detected in the studied region.

When solid material of a foam has low absorption loss (e.g., polystyrene with loss $\alpha = 1.00 \pm 0.12 \text{ cm}^{-1}$ at 0.5 THz [95, 96]), then foam scattering loss can become higher than foam absorption loss [86, 87]. Scattering loss becomes especially pronounced at higher frequencies when the scatterer (gas pocket) size becomes comparable to the wavelength of guided light. In fact, from the three samples used by Zhao et al. [86], the one with the largest average pore diameter $\sim 150 \text{ }\mu\text{m}$ had the highest extinction coefficient at frequencies above 2 THz. Therefore, in order to reduce the scattering, it is important to control the pore size and geometry.

As for the application of foams in THz frequency range we note the use of polystyrene foam as a substrate for imaging and for manufacturing of near-infrared dichroic filters [94, 97]. THz was also used for industrial non-destructive characterization of foams [98, 99] that allowed simultaneous monitoring of the chemical and structural information of the sample [99].

Surprisingly, no significant attention was given to foams as core materials for THz waveguiding. Although Mittleman et al. used polystyrene foam slabs to support the two-wire waveguide structure [30], the slabs were not used as a core or cladding material in those experiments. Most recently, our research group has demonstrated fabrication of 10 cm-long THz fibers from biodegradable silk foams that was used as a fiber core material [100].

Bulk polystyrene foam

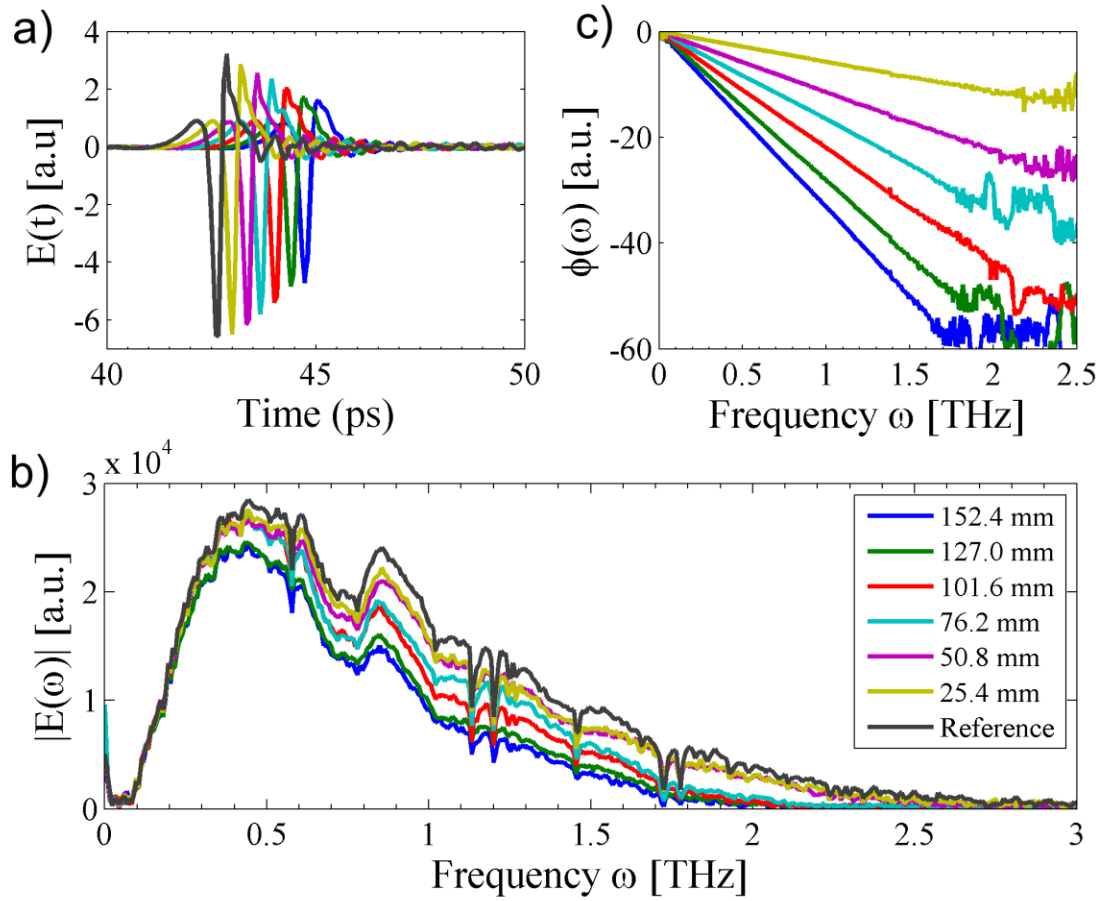


Figure 5.7 a) Time-domain electric field. b) Transmission spectra c) Unwrapped phase relative to the reference. Each color represents a particular length of polystyrene foam.

First, we present optical characterization of a polystyrene foam sample using a THz-TDS setup and a cutback method detailed in [32]. Six slabs of polystyrene foam from McMaster-Carr (item 9335K11) of dimensions 60x60x25.4 mm were placed in the path of a THz beam. Then, we conducted a series of seven measurements of the THz electric field by successively removing individual slabs. Figure 5.7 (a) presents time domain electric field traces for different effective thicknesses of a polystyrene foam sample (solid curves of different colors). The reference measurement corresponds to the pulse propagation through the empty system. During measurements, all THz optical components were fixed (see [100] for details). The corresponding transmission spectra and unwrapped phases are presented in Figure 5.7 (b), (c). Note that ambient water vapor has the adverse effect on the spectra, the transmission dips can be observed in the

vicinity of water absorption lines (for example, at 0.56, 1.11, and 1.41 THz). We are using nitrogen purging technique to reduce humidity in our setup, however it is impossible to completely remove the water vapor.

The complex transmission through the foam sample was calculated by assuming that interfaces between different foam slabs do not result in additional losses. Then, for a sample of length L_f we got (see [86] for details):

$$\begin{aligned} \frac{E_{foam}}{E_{ref}} &= t(\omega) e^{i\varphi(\omega)} \\ t(\omega) &= t_0 \exp(-\alpha_f(\omega)L_f); t_0 = \frac{4n_f(\omega)}{(n_f(\omega)+1)^2} \quad , \\ \varphi(\omega) &= \varphi_{foam}(\omega) - \varphi_{ref}(\omega) = -\frac{\omega}{c}(n_f(\omega)-1)L_f \end{aligned} \quad (5.1)$$

where $E_{foam}(\omega)$ and $E_{ref}(\omega)$ are the complex Fourier transforms of the THz signal, with and without the polystyrene foam, respectively. From this, we were able to extract the refractive index $n_f(\omega)$ and the foam extinction coefficient $\alpha_f(\omega)$ (see Figure 5.8). Consistent with the prior studies, the foam refractive index is essentially constant in the whole THz spectral range. Moreover, the foam extinction coefficient has a very low value of $< 0.15 \text{ cm}^{-1}$ for frequencies smaller than 1.5 THz. Overall, frequency dependence of the extinction coefficient can be well fitted with a forth order polynomial (Figure 5.8 (b)):

$$\begin{aligned} \alpha_f[cm^{-1}] &= a \cdot \nu^4 + b \cdot \nu^2 + c + d \cdot \left(\frac{\Gamma}{\Gamma^2 + (\nu - \nu_r)^2} \right) \\ a &= 0.01276; b = 0.03337; c = 0.00409; d = 0.01779 \quad . \\ \Gamma &= 0.1219 [THz] ; \nu_r = 0.7974 [THz] \\ \nu &\text{ is in } THz \end{aligned} \quad (5.2)$$

There, the fourth order polynomial (in frequency) describes a joint contribution of scattering and material absorption losses. Additionally, in the vicinity of 0.8 THz, one observes a broad resonance (fitted with Lorentzian) which is probably related to the spectral signature of gas (blowing agent) filling the pores.

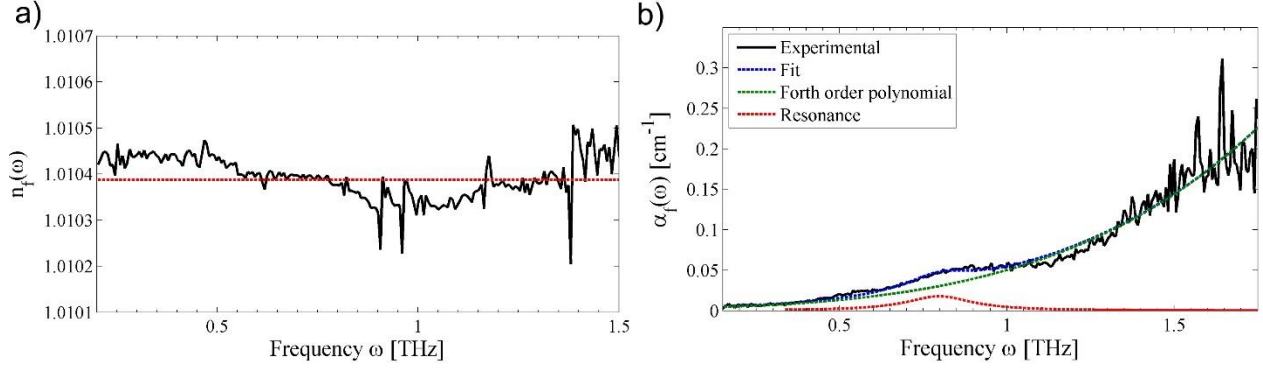


Figure 5.8 a) Effective refractive index. The mean is indicated by the dashed line. b) Extinction losses and fit with a forth order polynomial and Lorentzian function

Two-wire waveguide with a polystyrene foam cladding

As mentioned earlier, two-wire waveguides show outstanding guiding properties such as low propagation loss and low dispersion. The main obstacle for practical applications of a two-wire waveguide is the need for a cumbersome holder that is used to maintain the two wires straight and parallel along the total length of a waveguide. Furthermore, the fiber core is an air region which is exposed to the environment and is, therefore, sensitive to handling and perturbations in the environment.

Clearly, for practical applications a two-wire waveguide has to be encapsulated into a protective cladding that should not otherwise significantly affect the waveguide guidance properties. In this respect, foam constitutes an ideal material for the optical cladding of a two-wire waveguide as foam feature low loss, low dispersion and a refractive index close to that of air. Moreover, mechanically, foam is robust and can hermetically encapsulate two wires in its structure.

To demonstrate the foam potential as a cladding material for practical two-wire waveguides we performed a comparative study of the THz pulse transmission through a 14 cm-long two-wire waveguide with and without the foam cladding. Particularly, we first designed and, using a 3D printer, manufactured an ABS holder for a two-wire waveguide (Figure 5.9). The wires are wound on the four round metallic barrels (two on each side) that also control the inter-wire separation. Another function of the metallic barrels is to serve as a slit aperture, thus eliminating a large portion of the straight light that might otherwise propagate along the wire direction. The distance between copper wires is about 750 μm and is maintained constant along the waveguide length by applying tension. The waveguide was subsequently placed between two circular apertures, one at the

waveguide input end and the other at the waveguide output end. The apertures were aligned with the focal points of the two parabolic mirrors that couple THz pulse into the waveguide and then collect transmitted THz pulse for detection. The aperture is open to ~3mm which is the typical size of a THz beam in our system. In measurements with foam cladding, two polystyrene slabs of 6 x 20 x 130 mm in size were firmly pressed against the two metal wires.

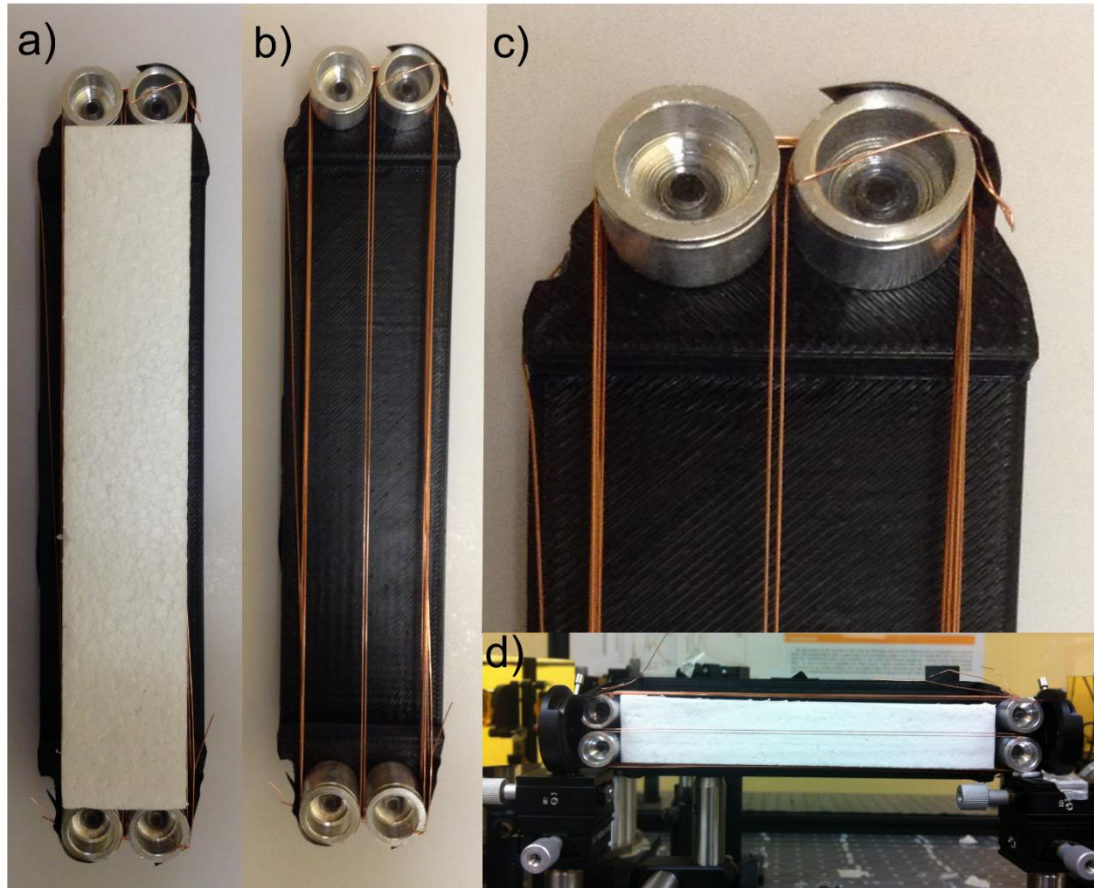


Figure 5.9 Photograph of the two-wire ABS 3D-printed holder a) with and b) without polystyrene foam. c) Magnification of the metal coupler used also as an aperture. d) Holder with two wires between two apertures inside the THz-TDS system.

To conduct our comparative studies we performed three types of measurements. In the first measurement we used two wires with polystyrene foam pressed firmly against the wires. In the second measurement, we removed the foam cladding and study pulse propagation in a bare two-wire waveguide with air core. Finally, without touching the holder we cut the wires and measured direct transmission of the THz pulse through the remaining apertures. This last measurement effectively measures the level of stray light in the system.

The pulse traces measured in these experiments and their corresponding Fourier transforms are presented in Figure 5.10. First, we confirm guidance in a two-wire waveguide by noting that the pulse transmitted with a waveguide (two wire) is 4 times stronger than the stray pulse (holder only). We also note that when using a classic two-wire in the air configuration, pulse bandwidth is limited to ~ 0.6 THz (0.2 – 0.8 THz transmission region). Also, the frequency of maximal pulse intensity is ~ 0.4 THz, which is determined directly by the inter-wire distance of 750 μm . In order to extend the waveguide operation range to higher frequencies one has to reduce the inter-wire separation.

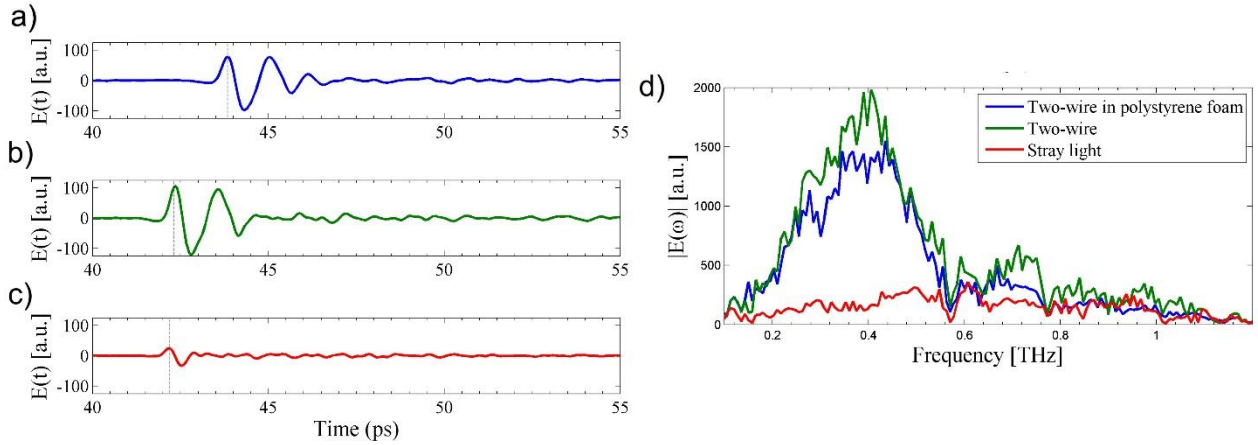


Figure 5.10 Time domain electric field of a) the two-wire waveguide embedded in polystyrene foam, b) the two wires only, and c) the ABS holder only. d) Transmission spectra of the corresponding electric field.

When adding polystyrene foam cladding, the THz pulse undergoes several changes. First, the pulse experiences a small retardation by 1.52 ps (as inferred from the temporal position of the peaks), from which we estimate that the average effective modal refractive index is ~ 1.003 . Pulse retardation is caused directly by the overlap of modal fields with a higher refractive index foam cladding. Remarkably, Fourier spectra of the transmitted pulses in the two waveguides (with and without foam cladding) are quite similar, with only a small decrease in the overall intensity in the case of a waveguide with foam cladding. From this we estimate that additional loss incurred by the waveguide mode due to addition of a foam cladding is on average $\sim 0.12 \text{ cm}^{-1}$.

From these measurements we conclude that polystyrene foams can indeed be used as optical cladding for two-wire THz waveguides, resulting in only a small degree of degradation in the waveguide performance. At the same time, addition of a mechanically robust and hermetical foam

cladding makes a two wire waveguide ready for practical applications that require convenient handling and low sensitivity to variations in the environmental conditions.

5.4 Two-wire THz fibers with microstructured dielectric cladding

In this section we describe an alternative approach that allows mechanical support and encapsulation of the metal wires. As we have demonstrated in the previous section, low-density foam can be, in principle, used as a cladding material in the two-wire waveguides. In this case, however, waveguide loss will be determined by that of foam, as this material will have significant presence in the immediate vicinity of the inter-wire gap (core region). In order to further reduce the effect of cladding material on the waveguide modal properties, it is reasonable to use microstructured claddings that minimize the amount of solid material in the inter-wire gap while nevertheless offering some kind of mechanical support to the metal wires, thus keeping the inter-wire distance fixed [123-125]. Another potential advantage of such microstructured claddings is that they allow convenient access to the inter-wire gap, which is beneficial for sensing applications. In the following, we present several possible realizations of such microstructured dielectric claddings and describe performance of the resulting hybrid metal/dielectric fibers.

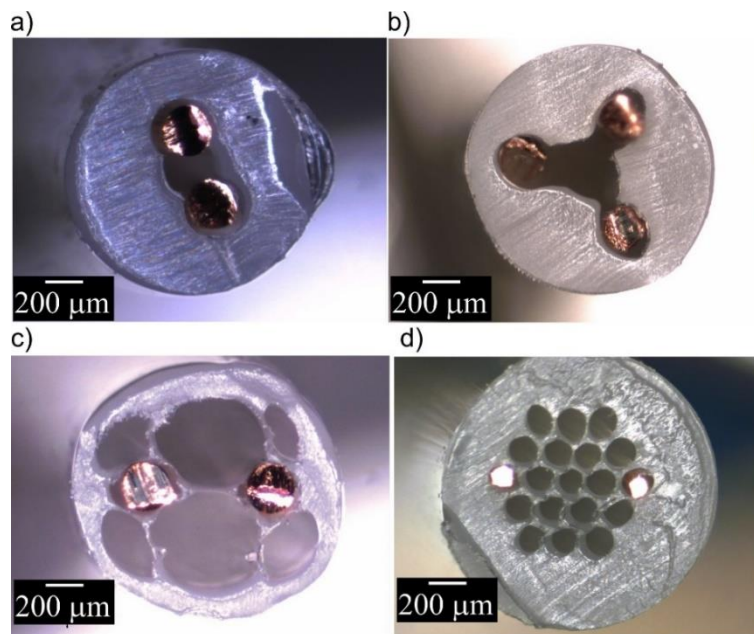


Figure 5.11. Cross sections of several hybrid fibers fabricated in our group. Microstructured claddings of these fibers feature: a) three-interconnected holes, b) four-interconnected holes, c) web of thin bridges that is used to support metallic wires, and d) three rings of holes positioned on a hexagonal lattice.

Two-wire waveguides encapsulated into porous microstructured claddings featuring subwavelength holes

In our group we have explored several designs of the microstructured claddings for application in two-wire waveguides. The proposed cladding structures are porous and feature several judiciously positioned holes [123]. In its simplest implementation, a hybrid fiber features dielectric cladding that has three interconnected circular holes (see Figure 5.17 (a), and Figure 4.4 (a)), where the central hole is empty and the two peripheral holes are filled with metal wires. More complex designs can feature a larger number of holes (see Figure 5.18 (e) or Figure 4.13 (a)), or a web of thin bridges that are used to support two metallic wires (see Figure 5.18 (c)). Clearly, such structures can be designed to hold more than two wires. All these microstructured cladding structures were realized in our group using fiber drawing technique. Particularly, microstructured preforms corresponding to the desired cladding geometries were first fabricated by CNC drilling of the polyethylene rods. The preforms were then drawn into fibers. During the drawing process, the size of the holes (in the fiber cladding) was controlled using overpressure. Finally, metallic wires were inserted into the drawn microstructured claddings to obtain hybrid two-wire fibers.

The guiding in hybrid two-wire waveguides is most efficient for the light polarized parallel to the line connecting the two wires. A typical modal pattern represents the mixture of a plasmonic mode, guided by the two wires, and a TIR (total internal reflection) mode of the fiber dielectric cladding. The presence of porous dielectric cladding significantly complicates the modal structure of a composite fiber. The modes of such fibers can be approximately classified as “cladding” modes and core-guided “plasmonic” modes. In order to distinguish core-guided plasmonic modes from the cladding modes, we also examined the dispersion relations, the losses, and the excitation efficiencies of the modes of a stand-alone porous cladding (red lines in Figure 5.12). Among all the modes of a composite fiber there is one (blue lines in Figure 5.12) that clearly has no corresponding analogue among the modes of a stand-alone porous cladding, we call such a mode the fundamental plasmonic mode of a composite fiber. Dispersion relation of the fundamental plasmonic mode extends into the low frequencies ($<0.1\text{THz}$), with the mode still well confined within the fiber. This can be of advantage when compared to the fundamental mode of a porous fiber which at low frequencies is strongly present in the air outside the fiber cladding. In practical terms, it means that even at low frequencies the fundamental plasmonic mode is suitable for guiding

THz light due to its strong confinement in the fiber and consequently, low sensitivity to the perturbations in the environment.

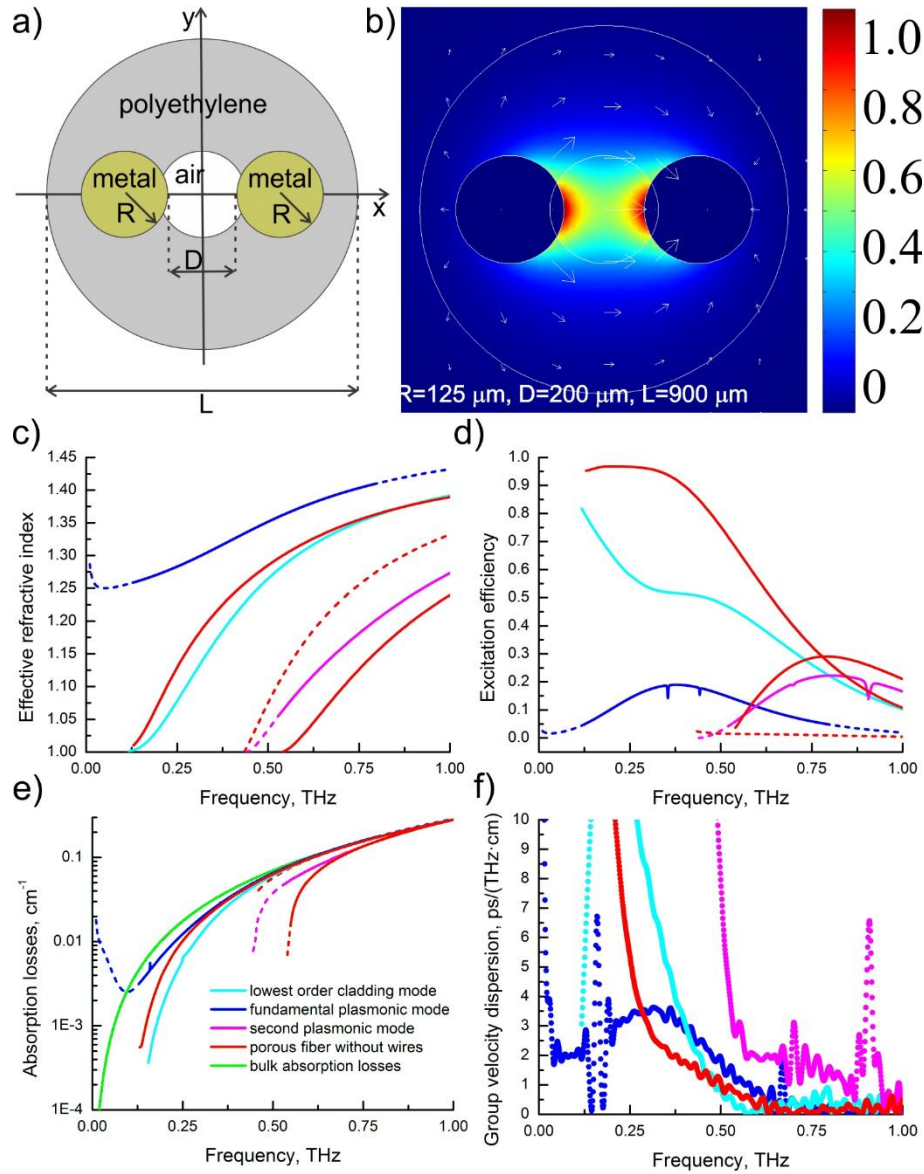


Figure 5.12. a) Schematic of a composite three-hole fiber. b) Longitudinal flux distribution for the fundamental plasmonic mode at 0.2 THz of a composite three-hole fiber. c) Effective refractive indices, d) excitation efficiencies, e) absorption losses, and f) group velocity dispersion for the various modes of a composite three-hole fiber. We use dotted curves at frequencies for which modal excitation efficiency drops below 5%. As an excitation source we use linearly polarized, diffraction limited Gaussian beam.

The cladding modes of a composite fiber (cyan curves in Figure 5.12, for example) have consistently lower absorption losses and lower modal group velocity dispersions compared to those

of a stand-alone porous cladding. This is a simple manifestation of the fact that placing metal wires in the structure of a porous fiber leads to more efficient modal expulsion from the neighboring dielectric into low-loss, low refractive index air regions.

Our simulations also show that absorption losses of the modes of a three-hole composite fiber can be quite smaller than the bulk material absorption losses of a dielectric cladding (green curve in Figure 5.12 (e)), which is a direct consequence of the modal localization in the fiber central air hole and air cladding. Meanwhile, losses and group velocity dispersions of the modes of a composite fiber are still much higher than those of a classical two-wire waveguide. In order to further decrease the absorption losses and broaden the waveguide's bandwidth it is essential to increase the fraction of power guided in the air by increasing the fiber porosity. Thus, in Figure 5.13 (a),(b) we present a seven-hole fiber with holes placed in the vertices of an equilateral triangular lattice. The two metal wires are placed in the two opposing holes of the fiber, resulting in the THz light guided predominantly in the central air hole (see Figure 5.13 (b)). In Figure 5.13 (c)-(f) we present dispersion relations, absorption losses, coupling efficiencies, and group velocity dispersion of the modes of a seven-hole composite fiber. Modal structure is dominated by the modes that are similar in nature to those of a three-hole fiber presented in Figure 5.12. However, transmission losses of a seven-hole fiber are significantly smaller than those of a three-hole fiber due to higher porosity of a seven-hole fiber. Another significant difference between the two fibers is observed in the modal properties of the second plasmonic mode. Particularly, the excitation efficiency of this mode in a seven-hole fiber is relatively high (20-70%) in the broad spectral range 0.59 THz-1.5 THz, while the maximal excitation efficiency of this mode in a three-hole fiber is only 20% at the near vicinity of 0.8 THz. At the same time, propagation losses of the second plasmonic mode in a seven-hole fiber are 3-10 times smaller than the cladding bulk absorption loss while the modal group velocity dispersion remains relatively low (~ 1 2ps/(THz.cm)) in a wide frequency range 0.65 THz-1.15 THz.

Although performance of the seven-hole hybrid fibers reported above is still considerably inferior to that of a classic two-wire waveguide, it is clear that one can consistently improve on the hybrid fiber performance by reducing modal overlap with the dielectric cladding structure. Moreover, if instead of solid plastics like Polyethylene, one would use low density foams, then using microstructured foam cladding presented in this section would lead to considerable

improvements to an already good performance of the two-wire waveguides with solid foam claddings.

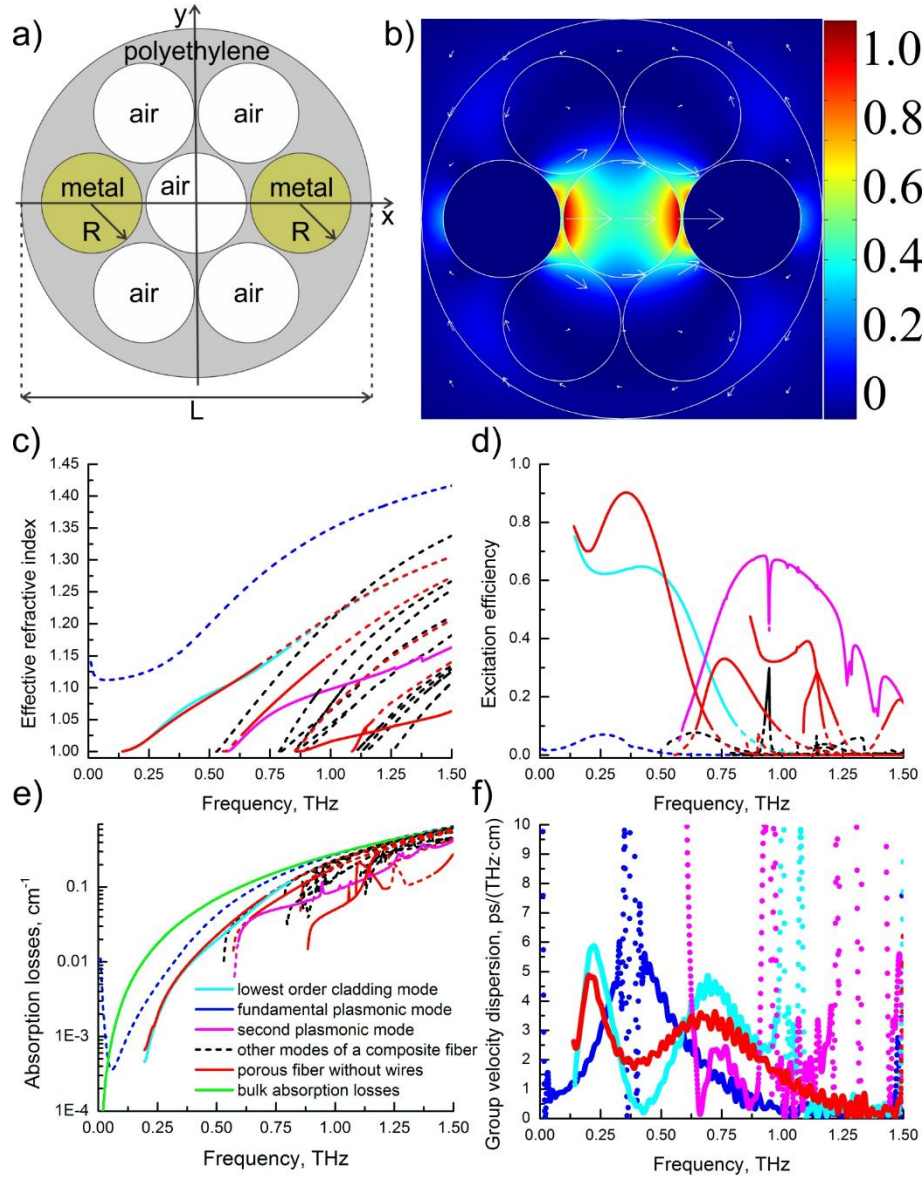


Figure 5.13. a) Schematics of a composite three-hole fiber. b) Longitudinal flux distribution for a typical guided mode of a composite seven-hole porous fiber. c) Effective refractive indices, d) excitation efficiencies, e) absorption losses, and f) group velocity dispersion for the various modes of a composite seven-hole fiber. We use dotted curves at frequencies for which modal excitation efficiency drops below 5%. As a source we assume linearly polarized, diffraction limited Gaussian beam.

Sensing applications with hybrid two-wire waveguides

Some plasmonic modes in the hybrid metal/dielectric waveguides detailed in the previous subsection can rapidly change their confinement with operation frequency. This interesting effect was studied in [126] in the context of resonant refractive index sensing. For example, in a three-hole hybrid waveguide shown in Figure 5.12, in the vicinity of 0.7 THz, localization of the second plasmonic modes changes from the core bound to the cladding bound. Particularly, at lower frequencies (0.5 – 0.7 THz) the plasmon is propagating at the air/metal interface with a significant amount of energy concentrated in the central air hole between the two wires (see Figure 5.14(a)). At higher frequencies (>0.7 THz), the plasmonic mode leaves the central air hole while localizing in the vicinity of the metal/plastic/air junctions (see Figure 5.14 (b)). Such resonant behavior is clearly interesting for sensing applications.

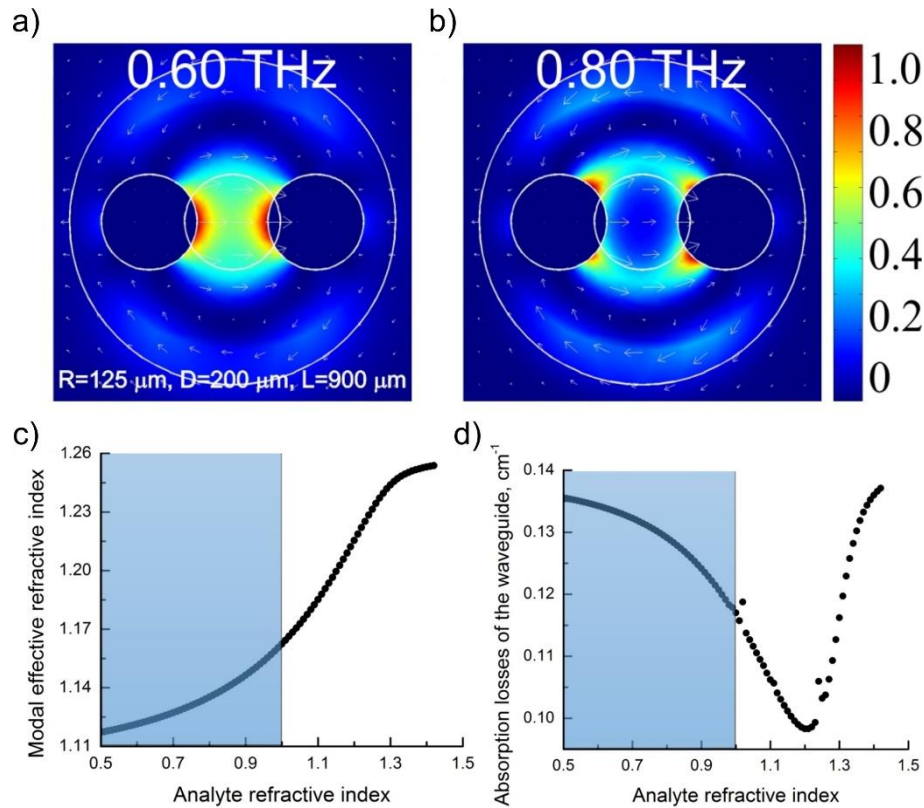


Figure 5.14. Longitudinal flux distribution for the second plasmonic mode at a) 0.60THz, b) 0.80 THz. Arrows show vectorial distribution of the corresponding transverse electric field. Changes in the optical properties of the plasmonic mode as a function of the analyte refractive index. c) Modal effective refractive index, d) absorption losses.

To demonstrate refractive index sensing in THz spectral range we assume that the central hole of the fiber is filled with analyte in gaseous or aerosol forms. In this case, the core refractive index is changed uniformly and throughout the fiber core. In the simulations we only vary the real part of the analyte refractive index while assuming that the gaseous analyte has negligible absorption. This is only to show the resonant nature of the transduction mechanism (unlike non-resonant, absorption-based sensing mechanism). In the following simulations we use 1.514 as a frequency independent refractive index of the polyethylene cladding with frequency dependent material loss $\alpha [cm^{-1}] = 0.28 \times \nu^2$ (ν is in THz) [127].

In Figure 5.14 (c),(d) we show how optical properties of the plasmonic mode change when varying the analyte refractive index (core refractive index). In these simulations we keep the operation frequency fixed at 0.71 THz. Strong changes in the fiber optical properties, with respect to changes in the analyte refractive index, are desirable for the optimal performance of a fiber refractometer. From Figure 5.14 (d) we note that by design, the rate of change in the modal absorption loss is the highest when the core refractive index is close to 1, which is most suitable for gaseous analytes. This is directly related to the choice of the operational frequency of 0.71 THz at which core guided mode shows significant changes in its localization preference from the hollow core at low frequencies into the plastic cladding at higher frequencies.

We now consider various factors that influence resolution of the hybrid fiber refractometer. In general, refractometer sensitivity can be defined as $S_a(n_a, \nu) = (\partial \alpha_m(n_a, \nu) / \partial n_a) / \alpha_m(n_a, \nu)$, where $\alpha_m(n_a, \nu)$ is the absorption loss of a plasmonic mode. From Figure 5.15 we notice that for a given value of the analyte refractive index, sensitivity can be optimized by the judicious choice of the operation frequency. Resolution of a sensor can then be calculated by assuming that a 1% change in the transmitted amplitude can be reliably detected. Thus, sensor resolution can be obtained as $0.01 / S_a(n_a, \nu)$. The maximal sensitivity is achieved at 1.0 THz and is equal to 6.98 RIU⁻¹, resulting in a sensor resolution of $1.4 \cdot 10^{-3}$ RIU. The geometric parameters of the fiber can be also optimized to increase sensor resolution.

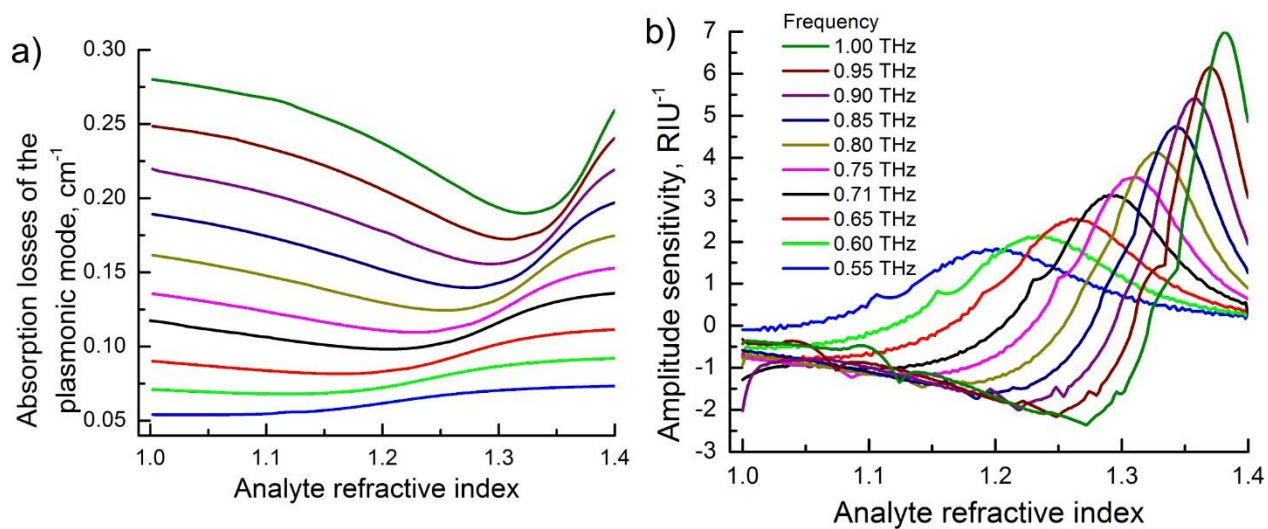


Figure 5.15. a) Absorption losses of the plasmonic mode, and corresponding b) sensitivity of the refractometer as a function the refractive index of the analyte at various values of the operation frequency.

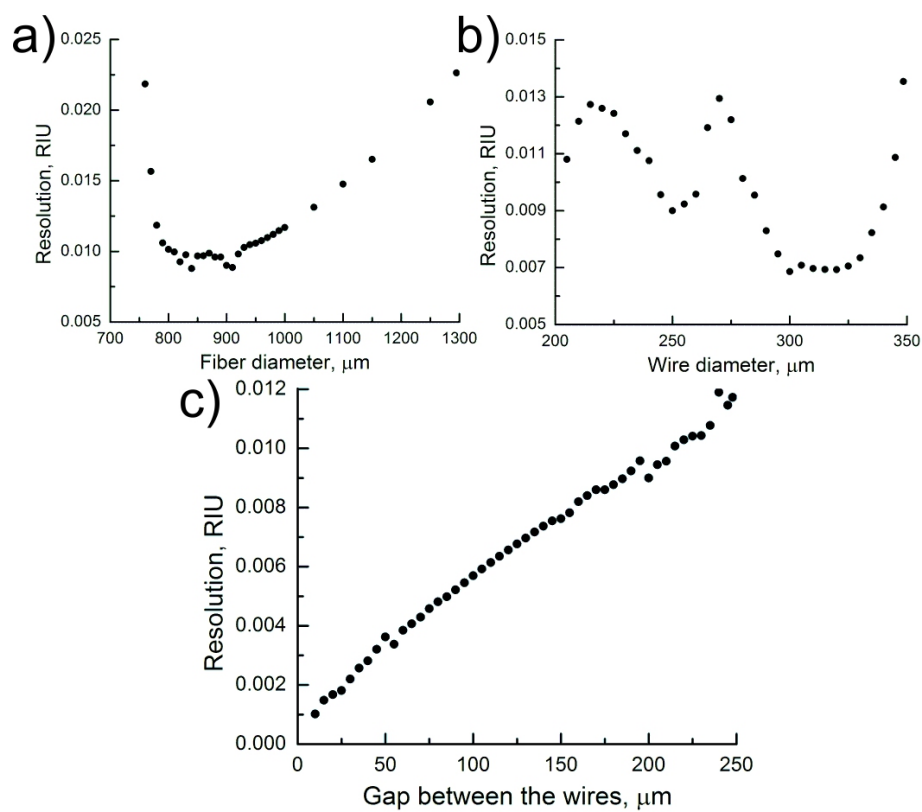


Figure 5.16. Resolution of the hybrid fiber-based refractometer as a function of a) fiber diameter, b) wire diameter, and c) gap between the wires.

In Figure 5.16 we present resolution of the refractometer for different values of the fiber diameter, the wire diameter, and the gap size between the wires. In these simulations we keep the operation frequency fixed at 0.71 THz and the analyte refractive index close to 1. Since plasmonic mode of a composite fiber is generally well confined within the central hole region of the fiber, the refractometer resolution is not strongly sensitive on the fiber and wire diameters (see Figure 5.16 (a),(b)). In contrast, inter-wire gap size has the strongest effect on the refractometer sensitivity (see Figure 5.16 (c)). There is practically a linear dependence of the resolution on the distance between the wires. Smaller gaps between the wires result in higher sensitivities. Thus, resolution as small as $3 \cdot 10^{-3}$ RIU can be achieved for the inter-wire separation of 50 μm .

Experimental characterization of hybrid fibers

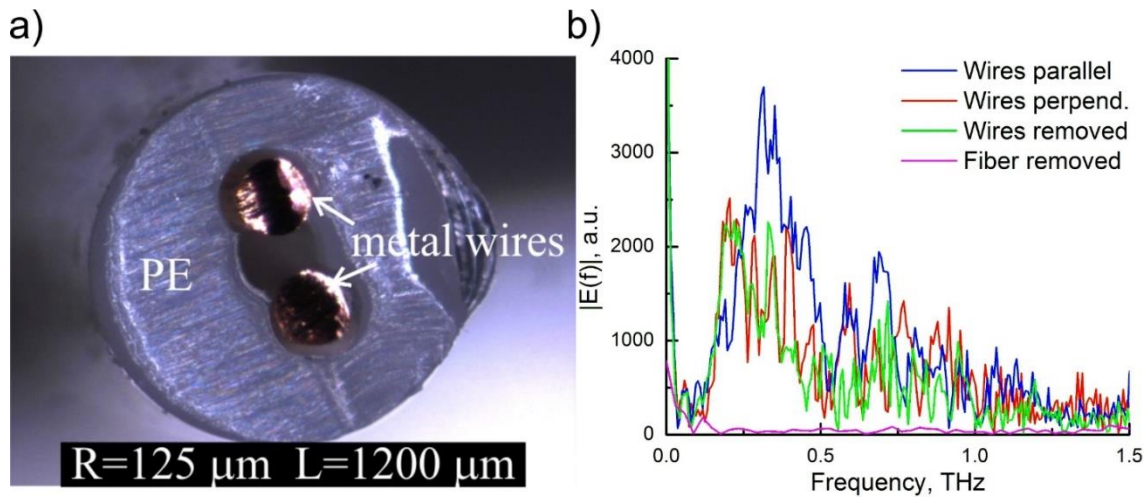


Figure.5.17 a) Cross section of a hybrid 20cm-long three-hole fiber. b) Experimentally measured transmission spectra, blue curve – wires oriented along the polarization of the input THz field, red curve – wires are perpendicular to the polarization of the input THz field, green curve – wires are removed, thus leaving behind a porous dielectric cladding, purple curve – the fiber is removed from the holders.

In this section we present optical characterization of several hybrid fibers featuring porous plastic claddings. We start with the three-hole hybrid fibers (see Figure.5.17 (a)) fabricated using fiber drawing technique [114, 115]. Specifically, three overlapping holes were drilled in a low density polyethylene (LDPE) rod with a diameter of 2.5 cm. The LDPE was chosen because of its low absorption in the THz region ($\alpha=0.28 \text{ cm}^{-1}$ at 1 THz) and the ease of thermal processing. The preform was subsequently drawn at 180°C without pressurization into fibers with a diameter of 1.2

mm. Finally, 250 μm -diameter copper wires were inserted into the two opposing holes of a plastic fiber. The diameter of the copper wires was chosen to match that of the fiber holes in order to reduce the potential misalignment inside the fiber. Using this method, 20 cm-long hybrid fibers were manufactured and later used in the measurements.

For optical characterization, a standard THz-TDS setup was used. The fiber input and output ends were placed at the focal points of the two parabolic mirrors. The two fiber ends were held by the metallic apertures that were closed around the fiber. The apertures were used both for mechanical support and for blocking the stray light that otherwise would propagate outside of the fiber. In Figure.5.17 (b) we show experimentally measured electric field transmission spectra. In our experiments we conducted four measurements. In the first of these measurements, polarization of the incoming THz light coincided with the direction of the line that connects the centers of the two metallic wires; we call this the “parallel” polarization. For this orientation of the wires, excitation of the plasmonic modes is most efficient and therefore, the total transmission through the fiber is the highest (blue curve in Figure.5.17 (b)). Then, we rotated the fiber so that polarization of the electric field became perpendicular to the line connecting the centers of the two metallic wires, we call this polarization “perpendicular”. In this case, excitation of the plasmonic modes is suppressed, thus, mostly the modes of a plastic cladding are excited. Not surprisingly, the corresponding transmission (red curve in Figure.5.17 (b)) is lower than in the case of “parallel” polarization. Then, we removed the metal wires and found that the resulting transmission spectrum of a bare plastic cladding (green curve in Figure.5.17 (b)) is similar to that of a hybrid fiber excited “perpendicularly”. This is undoubtedly related to the fact that, in both cases, the modes of plastic cladding are the most likely to be excited. Finally, we removed the fiber from the holders in order to determine the amount of stray light in the system (purple curve in Figure.5.17 (b)). We observed that almost no straight light can pass through a set of apertures (fiber support) in the absence of a fiber.

In Figure 5.18 we present several other examples of hybrid metal/dielectric fibers with porous dielectric claddings. Figure 5.18 (a),(c) depicts fibers featuring a thin web of plastic bridges that are used to support two metal wires. In Figure 5.18 (e) we show a fiber featuring a hexagonal lattice of air holes with two metal wires placed in the middle of the porous microstructure. For all these fibers we conducted optical characterizations similar to those presented in the previous paragraph. It is clear that for all of the hybrid fibers, transmission tends to be higher when

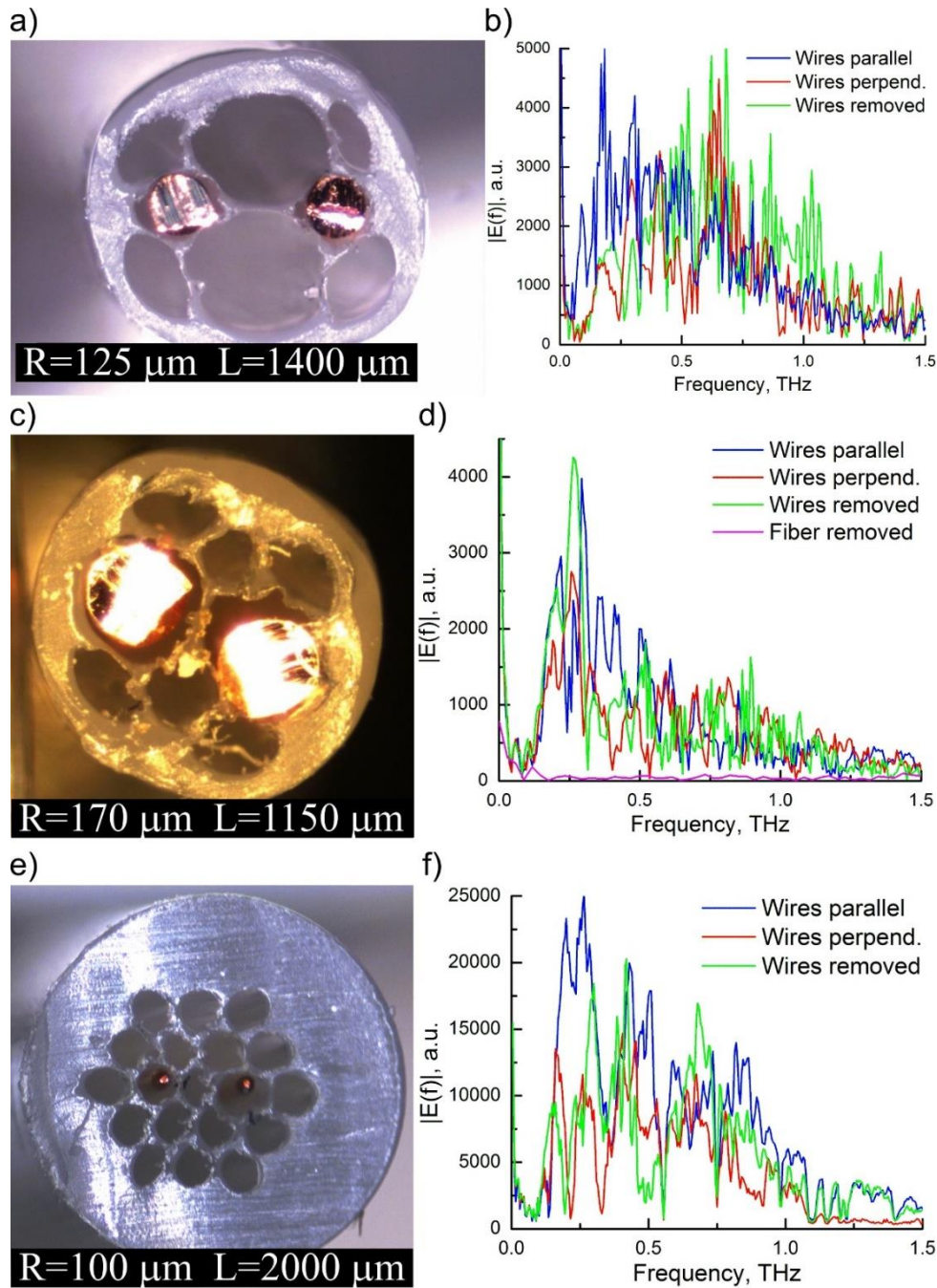


Figure 5.18 a) Cross section of a hybrid 10cm-long fiber with thin bridges supporting metallic wires and b) experimentally measured transmission spectra. c) Cross section of a hybrid 10cm-long fiber with thin bridges supporting larger metallic wires and d) experimentally measured transmission spectra. e) Cross section of a hybrid 5cm-long fiber with hexagonal lattice of air holes with two metallic wires and f) experimentally measured transmission spectra. For all the transmission spectra: blue curves – wires oriented along the polarization of the input THz field, red curves – wires are perpendicular to the polarization of the input THz field, green curves – wires are removed, thus leaving behind a porous dielectric cladding.

polarization of the incoming THz light coincides with the direction of the line connecting the centers of two metallic wires (“parallel” polarization). A spectral range in which a hybrid fiber is advantageous over an all-dielectric porous fiber of the same design (no wires) depends on the structure of the cladding and on the distance between the wires. Although our first experimental measurements of the hybrid fibers are encouraging, a more thorough analysis of cladding effect on the modal propagation parameters is still in order.

Fibers with embedded Indium wires

Another design of a hollow fiber with two or four metal wires has been demonstrated by Argyros et al. [61]. The Indium wires were embedded in the preform and then co-drawn together with the supporting material. The main advantage of the co-drawing method is in precise positioning of the thin metal wires inside of the fiber structure compared to manual insertion. Additionally, with the co-drawing method, several-meter-long fibers with wires can be fabricated while with the manual wire insertion method fiber length is typically limited to ~30 cm.

The investigated fiber (see Figure.5.19 (a)) has an inter-wire distance of approximately 2 mm. The wires have an elliptic shape with average diameters of 1.0 mm and 1.8 mm along the minor and the major axis, correspondingly. The fibers were made from Zeonex polymer which is known for its low loss in the THz region [62].

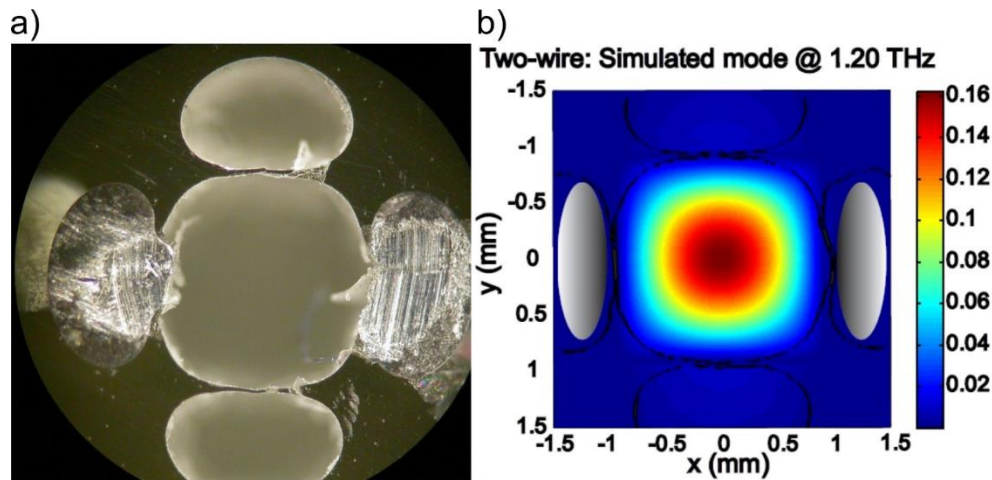


Figure.5.19 a) Cross section of a hollow core Zeonex fiber featuring two indium wires. Core diameter is ~2 mm. The indium wires are located at the left- and right-hand side of the hollow core and are seen silver; b) Field distribution (theory) in the HE_{11} -like mode at 1.2 THz. Adapted from [61].

In the THz frequency range, the lowest-loss mode compatible with the linearly polarized Gaussian beam of a standard THz source is a HE_{11} -like mode shown in Figure 5.19 (b). The numerical simulations indicate strong modal discrimination (with respect to their propagation losses) between the HE_{11} -like mode and the higher order modes. In the two-wire configuration, the HE_{11} -like mode is elliptical, which is most pronounced at low frequencies. At such frequencies, modal fields show significant presence in all three holes of the fiber and the modal sizes can differ by as much as 20% along the two axes. The authors have also investigated configurations with four metal wires surrounding the hollow core. Unsurprisingly, HE_{11} -like modes of the two-wire and four-wire fibers do not differ much in shape at high frequencies, with most of the modal field concentrated in the central hole. At lower frequencies however, HE_{11} -like mode of a two-wire fiber becomes more elongated compared to the mode of a four-wire fiber due to penetration of its modal field into the two peripheral holes.

Transmission through the fibers has been measured using a standard free-space THz-TDS setup. The cutback method was used to characterize fiber propagation loss and modal effective refractive index. To obtain a modal field profile, a metal pinhole with a diameter of 0.8 mm was placed at the fiber output end and scanned across the fiber cross section. The experimentally obtained modal profiles agree well with the field distribution of the simulated HE_{11} -like mode. Figure 5.20 (a) shows comparison of the measured and simulated power absorption coefficients. The experimentally measured absorption loss (by power) is 0.3 cm^{-1} for the two-wire configurations. The simulated absorption loss has a trend of decreasing towards higher frequencies due to enhanced confinement in the air-filled fiber core. At lower frequencies, modal fields can have a significant presence in the lossy plastic cladding, thus leading to rapid increase in the modal propagation loss. Experimentally, this is manifested by the presence of a low frequency cut-off at $\sim 0.5 \text{ THz}$.

The effect of the two-wire orientation with respect to the excitation beam polarization has been investigated by rotating the fiber around its axis. The comparison of the transmission spectra is shown in Figure 5.20 (b). In both cases, the same low-frequency cut-off was observed, at around 0.5 THz . The transmitted power for the polarization perpendicular to the wire plane was reduced in comparison with the polarization parallel to the wire plane.

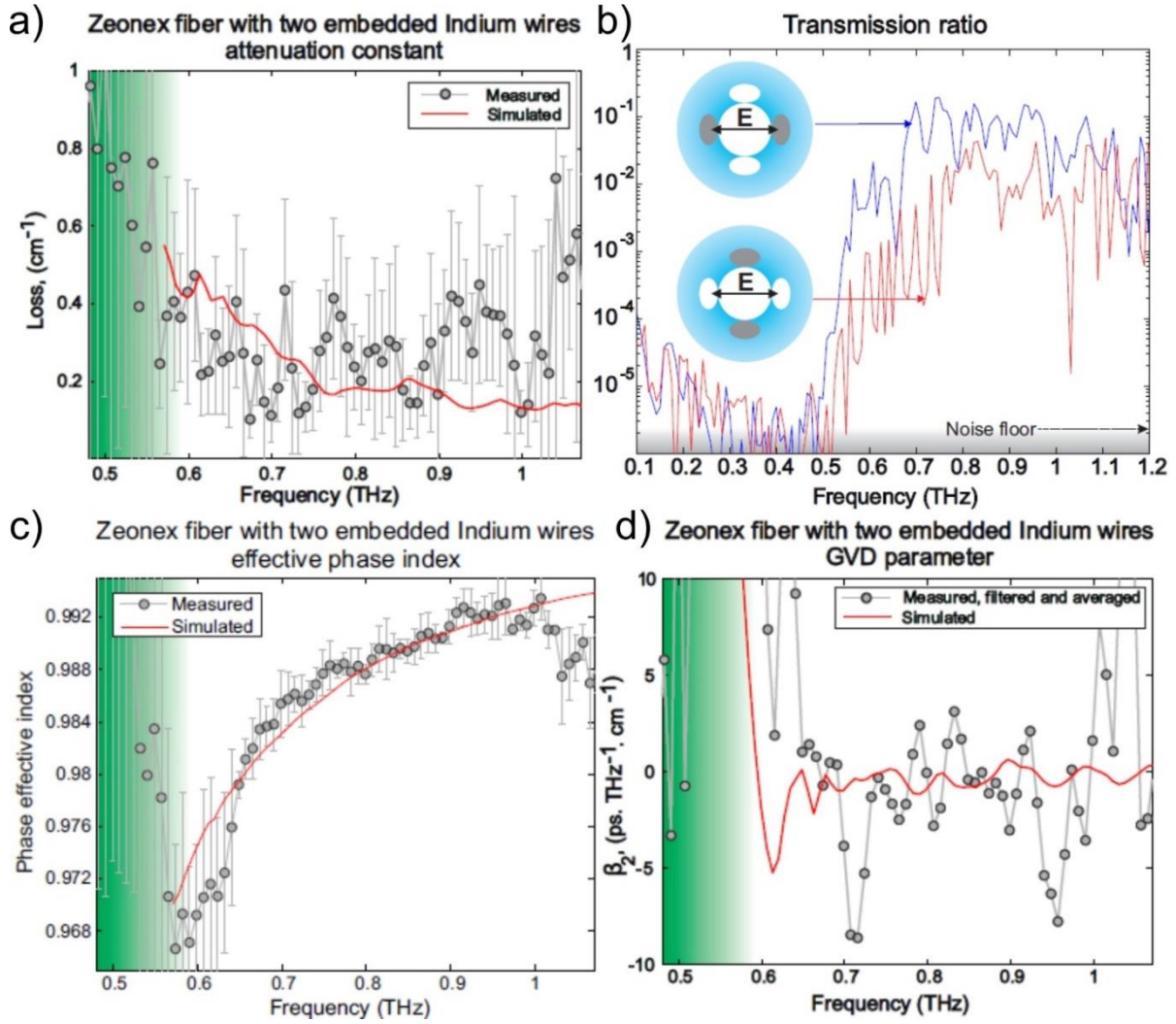


Figure 5.20 a) Loss coefficients as measured (grey) and as simulated (red line) for a two-wire fiber. b) Normalized transmission spectrum of 8 cm two-wire fiber with different wire plane orientation with respect to the electric field polarization as indicated. The indium wires are depicted as grey ellipses while the air region is the filled white space. c) Phase refractive indices as measured (grey) and as simulated (red line) for a two-wire fiber. d) The group velocity dispersion parameter determined from the measured data (grey) and as calculated from the simulation (red line) for a two-wire and fiber. Adapted from [61].

The effective refractive index is shown in Figure 5.20 (c), and its value is close to 1. The group velocity dispersion is calculated from the measured index data and is shown in Figure 5.20 (d). For the fiber with two-wires, GVD smaller than $5 \text{ ps}/(\text{THz} \cdot \text{cm})$ was found in the 0.65–1.0 THz frequency range. It was further demonstrated that fibers with two-wires show generally lower losses and lower dispersions than fibers with four wires.

Scaling of the hybrid fiber dimensions

It is interesting to note that the fibers discussed in section 4.3 and in section 1.1.4 of the literature review, appear to have very similar designs. Indeed, both fibers feature a porous microstructured cladding, a central air-filled hole (core), as well as two wires placed directly next to the hollow core. Although, the guiding mechanisms reported for these fibers are surprisingly different [128]. In particular, the waveguide of section 1.1.4 guides a HE_{11} -like mode [61] that is similar to a low-loss resonant ARROW mode of a thin plastic capillary [32]. In fact, both modes have effective refractive indices smaller than that of air and their field intensities are maximal at the core center. Moreover, in both cases, fiber guidance is most effective when the fiber hollow core size is much larger than the wavelength of guided light which is indeed the case for the fibers reported in [61]. Meanwhile, the waveguides discussed in section 4.3 guide hybrid plasmonic modes [123] which are characterized by the effective refractive indices that are higher than those of air. Moreover, the hybrid plasmonic modes feature modal fields that are bound to the surface of the metallic wires.

The main reason for the difference in the guiding mechanisms of the two fibers is simply related to the relative size of the two fibers. Particularly, fibers that guide hybrid plasmonic modes (section 4.3, [123]) have 10–20 times smaller diameters than fibers that guide ARROW-like modes (section 1.1.4, [61]). In [61] the authors start with a large hollow tube that is known to support ARROW-like modes in the hollow core and then add metallic inclusions. In this case, light interference in the tube walls is essential for the efficient modal confinement in the hollow core (see [32] for more details). Alternatively, in the previous section we start with a two-wire waveguide that features an inter-wire separation comparable to the wavelength of guided light. Such a waveguide is known to support a tightly confined plasmonic mode. Then, the porous dielectric cladding is added for mechanical support. In this case, the geometry of plastic cladding is not essential for guidance as the guided mode is supported directly by the two wires. The resulting fiber is therefore much smaller than in [61] and has a core size comparable to the wavelength of guided light.

If the only significant difference between these fibers is their size, then, it is interesting to see how the fiber guidance mechanism changes when the fiber size is continuously reduced. As a starting point for this study we take the structure of a three air-hole Zeonex fiber with two Indium

wires and a central hole-size of 2 mm as reported in [61]. We then continuously scale down the fiber dimensions to a factor of 100 while keeping the operational frequency fixed at 1.0 THz. In Figure 5.21 we present the longitudinal flux distribution of the most easily excitable mode of such fibers for different values of a scaling factor. The number below each figure indicates the size of the air gap between two metal wires. The easiest-to-excite mode is defined as a mode that has the highest excitation efficiency when using a linearly polarized Gaussian beam of 750 μm waist diameter as an excitation source.

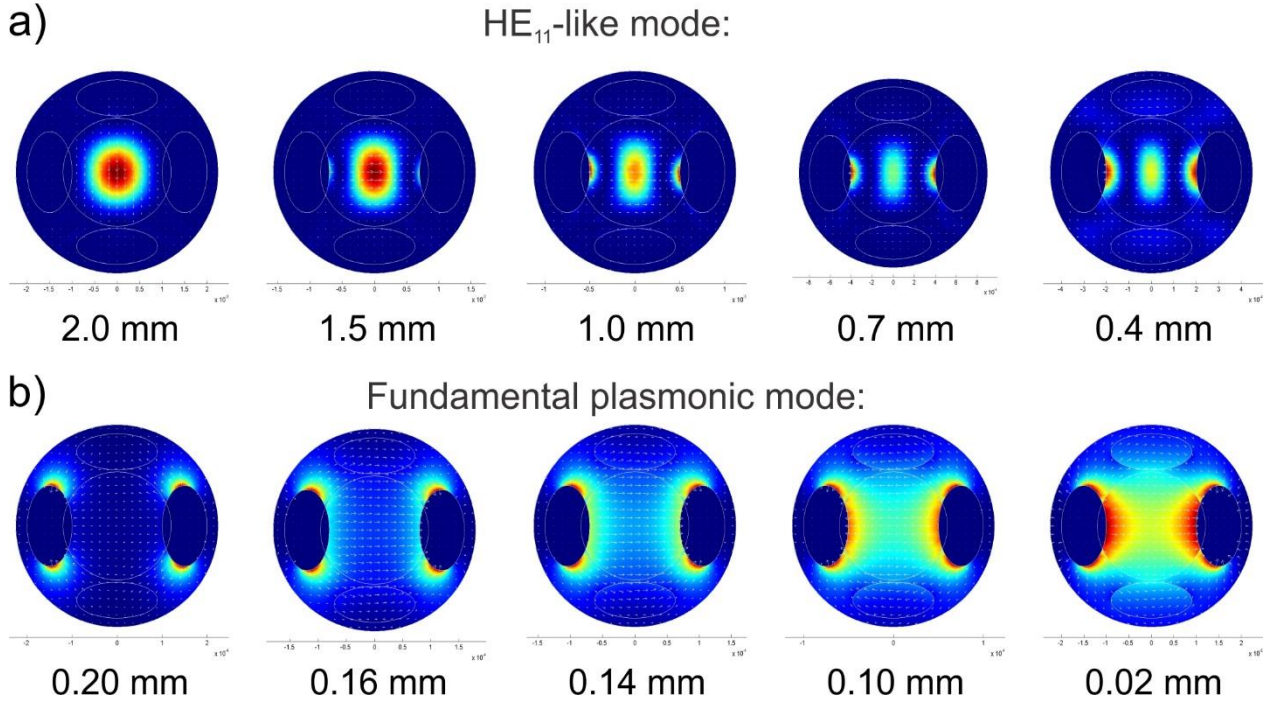


Figure 5.21 a) Core-bound HE_{11} -like modes similar to those reported in [61]. b) Plasmonic-like modes similar to those described in chapter 4.3 and paper [123]. The number below each graph indicates the size of the air gap between the two wires. Adapted from [128].

For the largest inter-wire gap (2 mm), the easiest-to-excite mode is a HE_{11} -like mode that can propagate in the hollow core even when metal wires are removed. However the use of metal wires is justified since their presence lowers the modal propagation losses as compared to those of a mode of corresponding all-dielectric waveguide with wires removed. This is because the field of the core-bound mode is efficiently expelled by the metal wires from the lossy plastic cladding, into the low-loss air region.

As we decrease the fiber size, we first observe a significant increase in the absorption losses of the HE_{11} -like mode. Moreover, its modal refractive index decreases from 0.99 for the largest

fiber down to 0.5 for the fiber with 0.4 mm gap between the two wires (see Figure 5.21 (a)). Finally, the mode disappears at inter-wire separations smaller than 0.4 mm.

At inter-wire separations of less than 0.4 mm, the easiest-to-excite mode is a hybrid plasmonic mode (see Figure 5.21 (b)). This mode is bound to the surfaces of the two metallic wires while also having some significant presence in the plastic cladding and in the air holes. For the inter-wire separations in the 0.2-0.4 mm range, the losses of this hybrid mode are high as the mode is mostly localized in the plastic cladding. When decreasing the inter-wire separation below 0.2 mm, the modal fields get pulled into the fiber central hole leading to a high fraction of the modal fields being located in the air gap between the two metallic wires; this is a classic property of a two-wire plasmonic waveguide.

From this study we conclude that the same hollow-core fiber featuring two metal wires can support low-loss air-bound ARROW modes at high frequencies, while changing its guidance mechanism to plasmonic (wire-bound modes) at lower frequencies when the wavelength of guided light becomes comparable or greater than the inter-wire separation. This conclusion is very intriguing as it signifies that hybrid metal/dielectric porous fibers can have a very large operational bandwidth while supporting tightly confined air-bound modes at all frequencies within their operational range.

5.5 Conclusion

In this review we detailed the state of development for hybrid metal/dielectric terahertz waveguides. We started with a summary of the outstanding guidance properties of the classic two-wire plasmonic waveguides. The fundamental mode of a two-wire waveguide has very low losses ($<0.01 \text{ cm}^{-1}$) and very low group velocity dispersion ($<0.1 \text{ ps}/(\text{THz}\cdot\text{cm})$) in the whole THz spectral range, with modal fields mostly confined in the inter-wire air gap. Excitation efficiency of the fundamental plasmonic mode is sensitive both to the operation frequency and to the various geometrical parameters such as metal wire diameter, inter-wire gap size, and relative position of the THz Gaussian beam used as a source. Through the judicious choice of the geometrical parameters of the waveguide, excitation efficiency of the fundamental mode can be optimized to reach levels higher than 50% within a broad frequency range $\sim 1 \text{ THz}$.

Next, we proposed the use of low-loss, low-refractive-index materials as optical cladding for the two-wire waveguides. The mechanical encapsulation of the metallic wires is necessary in order to simplify handling of the two-wire waveguides in practical applications, as well as to reduce the effect of the environment on the optical properties of the waveguide.

As one possible option for the two-wire waveguide cladding material, we considered low density polyethylene foam. Optical characterisation confirmed that foams have low loss $<0.2 \text{ cm}^{-1}$, as well as a low and almost constant refractive index ~ 1.01 in the whole THz frequency range. THz measurements using two wires sandwiched between two foam blocks have confirmed that in this hybrid waveguide the average (over frequency) modal refractive index has only slightly increased to ~ 1.003 , while the average modal loss have increased by only $\sim 0.12 \text{ cm}^{-1}$.

As another possible choice for the two-wire waveguide cladding material we considered highly porous microstructured claddings made of a low-loss plastic such as polyethylene. Several cladding structures have been fabricated using the fiber drawing technique. Most claddings feature a collection of air holes in plastic or a web of thin plastic bridges that are designed to mechanically support metallic wires. Optical characterization of hybrid waveguides fabricated using the aforementioned technique has confirmed that porous microstructured plastic claddings can indeed serve as a mechanical support for the two metallic wires. However, we have also discovered that meticulous care must be taken in order to minimize the negative effect of such claddings on the modal propagation properties such as loss and group velocity dispersion. For example, one has to reduce overlap of the modal fields with the lossy plastic cladding by increasing cladding porosity. Additionally, the size of the fiber microstructure (holes, etc.) has to be carefully matched with the size of the metal wires in order to avoid variations in the inter-wire gap along the waveguide length; otherwise, radiation losses can be significant.

Next, we reviewed several numerical studies of the modal structure and modal properties of the hybrid metal/dielectric THz fibers with porous microstructured cladding. The modes in such fibers can be generally classified as plasmonic-like and cladding-like. Tightly bound plasmonic modes of hybrid metal/dielectric THz fibers can exist even at very low frequencies attaining below 0.1 THz. When coupling to hybrid fibers using linearly-polarized Gaussian THz beams, efficient excitation of both cladding and plasmonic modes is possible. Consequently, it is important to make sure that consistent excitation conditions of hybrid waveguides are reached.

Furthermore, some plasmonic modes of the hybrid fibers show resonant dependence of their confinement properties on the operation frequency, geometrical parameters, and material refractive indices. Therefore, we review the possibility of using such modes for THz refractometry.

Finally, we conclude by mentioning that guidance mechanism of the hybrid fibers can change significantly when varying the operation frequency. Thus, hollow-core plastic fibers featuring two metal wires can support low-loss air-bound ARROW modes at high frequencies, while changing its guidance mechanism to plasmonic (wire-bound modes) at lower frequencies when the wavelength of guided light becomes comparable or greater than the inter-wire separation. This finding is particularly interesting as it suggests that metal/dielectric porous fibers can support tightly confined air-bound modes in a wide frequency range.

CHAPTER 6 ARTICLE 4: HYBRID PLASMONIC TERAHERTZ FIBERS FOR SENSING APPLICATIONS

This chapter is based on my paper “Hybrid plasmonic terahertz fibers for sensing applications,” published in Applied Physics Letters in 2013. There are no other contributors to this article besides me and my research supervisor. Therefore, my role in this article includes all the aspects of the novel fiber-based refractometer design. I am responsible for the initial idea of exploiting the transduction mechanism in hybrid metal/dielectric fiber for constructing a THz refractometer, optimization of the fiber geometry, and thorough analysis of its sensitivity.

In this chapter, a hybrid plasmonic THz fiber featuring two metallic wires in a porous dielectric cladding is studied for resonant sensing applications. In such design, introduction of even lossless analytes into the fiber core leads to significant changes in the modal losses, which is used as a transduction mechanism. With a refractive index resolution on the order of $\sim 10^{-3}$ RIU, the composite fiber-based sensor is capable of identifying various gaseous analytes and aerosols or measuring the concentration of dust particles in the air.

6.1 Introduction

Optical chemical and bio-sensors have attracted considerable attention in biochemistry and medicine where systems capable of highly sensitive, label-free and minimally invasive detection are in high demand [101, 102]. Terahertz electromagnetic waves with a spectrum lying between far infrared and microwave regions offer unique properties that are not available at other wavelengths. THz radiation is nonionizing due to its low photonic energy and many substances are predicted to have a specific spectral response in the terahertz range.

Most of the current THz sensors are realized in the non-resonant configurations where sample is interrogated directly by the THz light. In resonant sensors, changes in the sample properties are measured indirectly by studying variations in the optical properties of a resonant structure coupled to a sample. In resonant sensing method one typically employs resonant spectral transmission characteristics or photonic band-gap effect of sensing devices. The sensors detect shifts of the resonant wavelength in response to resonant structure changes caused by the presence of the analyte. These sensors include thin-film micro-strip lines resonators [103], photonic crystal

waveguides [104], metallized periodic groove structures integrated into parallel-plate waveguides [105], thin metallic meshes [106], planar double split-ring resonator arrays [107], resonant cavities integrated into parallel-plate waveguides [108], and dielectric pipe waveguides [109]. In the amplitude-based detection methodology one operates at a fixed wavelength and records changes in the amplitude of a signal, which are then reinterpreted in terms of changes in the analyte refractive index. Among the advantages of this type of sensors are low cost and ease of fabrication, since no precisely engineered resonant or photonic band-gap structure is required.

In this work, we describe a refractometer based on practical plasmonic THz fibers that feature two metallic wires inserted into porous dielectric cladding [see Figure 6.1 (a)]. For the purpose of this paper, we refer to such fibers as composite fibers. Introduction of even lossless analytes into the fiber core leads to significant changes in the modal losses, which is used as a transduction mechanism. With a refractive index resolution on the order of $\sim 10^{-3}$ RIU, the composite fiber-based sensor is capable of identifying various gaseous analytes and aerosols or measuring the concentration of dust particles in the air.

6.2 Wave guiding in composite fibers with two metal wires in dielectric cladding

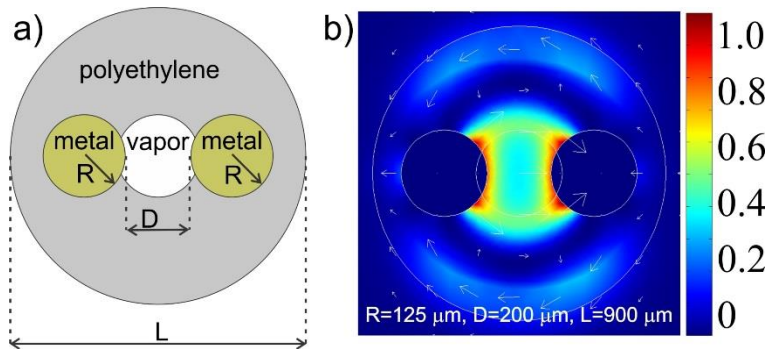


Figure 6.1 a) Schematic of the composite three-hole fiber. b) Longitudinal flux distribution for the plasmonic mode in a composite fiber at 0.71 THz. Arrows show vectorial distribution of the corresponding transverse electric field.

In general, two-wire plasmonic THz waveguides combine both low loss performance and low group velocity dispersion. Moreover, the field distribution in the fundamental mode of a two-wire waveguide is similar to that emitted by the dipole-type photoconductive THz antennas. This allows efficient excitation of the two-wire waveguides using standard THz sources [30, 123].

Finally, introduction of a porous cladding into the structure of a two-wire waveguide enables direct manipulations of such waveguides without the risk of perturbing the core-guided modes that are mostly confined in the gap between the wires.

The wave guiding in such composite fibers is most efficient for the light polarized parallel to the center line joining the two wires. A typical modal pattern represents the mixture of a plasmonic mode guided by the two wires, and a total internal reflection mode guided by the fiber plastic cladding. The presence of porous polyethylene cladding significantly complicates the modal structure of the waveguide. In order to distinguish predominantly plasmonic modes from the modes of a porous cladding, we also study the optical properties of the modes of a porous cladding alone (no wires). Among the modes of a composite fiber, there are plasmonic modes that have no corresponding analogue among the modes of a porous cladding. Plasmonic modes of a composite fiber are typically well confined within the central hole of a fiber cladding. In practical terms, it means that plasmonic modes are suitable for guiding THz light due to their strong confinement in the fiber hollow core and, as a consequence, relatively low loss and low group velocity dispersion, low sensitivity to bending, high tolerance to imperfections on the fiber surface and to perturbations in the environment. It is natural to expect high sensitivity of such sensors due to an almost perfect overlap between analytes filling the hollow core and optical modes of a sensor.

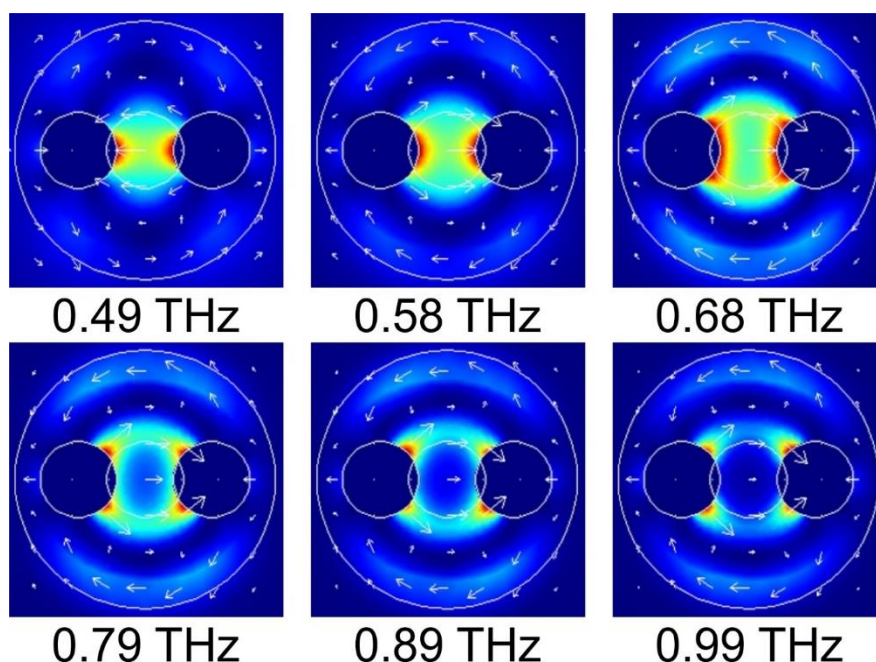


Figure 6.2 Longitudinal flux distribution for the plasmonic mode of a composite fiber at various frequencies.

6.3 Results and discussion

The outer diameter of the composite fiber in Figure 6.1 is $L = 900 \mu\text{m}$, the wire diameter is $2R = 250 \mu\text{m}$, the air hole diameter is equal to the wire diameter and the gap between the wires is $200 \mu\text{m}$. Theoretical modeling of modal excitation efficiency by a linearly polarized Gaussian beam (which is a typical field pattern produced using photoconductive antennas) shows that in the 0.5–1.0 THz frequency range there is an efficient excitation of plasmonic modes ($> 20\%$ coupling by power) that have high concentration of power in the cladding central hole. Transverse distribution of the longitudinal power flux of such mode at 0.71 THz is shown in Figure 6.1 (b). The choice of this frequency is justified by the fact that in its vicinity, localization of the mode changes from the core bound to cladding bound. At lower frequencies (0.5 – 0.7 THz) the plasmon is propagating at the air/metal interface with a significant amount of energy concentrated in the central air hole between the two wires. At higher frequencies (> 0.7 THz), the plasmonic mode leaves the central air hole, while localizing in the vicinity of the metal/plastic/air junctions (see Figure 6.2). Such behavior is advantageous for sensing applications.

To demonstrate sensing applications we first assume that the central hole of the fiber is filled with analyte in gaseous or aerosol forms. In this case, the core refractive index is changed uniformly and throughout the fiber core. In our simulations we only vary the real part of the analyte refractive index, while assuming that the gaseous analyte has negligible absorption. This is only to show the resonant nature of the transduction mechanism. Unequivocally, the same sensor will also detect changes in the analyte absorption. In the following simulations we use 1.514 as a frequency independent refractive index of the polyethylene cladding with frequency dependent material loss $\alpha [cm^{-1}] = 0.28 \times \nu^2$ (ν is in THz) [127].

In Figure 6.3 we show how optical properties of the plasmonic mode change when varying the analyte refractive index (core refractive index). In these COMSOL simulations we kept the operation frequency fixed at 0.71 THz. Clearly, strong changes in the fiber optical properties with respect to changes in the analyte refractive index are desirable for the optimal design of a fiber refractometer. From Figure 6.3 (b) we note, for example, that the rate of change in the modal absorption loss is the highest when the core refractive index is close to 1, which is most suitable for the design of refractometers operating with gaseous analytes. It should be noted that we present the modal effective refractive index and absorption losses for values of the analyte refractive index

below 1 only to demonstrate that the slope of these curves is the steepest (or nearest to the steepest value) for the values of analyte refractive index typical for analytes in a gaseous form. This high sensitivity of the modal loss on the value of the core refractive index is directly related to the choice of the operational frequency of 0.71 THz at which core guided mode shows significant changes in its localization preference from the hollow core at low frequencies into the plastic cladding at higher frequencies. Analysis of changes in the phase of transmitted light can give another modality for the multi-measurand detection using hybrid plasmonic THz fibers. Changes in the modal effective refractive index of the plasmonic guided mode [see Figure 6.3 (a)] can be determined from variations in the phase of transmitted light. However, the phase-based sensing approach is beyond the scope of this thesis and we rely on the absorption-based method which offers simplicity of implementation and lack of ambiguity in the interpretation of results, which is often the case with the phase sensitive methods.

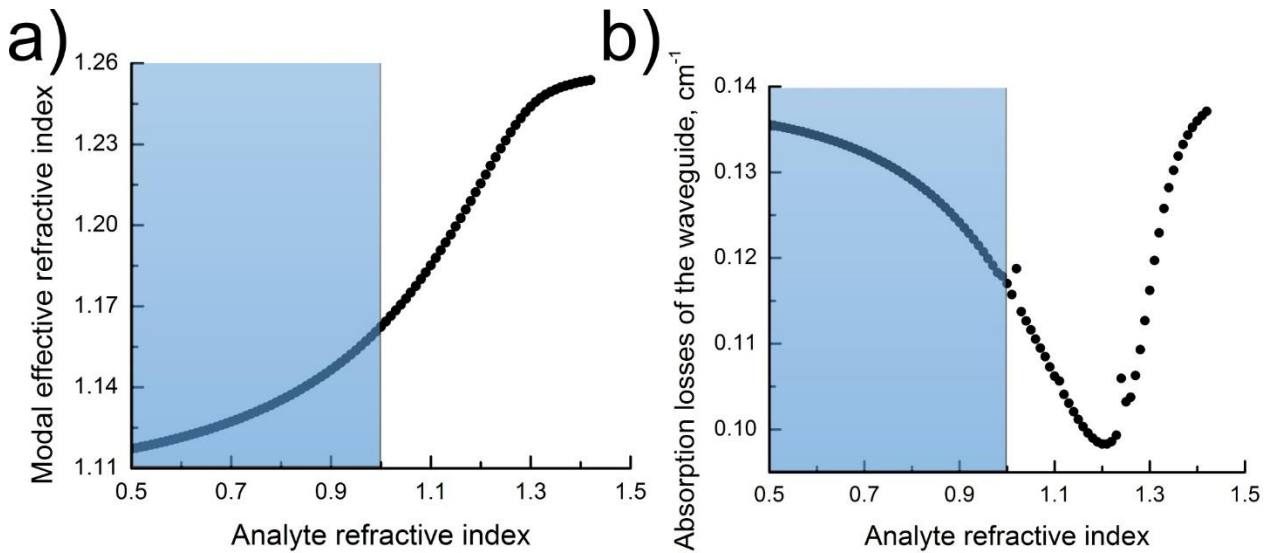


Figure 6.3 Changes in the optical properties of a plasmonic mode as a function of the analyte refractive index. a) Modal effective refractive index, b) absorption losses.

We now consider various factors that influence resolution of the refractometer. As before, we suppose that analyte is lossless. First of all, from Figure 6.4 we notice that for a given value of the analyte refractive index n_a , sensor's sensitivity can be optimized by the judicious choice of the operation frequency ν . Particularly, in Figure 6.4 (a) we present absorption losses of the plasmonic mode of a three-hole composite fiber as a function of the analyte refractive index for various choices of the operation frequency. As demonstrated in [129], for a given value of the analyte

refractive index, the optimal choice of the operation frequency is the one that maximizes an amplitude sensitivity defined as:

$$S_a(n_a, \nu) = (\partial \alpha_m(n_a, \nu) / \partial n_a) / \alpha_m(n_a, \nu) \quad (6.1),$$

where $\alpha_m(n_a, \nu)$ is the absorption loss of a plasmonic mode. Resolution of a sensor can then be calculated by assuming that 1% change in the transmitted amplitude can be reliably detected, from which sensor resolution is calculated as $0.01/S_a(n_a, \nu)$. Consider, for example, gaseous analytes with refractive index close to 1. From Figure 6.2 we observe that the nature of modal localization changes rapidly in the 0.7 - 0.9 THz frequency range from the core-guided to the cladding-guided. Consequently, this results in significant changes in the fiber absorption losses in this frequency range. Therefore, it is not surprising to find that the refractometer's sensitivity achieves its maximal value of 2.02 RIU^{-1} at 0.9 THz, with the corresponds resolution of $5 \times 10^{-3} \text{ RIU}$. The maximal sensitivity is achieved at 1.0 THz and is equal to 6.98 RIU^{-1} , resulting in the sensor resolution of $1.4 \times 10^{-3} \text{ RIU}$.

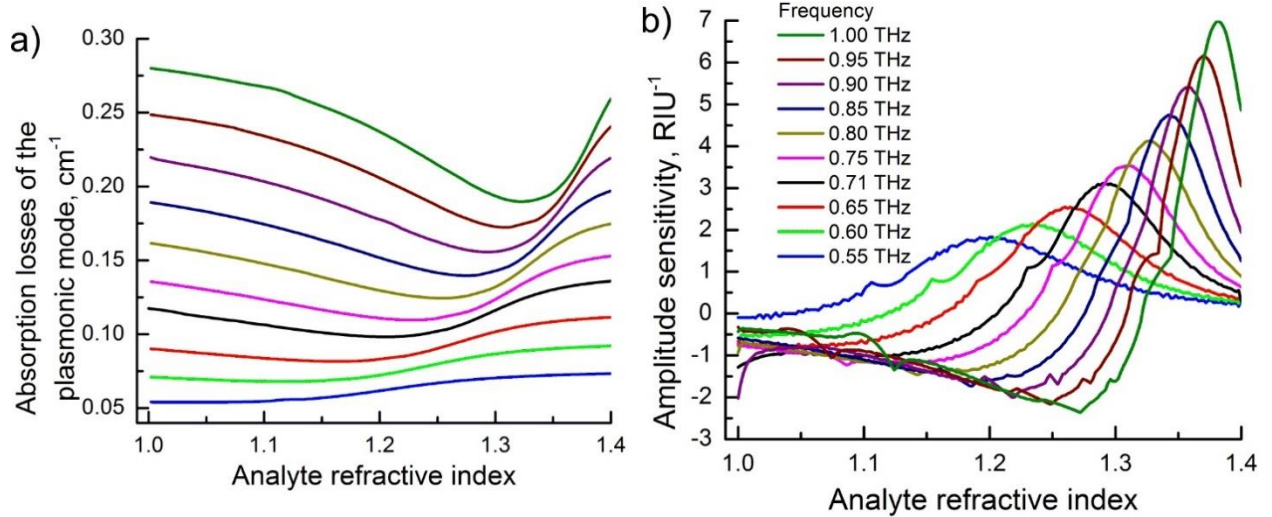


Figure 6.4 a) Absorption losses of the plasmonic mode, and corresponding b) Sensitivity of the refractometer as a function the refractive index of the analyte at various values of the operation frequency.

At this point, it is necessary to compare the sensitivity of the proposed sensor to that of the other devices reported in literature for optical refractive index sensing. Amplitude-based sensors are rarely studied in the terahertz range, the highest theoretical value of sensitivity was reported for

a fiber sensor composed of a subwavelength porous polymer fiber with a thin ferroelectric layer wrapped around it [130]. Phase matching of a plasmon-like mode with the fundamental core guided mode of a low loss porous fiber is highly sensitive to the gaseous analyte refractive index, which resulted in a resolution below $10^{-3} RIU$. More common spectral-based sensors include parallel-plate waveguides with a single [108] or multiple [131] resonant cavities with experimentally observed sensitivities of $91–225 GHz / RIU$, which yields a resolution of $4 \times 10^{-3} – 1.1 \times 10^{-2} RIU$ if we take into account a typical $1 GHz$ spectral resolution of a time domain THz setup. Vapor sensing has been shown by means of a simple pipe waveguide [109] where insertion of vapor into the hollow core of the pipe leads to a shift of resonant transmission dips. The experimentally obtained sensitivity is around $22.2 GHz / RIU$ (resolution $4.5 \times 10^{-2} RIU$ assuming $1 GHz$ resolution of a THz-TDS setup). Precisely engineered metamaterial array-based sensors [132, 133] have the highest experimentally shown sensitivity to the refractive index of the dielectric placed in direct contact with their surfaces. The resonant frequency shift results in $160–430 GHz / RIU$ sensitivity (resolution $2 \times 10^{-3} – 6 \times 10^{-3} RIU$). From the comparison of sensor resolutions it follows that the proposed device combines both the sensitivity comparable to that of the best demonstrated sensors while being cost effective and easy to manufacture.

The geometric parameters of the fiber can be also optimized to increase sensor resolution. Thus, Figure 6.5 presents resolution of the refractometer for different values of the fiber diameter, the wire diameter and the gap size between the wires. In these simulations we kept the operation frequency fixed at 0.71 THz and the analyte refractive index close to 1. Since plasmonic mode of a composite fiber is generally well confined within the central hole region of the fiber, the refractometer resolution is not strongly sensitive on the fiber and wire diameters [see Figure 6.5 (a), (b)]. In contrast, inter-wire gap size has the strongest influence on the refractometer resolution [see Figure 6.5 (c)]. There is virtually a linear dependence of the resolution on the distance between the wires. Smaller gaps between the wires result in faster (with frequency or core refractive index) changes in the nature of modal localization and, thus, result in higher sensitivities. Thus, resolution as small as $3 \times 10^{-3} RIU$ can be achieved for the inter-wire distance of 50 μm .

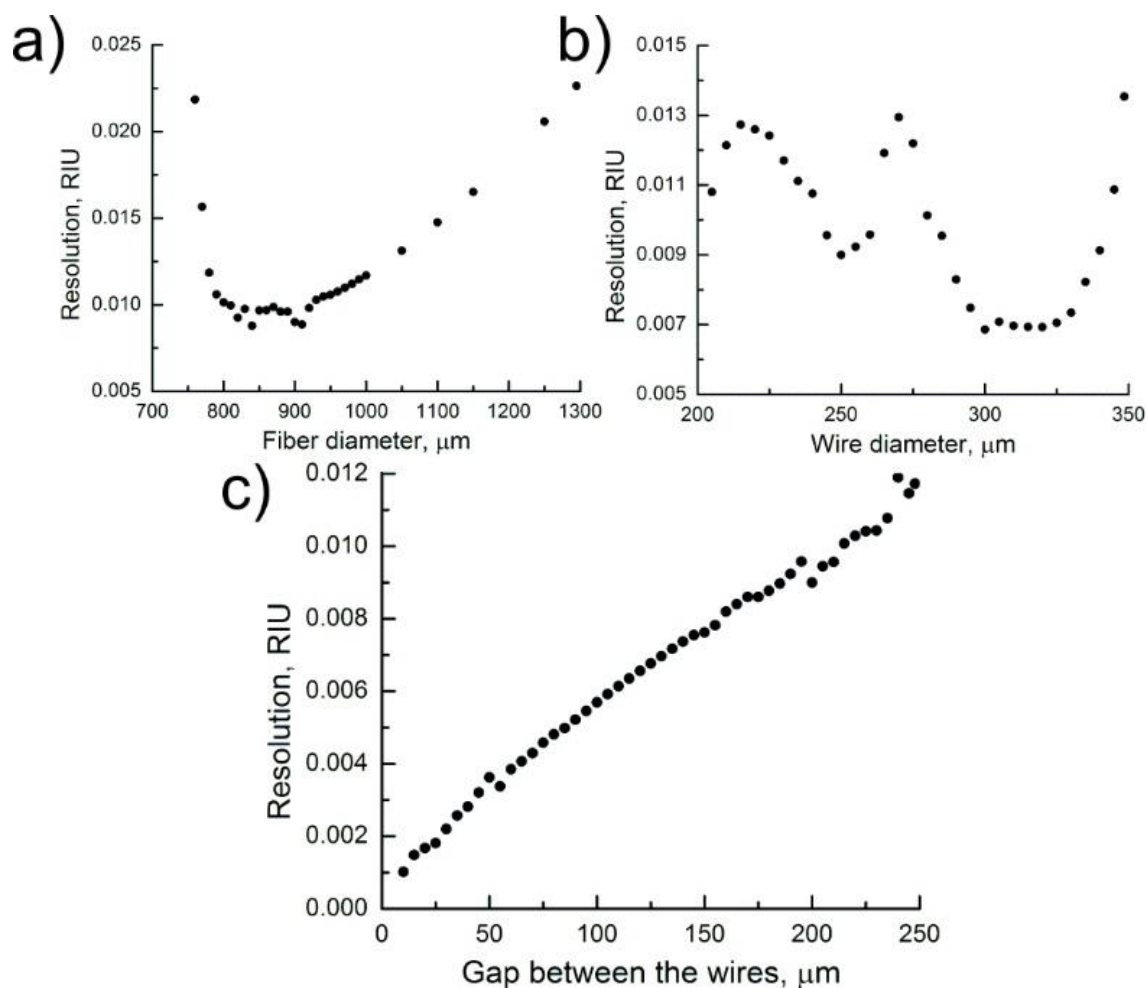


Figure 6.5 Resolution of the refractometer as a function of a) fiber diameter, b) wire diameter, c) gap between the wires.

6.4 Conclusion

In summary, we have proposed a hybrid refractometer based on practical plasmonic THz fibers that feature two metallic wires inserted into porous dielectric cladding. Introduction of even lossless analytes into the fiber core leads to significant changes in the modal losses, which is used as a transduction mechanism. Resolution of the refractometer has been investigated numerically as a function of the operation frequency and the geometric parameters of the fiber. Through the numerical simulation we have shown that amplitude-based detection method leads to sensitivities to the changes in the gaseous analyte refractive index on the order of $\sim 10^{-3}$ RIU.

CHAPTER 7 GENERAL DISCUSSION

Additional experimental results

Here I would like to discuss the additional experiments with the hybrid metal-wire/dielectric fibers that were not included in the previous chapters. During the last three years I have performed multiple measurements experimenting with different fiber designs.

For the characterization of the hybrid metal-wire/dielectric fibers it was the most important to compare their transmission with the all-dielectric fibers of the same design. Then in order to understand the modal structure of the hybrid fibers it was crucial to compare the transmission for different orientations of the incoming THz light polarization. Thus, a series of experiments has been conducted in which I studied the optical properties of the proposed fibers with and without metal wires in their structure for different polarization of THz radiation

In most of our experiments I conduct four measurements. In the first of these measurements, polarization of the incoming THz light coincides with the direction of the line that connects the centers of the two metallic wires (“parallel” polarization). For this orientation of the wires I expect the most efficient excitation of the plasmonic modes and therefore, the highest total transmission through the fiber. Then, I rotate the fiber so that polarization of the electric field became perpendicular to the line connecting the centers of the two metallic wires (“perpendicular” polarization). In this case, excitation of the plasmonic modes is suppressed, thus, mostly the modes of a plastic cladding are excited. Then, I remove the metal wires to find the resulting transmission spectrum of a bare plastic cladding. Finally, I remove the fiber from the holders in order to determine the amount of stray light in the system and confirm that almost no straight light can pass through a set of apertures (fiber support) in the absence of a fiber.

From Figure 7.1 and Figure 7.2 we notice that for most fibers the transmission is the highest in case of “parallel” to the excitation THz pulse orientation of the wires. It is especially pronounced at low frequencies where excitation efficiency of the fundamental plasmonic mode is the highest. Also I note that the resulting transmission spectrum of a bare plastic cladding is similar to that of a hybrid fiber excited “perpendicularly”. This is related to the fact that, in both cases, the modes of plastic cladding are the most likely to be excited.

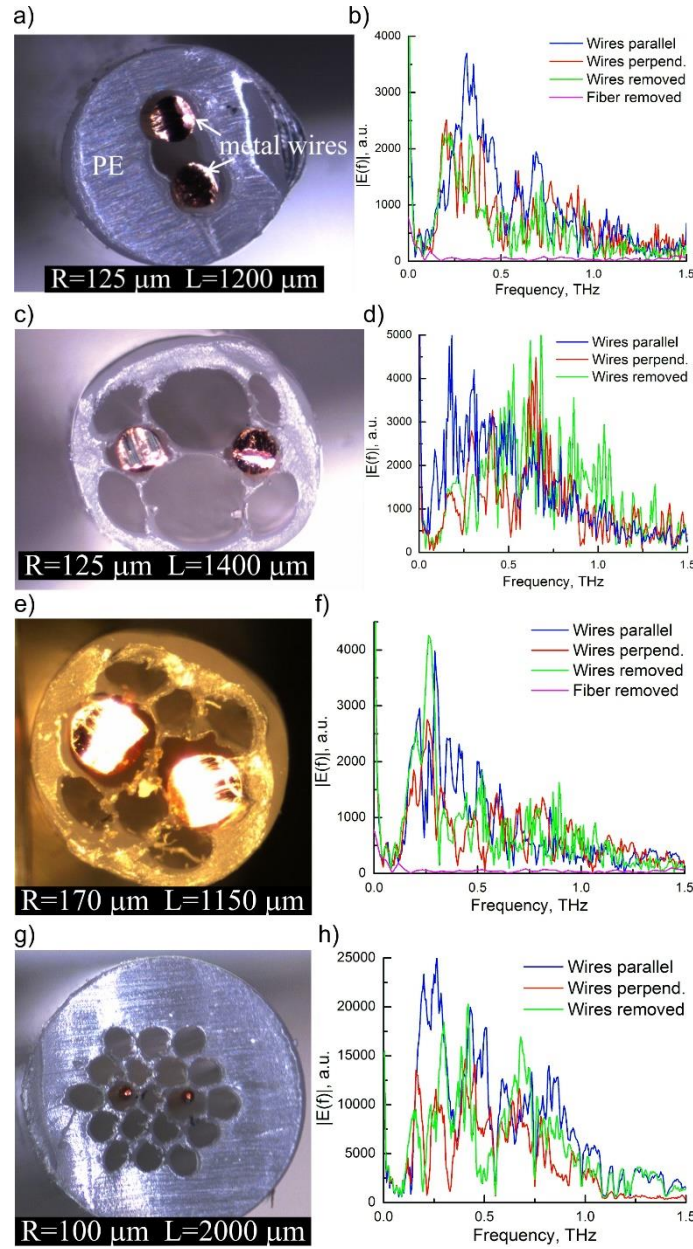


Figure 7.1 a) Cross section of a hybrid 20cm-long three-hole fiber. b) Experimentally measured transmission spectra; c) Cross section of a hybrid 10cm-long fiber with thin bridges supporting metallic wires and d) experimentally measured transmission spectra. e) Cross section of a hybrid 10cm-long fiber with thin bridges supporting larger metallic wires and f) experimentally measured transmission spectra. g) Cross section of a hybrid 5cm-long fiber with hexagonal lattice of air holes with two metallic wires and h) experimentally measured transmission spectra. For all the transmission spectra: blue curves – wires oriented along the polarization of the input THz field, red curves – wires are perpendicular to the polarization of the input THz field, green curves – wires are removed, thus leaving behind a porous dielectric cladding.

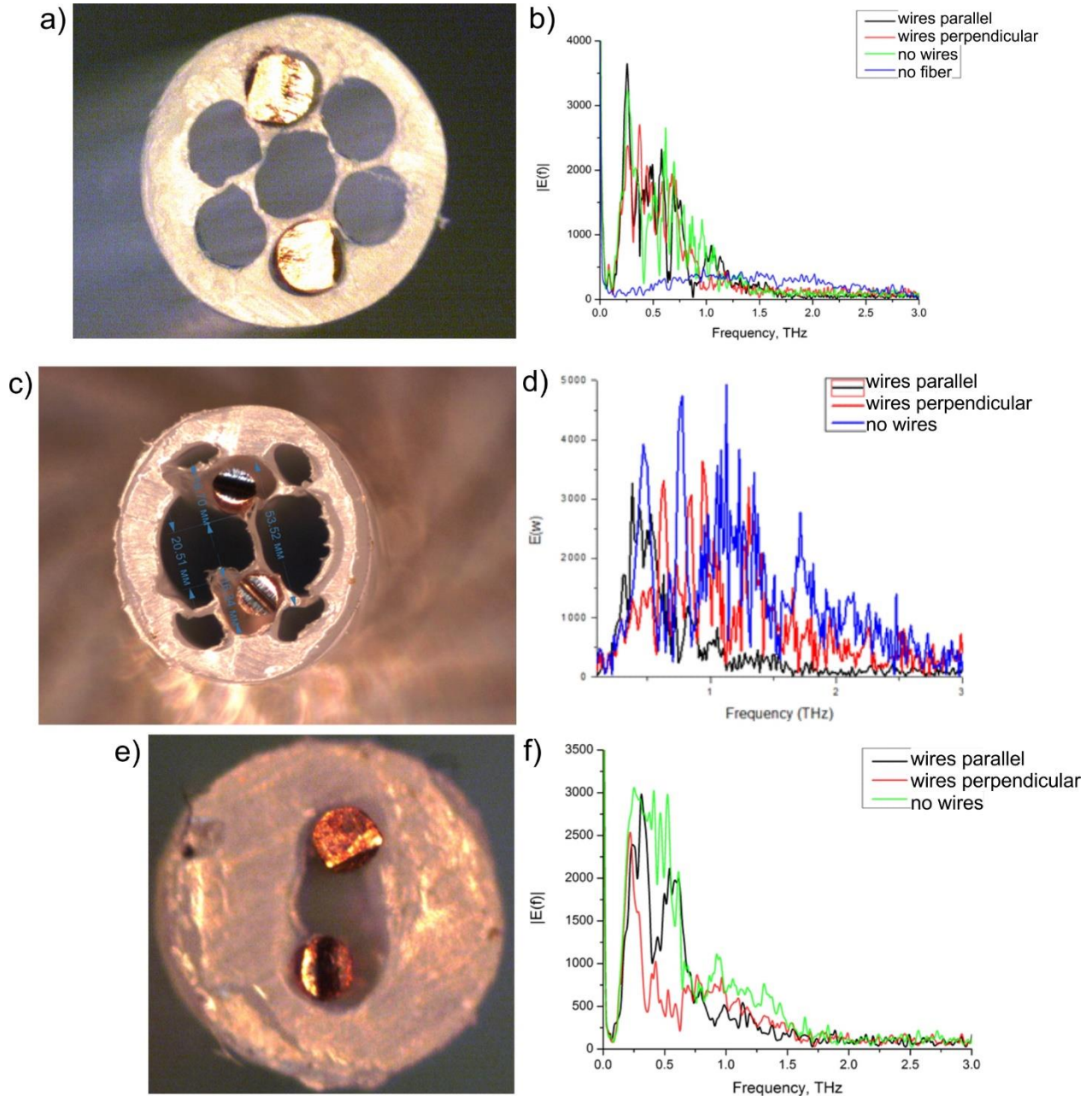


Figure 7.2. a) Cross section of a hybrid porous fiber with metal wires and b) experimentally measured transmission spectra; c) Cross section of a hybrid 10cm-long fiber with thin bridges supporting metallic wires and d) experimentally measured transmission spectra. e) Cross section of 3 hole fiber with two metallic wires and f) experimentally measured transmission spectra.

However from Figure 7.2 a)-b) we notice that in some measurements we observed almost complete transmission insensibility to the orientation of the wires or even their presence in the fiber. In Figure 7.2 c)-d) we show that for some fibers the presence of the metal wires is

advantageous only at low frequencies, and at higher frequencies the metal wires are rather blocking the incoming terahertz radiation than confining it in the air core of the fiber. The same statement is valid for the fiber from Figure 7.2 e)-f) where the “no wires” configuration demonstrates the highest transmission in the entire frequency region. These measurements do not correlate with the simulation results which predict an improved transmission of the hybrid metal-wire/dielectric fibers. In the next section I will explain the possible causes for such an inconsistency.

Waveguides performance limitations

The performance limitations of the waveguides described in this thesis mainly stem from two major factors. The first factor includes all types of fabrication imperfections. For example, to achieve the optimal transmission of any waveguide, one must ensure that its cross section is homogenous along the length of the waveguide and that all surfaces are smooth in order to reduce unnecessary reflection and scattering. In the particular case of two-wire waveguides, the most important requirement is to keep the wires perfectly straight and parallel to each other inside a long microstructured fiber.

The second factor lies in the choice of the material used for the fabrication of the waveguide. Low density polyethylene utilized both for planar waveguides and two-wire hybrid fibers is undoubtedly cheap, abundant, and easy to operate, however its absorption losses in the terahertz range are far from record low values. Therefore, in order to improve optical properties of THz waveguides, it may be more efficient to either use specifically designed polymers (Topaz, Zeonex etc.) or invest extra effort into improving fabrication methods. A simple replacement of the fiber material might potentially bring the absorption losses down by an order of magnitude.

Fiber cross section

As mentioned above, there are several challenges associated with the fiber fabrication process. The main problem is collapsing of the microstructured cladding during the drawing process, which is mainly due to surface tension. This problem can be partially solved by sealing one end of the preform and trapping air within the preform structure during the drawing process. While this generally allows us to avoid a complete hole collapse, it cannot prevent hole shrinking or shape changing. Thus, the drawing technique cannot guarantee a uniform cross section of the fiber along its length. This generally does not pose a significant problem for dielectric-only fibers,

however metal wire-based waveguides seem to be more sensitive to fabrication imperfections. The fundamental mode of the hybrid fiber is of plasmonic nature and is guided in the gap between the wires. Small changes in the dielectric cladding cross section might cause stronger deformation of the wires during the insertion and, thus, large bending losses.

To illustrate the issue in the Figure 7.3 I provide the cross sections of the input and the output facets of the same fiber provided in the same scale. One can observe that both outer diameter of the fiber changed and the separation between the wires reduced from 400 μm to 350 μm . Also I notice somewhat inconsistent structure of the waveguide inner geometry.

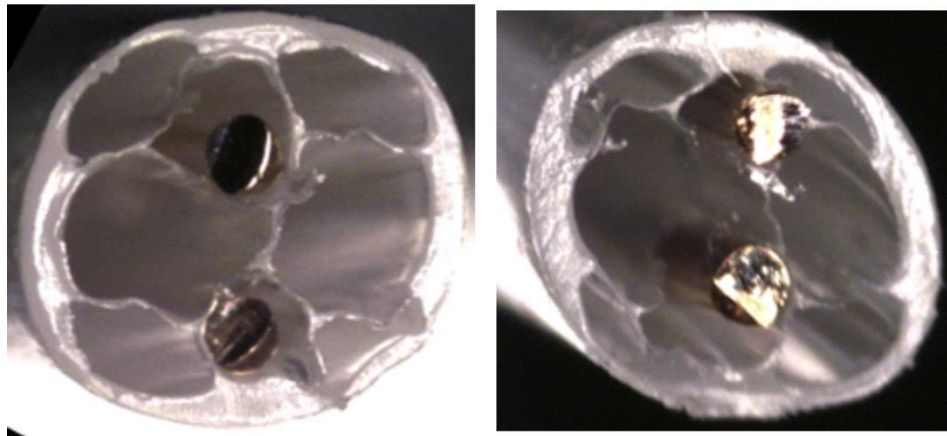


Figure 7.3 Two cross sections of the same highly porous hybrid fiber.

Coupling efficiency

Another complication in the design of such fibers lies in the ease of parasitic excitation of the cladding modes which prevents such fibers from showing losses comparable to that of low-loss hollow-core fibers. The large size of the fiber enables excitation of higher order modes. And the coupling into cladding modes is highly sensitive to the size of the input THz beam. The proper coupling should maximize the power guided by the fundamental mode and prevent excitation of higher order modes. To maximize the coupling in the desired fundamental mode of the waveguide, the terahertz beam must be focused such that its size is comparable to the distance between the wires. This would require precise and complicated alignment of optical hardware since the inter-wire distance is comparable or even lower than the wavelength. A hyper-hemispherical Si lens is used to focus the emitted THz radiation, which is subsequently focused by parabolic mirrors. However, due to a long optical path, it is practically impossible to bring the size of the THz beam

down to the diffraction limit. Focusing of a Gaussian beam by a parabolic mirror leads to a frequency dependent beam diameter d which can be approximated by [134]:

$$d_0 = \frac{4f\lambda}{\pi D}, \quad (7.1)$$

where D is the aperture size of the parabolic mirror, λ is the wavelength and f is the focal length of the parabolic mirror.

Commonly the knife-edge technique is employed to measure the beam profile of THz pulses. A non-transparent screen is moved across the optical path of the THz beam in small steps and the electric field in time-domain is measured for each step and then the electric field as a function of frequency and the position of the screen is calculated. For the Gaussian beam profile the field amplitude as a function of the displacement along the axis x perpendicular to the propagation line can be modeled by a complimentary error function $erfc(x)$. The derivative of this function yields the distribution of power inside the THz beam.

Alternatively, a simple technique that resolves the THz in both temporal and frequency domain is readily available [135]. The THz beam can be profiled utilizing an aperture fixed on a 2D translation stage placed in the beam path. For each position of the aperture a complete trace of the THz field is recorded. The accuracy of the method is limited by the minimal size of the aperture which allows a sufficient discrimination of the transmitted signal from noise.

In Figure 7.4 I present the experimental results of the beam size measurements. The aperture is placed in the center of the terahertz beam path at the focal distance from the parabolic lens focusing the radiation into the waveguide. The size of the aperture is changed between measurements and the transmitted pulse is recorded for each value of the aperture. Experimental measurements of the beam waist show that typically it is possible to focus a THz beam to the size of 1.5-3 mm, which is significantly larger than, for instance, the gap between the wires of the proposed hybrid fiber. A large discrepancy between the incoming THz beam size and the dimensions of the fiber causes inefficient coupling into the fiber's modes and leads to a low transmitted signal, which is then difficult to be discriminated over the noise level. Moreover, misalignment of the THz beam results in frequency shifted components, and narrowed spectra [136].

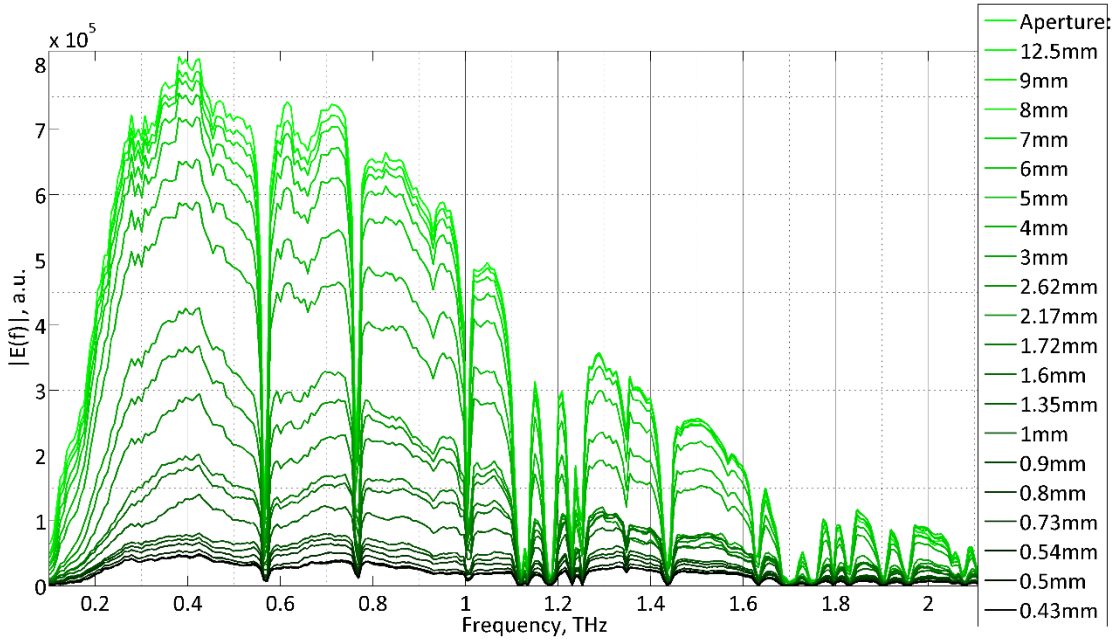


Figure 7.4. Terahertz field amplitude as a function of frequency for different sizes of the aperture.

Consequently, some alternative techniques for maximizing the coupling into the waveguide could be implemented. Adiabatic coupling taper is a promising method of enhancing coupling efficiency. A taper matches the parameters of the freely propagated terahertz beam on its input side and that of the waveguide mode on the output side.

Adiabatic terahertz field compression has been demonstrated in [137, 138] by means of double-tapered parallel plate waveguides. In the first paper the authors utilized Si lenses to couple radiation into and out of the waveguide which are prone to absorption and reflective losses, and in the second paper the authors managed to eliminate the lenses from the coupler geometry. In [139] a thick slot waveguide is proposed as an adiabatic coupler instead of the parallel plate waveguide. The approach reveals good experimental results, thus being very promising for coupling between mismatched in sizes THz sources and waveguides and enhancing THz field intensity in waveguides or sensors.

Characterization of terahertz waveguides

There are generally two different methods employed to measure the optical properties of terahertz waveguides. Using the first technique, one compares the two pulses. The first one being

a sample pulse which propagates through the entire optical system with all the mirrors, lenses and the waveguide included. For the second measurement, one excludes the waveguide keeping the rest of the optical hardware intact. The transmission and dispersion can then be calculated based on these two measurements.

The second technique is the cut-back method. The absorption coefficient is calculated by comparing the transmission through the waveguide segments of different lengths. The input facet of the fiber is fixed during the measurement and the fiber is repeatedly shortened by cutting its output end. The advantage of the cutback method is that it eliminates the waveguide coupling efficiency from losses calculation. However this technique brings some uncertainty factors. It is impossible to precisely guarantee that the output facet of the fiber before and after the cut will keep the same position, and that fiber coupling efficiency will remain constant after the cut. From what I have noticed in our experiments for the precision of the measurement it is more crucial to have the input facet of the fiber fixed reliably, thus it was glued to the aperture during the experiment. I have checked both the amplitude and the spectrum of the measured pulse to ensure the consistency of the measurement for each length of the fiber. I was making sure that after each cut the amplitude of the time-domain signal increases and that I also have a consistent increase of the pulse's spectrum amplitude in the whole frequency range (no major changes of transmission bandwidth).

To eliminate the difficulties associated with aforementioned methods, an alternative approach can be used. One of the possible method consists in using the second fiber that acts as a directional coupler with the sample fiber. The power transmitted to the directional coupler is proportional to the power guided in the sample fiber and it will decrease when the second fiber is being translated towards the output facet of the sample fiber. The sequence of power transmission measurements will allow to evaluate the losses of the sample fiber.

3D printing of terahertz waveguides/preforms

Due to the aforementioned imperfections caused by the fabrication method, it would be reasonable to consider switching to another fiber manufacturing technology. One possibility is to implement 3D printing for creating the dielectric terahertz waveguide. There was a time when this technology was solely associated with the manufacturing of large objects however, now, commercially available, reasonably priced 3D printers offer a resolution in tens of micrometers which is sufficient for even complex structured terahertz waveguides.

In [140] the authors demonstrate 3D printing of terahertz plasmonic waveguides. The authors exploit the characteristic short skin depth of metals at terahertz frequencies, the values of which are typically below 1 μm . The waveguides are printed in polymer resin and then a thin layer of gold is deposited on their surface. These waveguides support low loss propagation with the underlying layer exerting no effect on the optical characteristics of the waveguide. 3D printing facilitates fabrication of various complex waveguide structures, as well as waveguides with predefined values of bending radius. The authors mention somewhat higher losses compared to waveguides of the same structure which are fabricated using conventional techniques. This is due to greater surface roughness resulting from the printing process. However it is likely that the refinement of 3D printing technology will eventually allow us to eliminate existing problems.

3D printing of non-planar terahertz waveguides has been presented in [141]. In particular, the authors studied hollow core terahertz fibers and, in order to improve optical properties of the fibers, they implemented the same technique that is proposed in this thesis: they manually inserted metal wires into the voids of the fiber. Broadband single-mode THz guidance with relatively low propagation losses and high coupling efficiency has been demonstrated for such fibers. The rapid emergence of 3D printed terahertz waveguides, associated with the development of technology in recent years, suggests that this method might likely have a significant impact on terahertz waveguides.

In our group, we have recently started using the 3D printing technology to fabricate terahertz waveguides and waveguide preforms. The latter is the oversized version of the desired fiber geometry, which is prepared for drawing in a draw tower. When heated in the furnace of the draw tower the molten preform stretches into a fiber. The diameter of the fiber is controlled by adjusting the drawing temperature and pulling strength. Regularly the preforms are prepared using machine controlled drilling technique, thus the resolution of the preform geometry is limited by the smallest drill bit size available, which in our case equals to 2.0 mm. On the other hand, the actual resolution of even low-grade 3D printers is about 400 μm . Therefore, we expect the improvements in the quality of fibers produced in our lab and the ease of variability of the geometry parameters of preforms compared to the drilling technique. In Figure 7.5 we demonstrate our early samples of a 3D printed hollow core fiber and a porous 3D printed preform. The outer dimensions of the structures are approximately 3 cm.

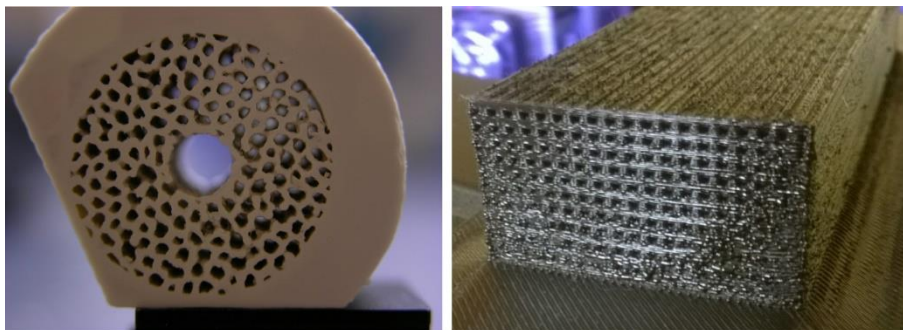


Figure 7.5. Cross section of a 3D printed hollow core fiber and a porous 3D printed preform.

As it has been discussed in the thesis, in order to achieve low-loss guidance it is crucial to increase the porosity of the fiber. As one can see from Figure 7.5, the air-filling factor of the printed structures is around 25%, which is quite low. A solution to this issue might be in using dissolvent for plastic (acetone, for example) to wash the excessive amount of the material from the preform of the fiber. By accurately controlling the dissolvent exposure time, thoroughly washing acetone with water after and applying the same technique multiple times, it will be possible to reduce the walls size of the waveguide structure to several tens of μm while maintaining the mechanical robustness of the waveguide.

Foam-based two-wire waveguides

In this thesis I discussed two alternative approaches to the improvement of hybrid metal wire/dielectric terahertz waveguides optical properties. Two-wire THz fibers with dielectric foam cladding offer protection of the guiding mode from the perturbations of the environment. Highly porous microstructured dielectric cladding does not require the use of cumbersome holders, and offer mechanical stability and ease of manipulation at the expense of somewhat higher absorption losses. To improve the optical properties of the hybrid waveguides, it would be beneficial to combine the design ideas of the two aforementioned types of waveguides. Foam-based microstructured fiber will offer flexibility and ease of manipulation of dielectric fibers and will simultaneously benefit from inherently low absorption loss of foam materials.

In order to fabricate a foam-based microstructured fiber one first has to choose a proper foam type for this application. There is always a balance between the air content in foam bubbles and the overall rigidity/flexibility of the resulting foam structure. So far, in our group we find that

polyurethane foam is the most suitable for the manufacturing of small terahertz waveguides. Then, the task is to produce (for example through 3D printing) a frame of the shape negative to that of the desired waveguide. The proper chosen type of foam also must not expand from its liquid phase too quickly so that the material can fill the whole volume uniformly. During the last step, the frame and the foam are separated, thus leaving a foam-based microstructured waveguide. We are currently working on the development this fabrication technique in our group.

Future research in the area

In the final section I would like to quickly mention the possibilities for future research that stem from the results presented in this thesis.

First, I would recommend an experimental investigation of multilayered dielectric waveguides for sensing of biological and chemical specimens in the terahertz region by placing the recognition elements into the waveguide microstructure. The multilayered dielectric waveguide exhibits small transmission losses, thus a sensor based on such a waveguide can have very long length, thus enabling high sensitivity of the sensor. Moreover, the convenience of the waveguide structure is in the ease of adjusting of the effective refractive index by changing the air spacing between the layers, as well as the number of layers in the core.

Recently, THz communications became an active research topic, driven by the availability of unregulated bandwidth and a promise of much higher transmission rates as compared to microwave communications. Communication applications rely heavily on the availability of high-quality low-loss and low-dispersion waveguides, and two-wire waveguides prove to be very promising for telecom applications. Besides parallel-wire based waveguides, it is now timely to develop signal-processing components required for THz communications that can be based on the same low-loss two-wire waveguide design. An important milestone will be the development of the waveguide Bragg grating, and ultimately THz ultra-fast low-cost communication systems.

CHAPTER 8 CONCLUSIONS

In the previous chapters I have reported the experimental and theoretical results that I have attained within the scope of my doctoral studies. In concluding, I would like to summarize the results and once again draw your attention towards some distinctive features of these completed projects. Moreover, I would like to propose routes for possible future improvements and new research avenues.

First, I have presented a novel design of a planar porous low-loss waveguide for THz frequency range with the waveguide structure consisting of multiple layers of thin polyethylene film that are separated by low-loss air layers of comparable thickness. The described waveguide can be also useful for sensing of biological and chemical specimens in the terahertz region by placing the recognition elements directly into the waveguide microstructure. The main advantage of the proposed planar porous waveguides is the convenient access to their optical mode, since the major portion of THz power launched into such a waveguide is confined within the air layers. Moreover, small spacing between the layers promotes rapid loading of the analyte into the waveguide due to strong capillary effect. The modal refractive index of porous waveguide is smaller compared to pure polymer and it is easy to adjust by changing the air spacing between the layers, as well as the number of layers in the core. The porous waveguide exhibits considerably smaller transmission losses than a bulk material. The transmission and absorption properties of such waveguides have been investigated both experimentally using THz-TDS spectroscopy and theoretically using finite element software. Good agreement between experimental data and theoretical results has been achieved.

Then, I have proposed a novel type of practical THz fibers that combines low-loss, low-dispersion and efficient excitation properties of the classic two-wire waveguides together with mechanical robustness, and ease of manipulation of the porous dielectric fibers. While optical properties of composite fibers are inferior to those of a classic two-wire waveguide, at the same time, composite fibers outperform porous fibers of the same geometry both in bandwidth of operation and in lower dispersion. I demonstrated that by increasing porosity of the fiber dielectric cladding its optical properties could be consistently improved.

In order to consistently improve the optical properties of a composite two-wire fiber one has to further increase porosity of its plastic cladding. The composite fibers presented here have

simple geometries, which are easy to fabricate. At the same time, it appears that more complex structures offering higher porosities have to be investigated in order to approach the outstanding low-loss, low-dispersion performance of the classic two-wire waveguides.

Optical characterization of hybrid waveguides fabricated using the aforementioned technique has confirmed that porous microstructured plastic claddings can indeed serve as a mechanical support for the two metallic wires. However, I have also discovered that meticulous care must be taken in order to minimize the negative effect of such claddings on the modal propagation properties such as loss and group velocity dispersion. For example, one has to reduce overlap of the modal fields with the lossy plastic cladding by increasing cladding porosity. Additionally, the size of the fiber microstructure (holes, etc.) has to be carefully matched with the size of the metal wires in order to avoid variations in the inter-wire gap along the waveguide length; otherwise, radiation losses can be significant.

As another possible option for the two-wire waveguide cladding material, I considered low density polyethylene foam. Optical characterization confirmed that foams have low loss $<0.2 \text{ cm}^{-1}$, as well as a low and almost constant refractive index ~ 1.01 in the whole THz frequency range. THz measurements using two wires sandwiched between two foam blocks have confirmed that in this hybrid waveguide the average (over frequency) modal refractive index has only slightly increased to ~ 1.003 , while the average modal loss have increased by only $\sim 0.12 \text{ cm}^{-1}$.

I have described a refractometer based on practical plasmonic THz fibers that feature two metallic wires inserted into porous dielectric cladding. Introduction of even lossless analytes into the fiber core leads to significant changes in the modal losses, which is used as a transduction mechanism. Resolution of the refractometer has been investigated numerically as a function of the operation frequency and the geometric parameters of the fiber. With a refractive index resolution on the order of $\sim 10^{-3}$ RIU, the composite fiber-based sensor is capable of identifying various gaseous analytes and aerosols or measuring the concentration of dust particles in the air.

REFERENCES

- [1] C. Fattinger and D. Grischkowsky, "Terahertz beams," *Applied Physics Letters*, vol. 54, pp. 490-492, 1989.
- [2] D. Grischkowsky, R. Kesselring and F. K. Kneubuehl, "Time-domain, far-infrared spectroscopy," in *4th International Conference on Infrared Physics*, 1988.
- [3] M. van Exter, C. Fattinger and D. Grischkowsky, "Terahertz time domain spectroscopy of water vapor," *Optics Letters*, vol. 14, pp. 1128-1130, 1989.
- [4] D. H. Auston, K. P. Cheung and P. R. Smith, "Picosecond photo-conducting Hertzian dipoles," *Applied Physics Letters*, vol. 45, no. 3, pp. 284-286, 1984.
- [5] D. H. Auston and M. C. Nuss, "Electrooptic generation and detection," *IEEE Journal of Quantum Electronics*, vol. 24, no. 2, pp. 184-197, 1988.
- [6] M. B. Ketchen, D. Grischkowsky, T. C. Chen, C.-C. Chi, I. N. Duling, N. J. Halas, J.-M. Halbout, J. A. Kash and G. P. Li, "Generation of sub-picosecond electrical pulses," *Applied Physics Letters*, vol. 48, pp. 751-753, 1986.
- [7] R. M. Woodward, V. P. Wallace, D. D. Arnone, E. H. Linfield and M. Pepper, "Terahertz Pulsed Imaging of Skin Cancer in the Time and Frequency Domain," *Journal of Biological Physics*, vol. 29, pp. 257-261, 2003.
- [8] K. Mitobe, M. Manabe, N. Yoshimura and T. Karabayashi, "Imaging of epithelial cancer in sub-terahertz electromagnetic wave," in *Conference Proceedings of IEEE Engineering in Medicine and Biology Society*, 2005.
- [9] E. Pickwell, W. P. Wallace, B. E. Cole, S. Ali, C. Longbottom, R. J. Lynch and M. Pepper, "Using terahertz pulsed imaging to measure enamel demineralisation in teeth.," in *Joint*

31st International Conference on Infrared Millimeter Waves and 14th International Conference on Terahertz Electronics, Shanghai, 2006.

- [10] J. F. Federici, B. Schulkin, F. Huang, D. Gary, R. Barat, F. Oliveira and D. Zimdars, "THz imaging and sensing for security applications? explosives, weapons and drugs," *Semiconductor Science and Technology*, vol. 20, p. S266, 2005.
- [11] R. H. Jacobsen, D. M. Mittleman and M. C. Nuss, "Chemical recognition of gases and," *Optics Letters*, vol. 21, no. 24, pp. 2011-2013, 1996.
- [12] J. Tang, L. Y. Deng, C. B. Tay, X. H. Zhang, J. W. Chai, H. Qin, H. W. Liu, T. Venkatesan and S. J. Chua, "Determination of carrier concentration dependent electron effective mass and scattering time of n-ZnO thin film by terahertz time domain spectroscopy," *Journal of Applied Physics*, vol. 115, p. 033111, 2014.
- [13] E. Knoesel, M. Bonn, J. Shan, F. Wang and T. F. Heinz, "Conductivity of solvated electrons in hexane investigated with terahertz time-domain spectroscopy," *Journal of Chemical Physics*, vol. 121, no. 1, pp. 394-404, 2004.
- [14] H. Cai, D. Wang and J. Shen, "Study of atmospheric pollution using terahertz wave," in *Infrared, Millimeter Wave, and Terahertz Technologies*, Beijing, China, 2010.
- [15] T. Uno and H. Tabata, "In situ Measurement of Combustion Gas Using Terahertz Time Domain Spectroscopy Setup for Gas Phase Spectroscopy and Measurement of Solid Sample," *Japanese Journal of Applied Physics*, vol. 49, p. 04DL17, 2010.
- [16] S. Ke, S. Yao-chun and J. A. Zeitler, "Terahertz Sensor for Non-Contact Thickness and Quality Measurement of Automobile Paints of Varying Complexity," *IEEE Transactions on Terahertz Science and Technology*, vol. 4, no. 4, pp. 432-439, 2014.
- [17] J. B. Jackson, J. Bowen, G. Walker, J. Labaune, G. Mourou, M. Menu and K. Fukunaga, "A Survey of Terahertz Applications in Cultural Heritage Conservation Science," *IEEE Transactions on Terahertz Science and Technology*, vol. 1, no. 1, pp. 220-231, 2011.

- [18] G. C. Walker, J. B. Jackson, D. Giovannacci, J. W. Bowen, B. Delandes, J. Labaune, G. Mourou, M. Menu and V. Detalle, "Terahertz analysis of stratified wall plaster at buildings of cultural importance across Europe," in *Optics for Arts, Architecture, and Archaeology IV*, Munich, Germany, 2013.
- [19] K. Fukunaga, I. Hosako, I. N. Duling and M. Picollo, "Terahertz imaging systems: a non-invasive technique for the analysis of paintings," in *O3A: Optics for Arts, Architecture, and Archaeology II*, Munich, Germany, 2009.
- [20] H. Hoshina, Y. Sasaki, A. Hayashi, C. Otani and K. Kawase, "Noninvasive mail inspection system with terahertz radiation.H," *Applied Spectroscopy*, vol. 63, no. 1, pp. 81-86, 2009.
- [21] Z. Yan, Y. Ying, H. Zhang and H. Yu, "Research progress of terahertz wave technology in food inspection," in *Terahertz Physics, Devices, and Systems*, Boston, 2006.
- [22] S. Koenig, D. Lopez-Diaz, J. Antes, F. Boes, F. Henneberger, A. Leuther, A. Tessmann, R. Schmogrow, D. Hillerkuss, R. Palmer, T. Zwick, C. Koos, W. Freude, O. Ambacher, J. Leuthold and I. Kallfass, "Wireless sub-THz communication system with high data rate," *Nature Photonics*, vol. 7, pp. 977-981, 2013.
- [23] S. X. She, "Metal-clad multilayer dielectric waveguide: accurate perturbation analysis," *Journal of the Optical Society of America A*, vol. 7, no. 9, pp. 1582-1590, 1990.
- [24] D. Hao, P. Gerard and P. Benech, "Radiation modes of lossless multilayer dielectric waveguides," *IEEE Journal of Quantum Electronics*, vol. 31, no. 2, pp. 411-416, 1995.
- [25] D. M. Shyroki and A. V. Lavrichenko, "Dielectric multilayer waveguides for TE and TM mode matching," *Journal of Optics A: Pure and Applied Optics*, vol. 5, pp. 192-198, 2003.

- [26] M. Wächter, M. Nagel and H. Kurz, "Frequency-dependent characterization of THz Sommerfeld wave propagation on single-wires," *Optics Express*, vol. 13, pp. 10815-10822, 2005.
- [27] A. Sommerfeld, "Ueber die Fortpflanzung elektrodynamischer Wellen längs eines Drahtes," *Annalen der Physik und Chemie*, vol. 67, pp. 233-290, 1899.
- [28] F. Sobel, F. Wentworth and J. C. Wiltse, "Quasi-Optical Surface Waveguide and Other Components for the 100- to 300-Gc Region," *IEEE Transactions on Microwave Theory and Techniques*, vol. 9, pp. 512-518, 1961.
- [29] M. J. King and J. C. Wiltse, "Surface-Wave Propagation on Coated or Uncoated Metal Wires at Millimeter Wavelengths," *IEEE Transactions on Antennas and Propagation*, vol. 10, pp. 246-254, 1962.
- [30] M. Mbonye, R. Mendis and D. Mittleman, "A terahertz two-wire waveguide with low bending loss," *Applied Physics Letters*, vol. 95, p. 233506, 2009.
- [31] Y.-S. Jin, G.-J. Kim and S.-G. Jeon, "Terahertz dielectric properties of polymers," *Journal of the Korean Physical Society*, vol. 49, pp. 513-517, 2006.
- [32] B. Ung, A. Mazhorova, A. Dupuis, M. Rozé and M. S. Skorobogatiy, "Polymer microstructured optical fibers for terahertz wave guiding," *Optics Express*, vol. 19, pp. B848-B861, 2011.
- [33] M. Roze, B. Ung, A. Mazhorova, M. Walther and M. Skorobogatiy, "Suspended core subwavelength fibers: towards practical designs for low-loss terahertz guidance," *Optics Express*, vol. 19, pp. 9127-9138, 2011.
- [34] L.-J. Chen, H.-W. Chen, T.-F. Kao, J.-Y. Lu and C.-K. Sun, "Low-loss subwavelength plastic fiber for terahertz waveguiding," *Optics Letters*, vol. 31, pp. 308-310, 2006.

- [35] T. Ito, Y. Matsuura, M. Miyagi, H. Minamide and H. Ito, "Flexible terahertz fiber optics with low bend-induced losses," *Journal of the Optical Society of America B*, vol. 24, pp. 1230-1235, 2007.
- [36] J. A. Harrington, R. George, P. Pedersen and E. Mueller, "Hollow polycarbonate waveguides with inner Cu coatings for delivery of terahertz radiation," *Optics Express*, vol. 12, pp. 5263-5268, 2004.
- [37] B. Bowden, J. A. Harrington and O. Mitrofanov, "Silver/polystyrene-coated hollow glass waveguides for the transmission of terahertz radiation," *Optics Letters*, vol. 32, pp. 2945-2947, 2007.
- [38] A. Dupuis, K. Stoeffler, B. Ung, C. Dubois and M. Skorobogatiy, "Transmission measurements of hollow-core THz Bragg fibers," *Journal of the Optical Society of America B*, vol. 28, pp. 896-907, 2011.
- [39] C.-H. Lai, B. You, J.-Y. Lu, T.-A. Liu, J.-L. Peng, C.-K. Sun and H. Chang, "Modal characteristics of antiresonant reflecting pipe waveguides for terahertz waveguiding," *Optics Express*, vol. 18, pp. 309-322, 2010.
- [40] S. Sato, T. Katagiri and Y. Matsuura, "Fabrication method of small-diameter hollow waveguides for terahertz waves," *Journal of the Optical Society of America*, vol. 29, pp. 3006-3009, 2012.
- [41] A. Mazhorova, A. Markov, B. Ung, M. Rozé, S. Gorgutsa and M. Skorobogatiy, "Thin chalcogenide capillaries as efficient waveguides from mid-infrared to terahertz," *Journal of the Optical Society of America B*, vol. 29, pp. 2116-2123, 2012.
- [42] C.-H. Lai, Y.-C. Hsueh, H.-W. Chen, Y.-J. Huang, H. Chang and C.-K. Sun, "Low-index terahertz pipe waveguides," *Optics Letters*, vol. 34, pp. 3457-3459, 2009.

- [43] R. Mendis and D. Grischkowsky, "Undistorted guided-wave propagation of subpicosecond terahertz pulses," *Optics Letters*, vol. 26, pp. 846-848, 2001.
- [44] M. Nagel, A. Marchewka and H. Kurz, "Low-index discontinuity terahertz waveguides," *Optics Express*, vol. 14, pp. 9944-9954, 2006.
- [45] D. Saeedkia and S. Safavi-Naeini, "Modeling and Analysis of a Multilayer Dielectric Slab Waveguide With Applications in Edge-Coupled Terahertz Photomixer Sources," *Journal of Lightwave Technology*, vol. 25, no. 1, pp. 432-439, 2007.
- [46] V. Paeder, J. Darmono and K. Unterrainer, "Ultra-thin terahertz waveguides on periodic dielectric multilayers," in *Infrared, Millimeter, and Terahertz Waves (IRMMW-THz)*, 2013.
- [47] B. Scherger, M. Scheller, N. Vieweg, S. T. Cundiff and M. Koch, "Paper terahertz wave plates," *Optics Express*, vol. 19, no. 25, pp. 24884-24889, 2011.
- [48] M. Scheller, C. Jordens and M. Koch, "Terahertz form birefringence," *Optics Express*, vol. 18, no. 10, pp. 10137-10142, 2010.
- [49] K. Wang and D. Mittleman, "Metal wires for terahertz guiding," *Nature*, vol. 432, pp. 376-379, 2004.
- [50] K. Wang and D. Mittleman, "Guided propagation of terahertz pulses on metal wires," *Journal of the Optical Society of America B*, vol. 22, pp. 2001-2008, 2005.
- [51] J. A. Deibel, K. L. Wang, M. D. Escarra and D. M. Mittleman, "Enhanced coupling of terahertz radiation to cylindrical wire waveguides," *Optics Express*, vol. 14, pp. 279-290, 2006.
- [52] J. A. Deibel, M. Escarra, N. Berndsen, K. Wang and D. M. Mittleman, "Finite-Element Method Simulations of Guided Wave Phenomena at Terahertz Frequencies," *Proceeding of the IEEE*, vol. 95, no. 8, pp. 1624-1640, 2007.

- [53] N. C. J. v. d. Valk and P. C. M. Planken, "Effect of adielectric coating on terahertz surface plasmon polaritons on metal wires," *Applied Physics Letters*, vol. 87, p. 071106, 2005.
- [54] H. Cao and A. Nahata, "Coupling of terahertz pulses onto a single metal wire waveguide using milled grooves," *Optics Express*, vol. 13, pp. 7028-7034, 2005.
- [55] X.-Y. He, "Investigation of terahertz Sommerfeld wave propagation along conical metal wire," *Journal of the Optical Society of America B*, vol. 26, pp. A23-A28, 2009.
- [56] H. Pahlevaninezhad, T. Darcie and B. Heshmat, "Two-wire waveguide for terahertz," *Optics Express*, vol. 18, pp. 7415-7420, 2010.
- [57] H. Pahlevaninezhad, T. E. Darcie and B. Heshmat, "Coupling of terahertz waves to a two-wire waveguide," *Optics Express*, vol. 18, pp. 22614-22624, 2010.
- [58] P. Tannouri, M. Peccianti, P. L. Lavertu, F. Vidal and R. Morandotti, "Quasi-TEM mode propagation in twin-wire THz waveguides ," *Chinese Optics Letters*, vol. 09, p. 110013, 2011.
- [59] J. Dickason and K. Goosen, "Loss analysis for a two wire optical waveguide for chip-to-chip communication," *Optics Express*, vol. 21, pp. 5526-5532, 2013.
- [60] M. Mridha, A. Mazhorova, M. Clerici, I. Al-Naib, M. Daneau, X. Ropagnol, M. Peccianti, C. Reimer, M. Ferrera, L. Razzari, F. Vidal and R. Morandotti, "Active terahertz two-wire waveguides," *Optics Express*, vol. 22, no. 19, pp. 22340-22348, 2014.
- [61] J. Anthony, R. Leonhardt and A. Argyros, "Hybrid hollow core fibers with embedded wires as THz waveguides," *Optics Express*, vol. 21, pp. 2903-2912, 2013.
- [62] J. Anthony, R. Leonhardt, A. Argyros and M. C. J. Large, "Characterization of a microstructured Zeonex terahertz fiber," *Journal of the Optical Society of America B*, vol. 28, pp. 1013-1018, 2011.

- [63] Y. Matsuura and E. Takeda, "Hollow optical fibers loaded with an inner dielectric film for terahertz broadband spectroscopy," *Journal of the American Optical Society B*, vol. 25, no. 12, pp. 1949-1954, 2008.
- [64] L. Vincetti, "Hollow core photonic band gap fiber for THz applications," *Microwave and Optical Technology Letters*, vol. 51, pp. 1711-1714, 2009.
- [65] M. Skorobogatiy and A. Dupuis, "Ferroelectric all-polymer hollow Braggfibers for terahertz guidance," *Applied Physics Letters*, vol. 90, p. 113514, 2007.
- [66] R.-J. Yu, B. Zhang, Y.-Q. Zhang, C.-Q. Wu, Z.-G. Tian and X.-Z. Bai, "Proposal for ultralow loss hollow-core plastic Bragg fiber with cobwebstructuredcladding for terahertz waveguiding," *IEEE Photonics Technology Letters*, vol. 19, no. 12, pp. 910-912, 2007.
- [67] C. S. Ponseca, R. Pobre, E. Estacio, N. Sarukura, A. Argyros, M. C. J. Large and M. A. van Eijkelenborg, "Transmission of terahertz radiation using a microstructured polymer optical fiber," *Optics Letters*, vol. 33, no. 9, pp. 902-904, 2008.
- [68] J. Anthony, R. Leonhardt, S. G. Leon-Saval and A. Argyros, " THz propagation in kagome hollow-core microstructured fibers," *Optics Express*, vol. 19, no. 19, pp. 18470-18478, 2011.
- [69] L. Vincetti, "Numerical analysis of plastic hollow core microstructured fibers for terahertz applications," *Optical Fiber Technology*, vol. 15, no. 4, pp. 398-401, 2009.
- [70] H. Han, H. Park, M. Cho and J. Jim, "Terahertz pulse propagation in a plastic photonic crystal fiber," *Applied Physics Letters*, vol. 80, no. 15, pp. 2634-2636, 2002.
- [71] K. Nielsen, H. K. Rasmussen, A. J. L. Adam, P. C. M. Planken, O. Bang and P. U. Jepsen, "Bendable, low-loss Topas fibers for the terahertz frequency range," *Optics Express*, vol. 17, no. 10, pp. 8592-8601, 2009.

- [72] S. Atakaramians, S. Afshar , H. Ebendorff-Heidepriem, M. Nagel, B. M. Fischer, D. Abbott and T. M. Monro, "THz porous fibers: design, fabrication and experimental characterization," *Optics Express*, vol. 17, no. 16, pp. 14053-14062, 2009.
- [73] S. Atakaramians, S. Afshar, M. Nagel, H. K. Rasmussen, O. Bamg, T. M. Monro and D. Abbott, "Direct probing of evanescent field for characterization of porous terahertz fibers," *Applied Physics Letters*, vol. 98, p. 121104, 2011.
- [74] A. Dupuis, A. Mazhorova, F. Désévéday, M. Rozé and M. Skorobogatiy, "Spectral characterization of porous dielectric subwavelength THz fibers," *Optics Express*, vol. 18, no. 13, pp. 13813-13828, 2010.
- [75] C. Themistos, B. Rahman, M. Rajarajan, V. Rakocevic and K. Grattan, "Finite Element Solutions of Surface-Plasmon Modes in Metal-Clad Dielectric Waveguides at THz Frequency," *Journal of Lightwave Technology*, vol. 24, pp. 5111-5118, 2006.
- [76] O. Mitrofanov, R. James, F. A. Fernandez, T. K. Mavrogordatos and J. A. Harrington, "Reducing Transmission Losses in Hollow THz Waveguides," *IEEE Transactions of Terahertz Science and Technology*, vol. 1, no. 1, pp. 124-132, 2011.
- [77] S. R. Andrews, "Microstructured terahertz waveguides," *Journal of Physics D: Applied Physics*, vol. 47, p. 374004, 2014.
- [78] C. Yeh, F. Shimabukuro and P. H. Siegel, " Low-loss terahertz ribbon waveguides," *Applied Optics*, vol. 44, no. 28, pp. 5937-5946, 2005.
- [79] A. Ishikawa, S. Zhano, D. A. Genov, G. Bartal and X. Zhang, "Deep subwavelength terahertz waveguides using gap magnetic plasmon," *Physical Review Letters*, vol. 102, no. 4, p. 043904, 2009.

- [80] F. A. Vallejo and L. M. Hayden, "Design of ultra-broadband terahertz polymer waveguide emitters for telecom wavelengths using coupled mode theory," *Optics Express*, vol. 21, no. 5, pp. 5842-5858, 2013.
- [81] M. Szymanski, A. Szerling and K. Kosiel, "Theoretical investigation of metal-metal waveguides for terahertz quantum-cascade lasers," *Optical and Quantum Electronics*, vol. 47, pp. 843-849, 2015.
- [82] A. H. Landrock, Handbook of plastic foams, William Andrew Publishing, 1995.
- [83] M. Chanda, Plastics fabrication and recycling, CRC Press, 2009.
- [84] K. C. Frisch and J. H. Saunders, Plastic foams, Marcel Dekker, 1973.
- [85] S.-T. Lee, Foam extrusion : principles and practice, Technomic Pub. Co, 2000.
- [86] G. Zhao, M. Mors, T. Wenckebach and P. C. M. Planken, "Terahertz dielectric properties of polystyrene foam," *Journal of the Optical Society of America B*, vol. 18, pp. 1476-1479, 2002.
- [87] C. Roman, O. Ichim, L. Sarger, V. Vigneras and P. Mounais, "Terahertz dielectric characterisation of polymethacrylimide rigid foam : The perfect sheer plate?," *Electronics Letters*, vol. 40, pp. 1167-1169, 2004.
- [88] M. Scheller, C. Jensen and M. Koch, "Applications of effective medium theories in the terahertz regime," in *Recent Optical and Photonic technologies*, K. Y. Kim, Ed., InTech, 2010, pp. 231-250.
- [89] T. C. Choy, Effective Medium Theory : Principles and applications, Oxford University Press, 1999.

- [90] C. R. Dietlein, J. E. Bjarnason and E. N. Grossman, "Absorption, transmission, and scattering of expanded polystyrene at millimetre-wave and terahertz frequencies," *Proceedings of SPIE*, vol. 6948, p. 69480E, 2008.
- [91] J. Pearce, Z. Jian and D. Mittleman, "'Propagation of terahertz pulses in random media," *Philosophical Transactions of the Royal Society A*, vol. 362, pp. 301-314, 2004.
- [92] J. Pearce, Z. Jian and D. Mittleman, "Statistics of multiply scattered broadband terahertz pulses," *Physical Review Letters*, vol. 91, p. 043903, 2003.
- [93] Z. Jian, J. Pearce and D. Mittleman, "Characterizing individual scattering events by measuring the amplitude and phase of the electric field diffusing through a random medium," *Physical Review Letters*, vol. 91, p. 033903, 2003.
- [94] S. Wang and X.-C. Zhang, "Pulsed terahertz tomography," *Journal of Physics D: Applied Physics*, vol. 37, pp. R1-R36, 2004.
- [95] P. D. Cunningham, N. N. Valdes, F. A. Vallejo, L. M. Hayden, B. Polishak, X.-H. Zhou, J. Luo, A. K.-Y. Jen, J. C. Williams and R. J. Twieg, "Broadband terahertz characterization of the refractive index and absorption of some important polymeric and organic electro-optic materials," *Journal of Applied Physics*, vol. 109, p. 043505, 2011.
- [96] R. Piesiewicz, C. Jansen, S. Wietzke, D. Mittleman, M. Koch and T. Kürner, "Properties of building and plastic materials in the THz range," *International Journal of Infrared and Millimeter Waves*, vol. 28, pp. 363-371, 2007.
- [97] X.-C. Zhang, "Three-dimensional terahertz wave imaging," *Philosophical Transactions of the Royal Society A*, vol. 362, pp. 283-299, 2004.
- [98] B. Pradarutti, S. Riehemann, G. Notni and A. Tunnerman, "Terahertz imaging for styrofoam inspection," *Proceedings of SPIE*, vol. 6772, p. 67720P, 2007.

- [99] A. Abina, U. Puc, A. Jeglic and A. Zidansek, "Structural analysis of insulating polymer foams with terahertz spectroscopy and imaging," *Polymer Testing*, vol. 32, pp. 739-747, 2013.
- [100] H. Guerboukha, G. Yan, O. Skorobogata and M. Skorobogatiy, "Silk Foam Terahertz Waveguides," *Optics Express*, vol. submitted, 2014.
- [101] N. Laman, S. Harsha, D. Grischkowsky and J. Melinger, "High-Resolution Waveguide THz Spectroscopy of Biological Molecules," *Biophysical Journal*, vol. 94, pp. 1010-1020, 2008.
- [102] C. Markos, W. Yuan, K. Vlachos, G. Town and O. Bang, "Label-free biosensing with high sensitivity in dual-core microstructured polymer optical fibers," *Optics Express*, vol. 19, pp. 7790-7798, 2011.
- [103] M. Nagel, P. H. Bolivar, M. Brucherseifer, A. B. H. Kurz and R. Büttner, "Integrated THz technology for label-free genetic diagnostics," *Applied Physics Letters*, vol. 80, pp. 154-156, 2002.
- [104] H. Kurt and D. Citrin, "4Coupled-resonator optical waveguides for biochemical sensing of nanoliter volumes of analyte in the terahertz region," *Applied Physics Letters*, vol. 87, p. 241119, 2005.
- [105] M. Nagel, P. H. Bolivar and H. Kurz, "Modular parallel-plate THz components for cost-efficient biosensing systems," *Semiconductor Science and Technology*, vol. 20, p. S281, 2005.
- [106] H. Yoshida, Y. Ogawa, Y. Kawai, S. Hayashi, A. Hayashi, C. Otani, E. Kato, F. Miyamaru and K. Kawase, "Terahertz sensing method for protein detection using a thin metallic mesh," *Applied Physics Letters*, vol. 91, p. 253901, 2007.

- [107] J. O'Hara, R. Singh, I. Brener, E. Smirnova, J. Han, A. Taylor and W. Zhang, "Thin-film sensing with planar terahertz metamaterials: sensitivity and limitations," *Optics Express*, vol. 16, pp. 1786-1795, 2008.
- [108] R. Mendis, V. Astley, J. Liu and D. M. Mittleman, "Terahertz microfluidic sensor based on a parallel-plate waveguide resonant cavity," *Applied Physics Letters*, vol. 95, p. 171113, 2009.
- [109] B. You, J. Lu, C. Yu, T. Liu and J. Peng, "Terahertz refractive index sensors using dielectric pipe waveguides," *Optics Express*, vol. 20, pp. 5858-5866, 2012.
- [110] M. Skorobogatiy, *Nanostructured and Subwavelength Waveguides: fundamentals and applications*, Wiley, 2012.
- [111] D. Grischkowsky, "Optoelectronic characterization of transmission lines and waveguides by terahertz time-domain spectroscopy," *IEEE Journal of Selected Topics in Quantum Electronics*, vol. 6, pp. 1122-1135, 2000.
- [112] A. Mazhorova, A. Markov, A. Ng, R. Chinnappan, O. Skorobogata, M. Zourob and M. Skorobogatiy, "Label-free bacteria detection using evanescent mode of a suspended core terahertz fiber," *Optics Express*, vol. 20, pp. 5344-5355, 2012.
- [113] A. Mazhorova, J. F. Gu, A. Dupuis, M. Peccianti, O. Tsuneyuki, R. Morandotti, H. Minamide, M. Tang, Y. Wang, H. Ito and M. Skorobogatiy, "Composite THz materials using aligned metallic and semiconductor microwires, experiments and interpretation," *Optics Express*, vol. 18, pp. 24632-24647, 2010.
- [114] A. Markov, S. Gorgutsa, H. Qu and M. Skorobogatiy, "Practical Metal-Wire THz Waveguides," 14 06 2012. [Online]. Available: <http://arxiv-web3.library.cornell.edu/abs/1206.2984>.

- [115] A. Markov, S. Gorgutsa, H. Qu and M. Skorobogatiy, "THz wire waveguides," in *Plasmonics, Gordon Research Conference*, Maine, USA, June, 2012.
- [116] M. Ordal, R. Bell, R. Alexander, L. L. Jr and M. Querry, "Optical properties of fourteen metals in the infrared and far infrared," *Applied Optics*, vol. 24, pp. 4493-4499, 1985.
- [117] E. J. Zeman and G. C. Schatz, "An accurate electromagnetic theory study of surface enhancement factors for silver, gold, copper, lithium, sodium, aluminum, gallium, indium, zinc, and cadmium," *The Journal of Physical Chemistry*, vol. 91, pp. 634-643, 1987.
- [118] Y.-S. Lee, *Principles of Terahertz Science and Technology*, Springer, 2008.
- [119] A. Hassani, A. Dupuis and M. Skorobogatiy, "Low loss porous terahertz fibers containing multiple subwavelength holes," *Applied Physics Letters*, vol. 92, p. 071101, 2008.
- [120] A. Hassani, A. Dupuis and M. Skorobogatiy, "Porous polymer fibers for low-loss Terahertz guiding," *Optics Express*, vol. 16, pp. 6340-6351, 2008.
- [121] A. Dupuis, J. Allard, D. Morris, C. Dubois and M. Skorobogatiy, "Fabrication and THz loss measurements of porous subwavelength fibers using a directional coupler method," *Optics Express*, pp. 8012-8028, 2009.
- [122] M. Wachter, M. Nagel and H. Kurz, "Frequency-dependent characterization of THz Sommerfeld wave propagation on single-wires," *Optics Express*, vol. 13, no. 26, pp. 10815-10822, 2005.
- [123] A. Markov and M. Skorobogatiy, "Two-wire terahertz fibers with porous dielectric support," *Optics Express*, vol. 21, pp. 12729-12743, 2013.
- [124] B. Vidal, T. Nagatsuma, N. J. Gomes and T. E. Darcie, "Photonic Technologies for Millimeter- and Submillimeter-Wave Signals," *Advances in Optical Technologies*, vol. 2012, p. 925065, 2012.

- [125] H. Pahlevaninezhad, "Design and implementation of efficient terahertz waveguides," Ph.D. Thesis, University of Victoria , 2012.
- [126] A. Markov and M. Skorobogatiy, "Hybrid plasmonic terahertz fibers for sensing applications," *Applied Physics Letters*, vol. 103, p. 181118, 2013.
- [127] A. Markov, A. Mazhorova and M. Skorobogatiy, "Planar porous THz waveguides for low-loss guidance and sensing applications," *IEEE Transactions on Terahertz Science and Technology*, vol. 3, p. 96, 2013.
- [128] A. Markov, H. Guerboukha, A. Argyros and M. Skorobogatiy, "A complementary study to "Hybrid hollow core fibers with embedded wires as THz waveguides" and "Two-wire terahertz fibers with porous dielectric support" comment," *Optics Express*, vol. 21, pp. 27802-27803, 2013.
- [129] M. Skorobogatiy, "Resonant bio-chemical sensors based on Photonic Bandgap waveguides and fibers," in *Optical guided-wave Chemical and Biosensors II*, M. Zourob and A. Lakhtakia, Eds., Berlin Heidelberg , Springer-Verlag, 2010, pp. 43-72.
- [130] A. Hassani and M. Skorobogatiy, "Surface plasmon resonance-like integrated sensor at terahertz frequencies for gaseous analytes," *Optics Express*, vol. 16, pp. 20206-20214, 2008.
- [131] V. Astley, K. S. Reichel, J. Jones, R. Mendis and D. M. Mittleman, "Terahertz multichannel microfluidic sensor based on parallel-plate waveguide resonant cavities," *Applied Physics Letters*, vol. 100, p. 231108, 2012.
- [132] B. Li, S. Yan, W. Xiong, J. Shen and J. Yao, "Terahertz-metallic aperture arrays designing," *Chinese Optics Letters*, vol. 10(s1), p. S13102, 2012.
- [133] B. Reinhard, K. M. Schmitt, V. Wollrab, J. Neu, R. Beigang and M. Rahm, "Metamaterial near-field sensor for deep-subwavelength thickness measurements and sensitive

- refractometry in the terahertz frequency range," *Applied Physics Letters*, vol. 100, p. 221101, 2012.
- [134] A. E. Siegman, *Lasers*, Sausalito, USA: University Science Books, 1986.
- [135] J. F. Molloy, M. Naftaly and R. A. Dudley, "Characterisation of Terahertz Beam Profile and Propagation through Complex Quasi-Optic Systems," *Terahertz Science and Technology*, vol. 4, no. 3, pp. 99-103, 2011.
- [136] S. Mickan, J. Xu, J. Munch, X.-C. Zhang and D. Abbott, "The limit of spectral resolution in THz time-domain spectroscopy," *Proceedings of SPIE*, vol. 5277, pp. 54-64, 2004.
- [137] J. Zhang and D. Grischkowsky, "Adiabatic compression of parallel-plate metal waveguides for sensitivity enhancement of waveguide THz time domain spectroscopy," *Applied Physics Letters*, vol. 86, p. 061109, 2005.
- [138] A. Shutler and D. Grischkowsky, "Gap independent coupling into parallel plate terahertz waveguides using cylindrical horn antennas," *Journal of Applied Physics*, vol. 112, p. 073102, 2012.
- [139] L. Smith, F. Ahmed, A. Jooshesh, J. Zhang, M. Jun and T. Darcie, "THz Field Enhancement by Antenna Coupling to a Tapered Thick Slot Waveguide," *Journal of Lightwave Technology*, vol. 32, no. 20, pp. 3676-3682, 2014.
- [140] S. Pandey, B. Gupta and A. Nahata, "Terahertz plasmonic waveguides created via 3D printing," *Optics Express*, vol. 21, no. 21, pp. 24422-24430, 2013.
- [141] N. Yudasari, D. Vogt, J. Anthony and R. Leonhardt, "Hollow core terahertz waveguide fabricated using a 3D printer," in *IRMMW-THz 2014*, Tucson, 2014.

APPENDIX:

SCIENTIFIC OUTCOMES OF MY DOCTORAL RESEARCH

Journal papers:

1. H. Guerboukha, **A. Markov**, H. Qu, M. Skorobogatiy, "Fast rotary linear optical delay line for THz time-domain spectroscopy," submitted to IEEE Transactions on Terahertz Science and Technology, (2015)
2. T. Ma, **A. Markov**, L. Wang, M. Skorobogatiy, "Graded index porous optical fibers – dispersion management in terahertz range," Optics Express, vol. 23, pp. 7856-7869 (2015)
3. Invited: **A. Markov**, H. Guerboukha, M. Skorobogatiy, "(30th anniversary) Hybrid metal-dielectric terahertz waveguides: challenges and opportunities," JOSA B, Special 30th Anniversary Issue (Invited Only), vol. 31, pp. 2587–2600 (2014)
4. **A. Markov** and M. Skorobogatiy, "Hybrid plasmonic terahertz fibers for sensing applications," Appl. Phys. Lett., vol. 103, 181118 (2013)
5. **A. Markov**, H. Guerboukha, A. Argyros, and M. Skorobogatiy, "A complementary study to “Hybrid hollow core fibers with embedded wires as THz waveguides” and “Two-wire terahertz fibers with," Opt. Express, vol. 21, pp. 27802-27803 (2013)
6. C. Reinhardt, A.B. Evlyukhin, W. Cheng, T. Birr, **A. Markov**, B. Ung, M. Skorobogatiy, and B.N. Chichkov, "Bandgap-confined large mode waveguides for surface plasmon-polaritons," JOSA B, vol. 30, pp. 2898–2905 (2013)
7. G. Yan, **A. Markov**, Y. Chinifooroshan, S. M Tripathi, W. J Bock, and M. Skorobogatiy, "Low-Loss THz Waveguide Bragg Grating using a Two-Wire Waveguide and a Paper Grating," Optics Letters, vol. 38, pp. 3089–3092 (2013)
8. G. Yan, **A. Markov**, Y. Chinifooroshan, S. M Tripathi, W. J Bock, and M. Skorobogatiy, "Resonant THz sensor for paper quality monitoring using THz fiber Bragg gratings," Optics Letters, vol. 38, pp. 2200-2202 (2013)
9. **A. Markov**, M. Skorobogatiy, "Two-wire terahertz fibers with porous dielectric support," Optics Express, vol. 21, pp. 12729-12743 (2013)

10. **A. Markov**, A. Mazhorova, and M. Skorobogatiy, "Planar porous THz waveguides for low-loss guidance and sensing applications," IEEE Transactions on Terahertz Science and Technology, vol. 3, pp. 96-102 (2013)
11. A. Mazhorova, **A. Markov**, B. Ung, M. Rozé, S. Gorgutsa, and M. Skorobogatiy, "Thin chalcogenide capillaries as efficient waveguides from mid-infrared to terahertz," JOSA B, Vol. 29 Issue 8, pp. 2116-2123 (2012)
12. A. Mazhorova, **A. Markov**, A. Ng, R. Chinnappan, O. Skorobogata, M. Zourub, and M. Skorobogatiy., "Label-free bacteria detection using evanescent mode of a suspended core terahertz fiber," Optics Express, vol. 20 (5), pp. 5344-5355, (2012)
13. **A. Markov**, C. Reinhardt, B. Ung, A. Evlyukhin, W. Cheng, B. Chichkov, and M. Skorobogatiy "Photonic bandgap plasmonic waveguides," Optics Lett., vol. 36, pp.2468-2470 (2011)

Conference proceedings:

1. **Invited talk: A. Markov**, H. Guerboukha, M. Skorobogatiy, "Hybrid Metal-dielectric THz Fibers: a review," Photonics North, Canada (2015)
2. **A. Markov**, T. Ma, M. Skorobogatiy, "Graded Index Porous Optical Fibers – Dispersion Management in Terahertz Range," CLEO, JW2A.56, USA (2015)
3. **A. Markov**, H. Guerboukha, M. Skorobogatiy, "Hybrid Metal Wire-Dielectric THz Fibers: Design and Perspectives," CLEO, JW2A.55, USA (2015)
4. **Invited talk: A. Markov**, H. Guerboukha, M. Skorobogatiy, "Hybrid Metal-dielectric THz Fibers: Design And Perspectives," 39th Int. Conf. on Infrared, Millimeter, and THz Waves, W2B-21.1, USA (2014)
5. **A. Markov**, G. Yan, M. Skorobogatiy, "Low-Loss THz Waveguide Bragg Grating Using A Two-Wire Waveguide And A Paper Grating," 39th Int. Conf. on Infrared, Millimeter, and THz Waves, M2B-3.1, USA (2014)
6. **A. Markov**, "Hybrid Plasmonic Terahertz Fibers for Sensing Applications," Frontiers in Optics (FiO), FTu4B.2, Orlando, Florida, USA, October, 2013

7. **Invited: A. Markov**, H. Guerboukha, M. Skorobogatiy, "Plasmonic Two Wire Terahertz Fibers with Highly Porous Dielectric Support ," IEEE Photonics Conference (IPC), Washington, USA, September, 2013
8. **A. Markov**, H. Guerboukha, M. Skorobogatiy, "Plasmonic Two Wire Terahertz Fibers With Porous Dielectric Support " International Conference on Infrared, Millimeter, and Terahertz Waves (IRMMW-THz), 2352610 , Germany, September, 2013
9. **A. Markov**, M. Skorobogatiy, "Hybrid Plasmonic Terahertz Fibers for Sensing," OSA Optical Sensors, SM1C.3, Rio Grande, Puerto Rico, July, 2013
10. **A. Markov**, S. Gorgutsa, H. Qu, M. Skorobogatiy, "Plasmonic Two Wire Terahertz Fibers with Highly Porous Dielectric Support," Conference on lasers and Electro Optics (CLEO 2013), CTh1K.4, San Jose, USA, June, 2013
11. A. Mazhorova, **A. Markov**, B. Ung, M. Rozé, S. Gorgutsa, and M. Skorobogatiy, "THz wave guiding using hollow capillaries," (OPTICS-7-26-3), Photonics North, Canada, 2012
12. **A. Markov**, S. Gorgutsa, H. Qu and M. Skorobogatiy, "THz wire waveguides," Plasmonics, Gordon Research Conference, Maine, USA, June, 2012.
13. **A. Markov**, C. Reinhardt, B. Ung, A. Evlyukhin, W. Cheng, B. Chichkov, M. Skorobogatiy, "Photonic Bandgap Plasmonic Waveguides," JTh2A.110, CLEO, San Jose, CA, USA, 2012
14. C. Reinhardt, A. Evlyukhin, W. Cheng, R. Kiyan, A. Kuznetsov, B. Chichkov, M. Skorobogatiy, and **A. Markov**, "Plasmonic Waveguides with Photonic Bandgab Confinement," NanoMeta 2011, TUE4f.60, Austria 2011.